Université de Lille

École doctorale ED Régionale SPI 72

Impulsive and Dependent Interference in IoT Networks
(Interférence Impulsive et Dépendante dans Les Réseaux IoT)

Auteur : Ce ZHENG

Présentée et soutenue publiquement le 08/12/2020
pour l'obtenir le titre de **Docteur**
*de l'*Université de Lille
Spécialité: Micro et nano technologies, acoustique et
télécommunications.

Composition du jury (prévu):

Rapporteurs :   **Mylene Pischella**
Associate professor, CNAM, France
Claude Oestges
Full professor, UCLouvain, Belgium

Examinateurs :   **Jean-François Hélard** (président du jury)
Professor, IETR INSA Rennes, France
Lina Mroueh
Associate Professor, ISEP - École d'ingénieurs du
Numérique, France

Troels Pedersen
Associate Professor, Aalborg University, Denmark
Directeur de thèse :   **Laurent Clavier**
Professeur, IEMN, IMT Lille Douai, Université de
Lille, France
Co-directeur de thèse :   **Jean-Marie Gorce**
Professor, Inria, INSA Lyon, France
Co-encadrant :   **Malcolm Egan**
Chargé de Recherche, Inria, INSA Lyon, France
Invité :   **Gareth W. Peters**
Chair Professor in Statistics for Risk and
Insurance, Heriot-Watt University, UK

To my family and friends.

"Life can only be understood backwards, but it must be lived forwards."

Soren Kierkegaard

"I just wondered how things were put together."

Claude Shannon

Acknowledgements

It marks three years since my first arrival in France. In April 2017, I saw a Ph.D. opening on IRACON website and sent my CV to Professor Laurent CLAVIER and Professor Jean-Marie GORCE. After several interviews, I finally got the offer on this thesis. This opens a gate towards a new life.

I would first like to express my special appreciation and gratitude to two supervisors who helped me most— Laurent Clavier and Malcolm Egan for their mentorship throughout my Ph.D. candidature. They have been nice and patient to me. They are willing to spend time on supervising me on my project and answering all my silly questions and helping me out when I got stuck, It is impossible to achieve this thesis without their help and contribution. Besides, I also got extra assistance from Professor Gareth. W. Peters.

I also want to thank my second supervisor, Professor Jean-Marie who brought me into the ARBURST project. In this project, I met many awesome professors and team members, Jean-Yves Baudais, Philippe Mary, Anne Savard and Dadja Anade.

A nice and unforgettable memory is in Denmark thanks to Professor Troels Pedersen who treated me well. Although the initial goal is not reached, I learned a lot from working with him. In Aalborg university, I met many good professors and students. Carles Navarro Manchon, Petar Popovski, Ignacio Rodriguez Larrad, Ayush Bharti and Sajad Rezaie.

I thank all my former and colleges in IRCICA lab, Mauro Lopes De Freitas, Umber Noreen, Nicolas de Araujo Moreira, Yasser Mestrah, Sofiane Kharbech and Angesom Ataklity Tesfay.

In Lille, I met lots of friends, all of them are very nice to me: Min Li, Liuqing Pang, Shanshan Xu, Kunpeng Long, Lei Shi, Fei Xiao, Honghong Xiao, Zhixiong Gong, Dom Grums and etc.

What is more, thanks for the time and effors of my jury members: Professor Claude Oestges, Mylene Pischella, Jean-Francois Hélard, Lina Mroueh.

Last but not least, I am very grateful with the support from my parents and my girlfriend, Fen Mao.

Life is magnificent. I never thought I would end up in France but here I am. I want to rethank to all the people I mentioned above and also to the people whom I didnt mentioned but directly or indirectly helped me during my study.

Abstract

Title: *Impulsive and Dependent Interference in IoT Networks*
(Interférence Impulsive et Dépendante dans Les Réseaux IoT)

The number of devices in wireless Internet of Things (IoT) networks is now rapidly increasing and is expected to continue growing in the coming years. To support this massive connectivity, a number of new technologies, collectively known as Low Power Wide Area Network (LPWAN), have been developed. Many devices in LPWANs limit their transmissions by duty cycle constraints; i.e., the proportion of time allocated for transmission. For nearby wireless networks using the same time-frequency resources, the increasing number of devices leads to a high level of unintended signals, known as interference.

In this thesis, we characterize the statistics of interference arising from LPWANs, with a focus on protocols related to Narrowband IoT (NB-IoT) and emerging approaches such as Sparse Code Multiple Access (SCMA). Such a characterization is critical to improve signal processing at the receiver in order to mitigate the interference.

We approach the characterization of the interference statistics by exploiting a mathematical model of device locations, signal attenuation, and the access protocols of individual interfering devices. While there has been recent work developing empirical models for the interference statistics, this has been limited to studies of the interference power, which has limited utility in receiver design. The approach adopted in this thesis has the dual benefits of providing a model for the amplitude and phase statistics and while also yielding insights into the impact of key network parameters.

The first contribution in this work is to revisit interference in a single subcarrier system, which is widely used in current implementations of IoT networks. A basic model in this scenario distributes interfering devices according to a homogeneous Poisson point process. It has been long known that the resulting interference is well approximated via an α-stable model, rather than a Gaussian model. In this work, the α-stable model is shown via theoretical and simulation results to be valid in a wider range of models, including the presence of guard zones, finite network radii, and non-Poisson point processes governing device locations.

The second contribution in this thesis is the study, for the first time, of interference statistics in multi-carrier IoT networks, including those that exploit NB-IoT and SCMA. Motivated by the results in the single subcarrier setting, a multivariate model based on α-stable marginals and copula

theory is developed. This model is verified by extensive simulations and further justified via a new, near-optimal, parameter estimation algorithm, which has very low complexity.

The third part of this thesis applies the characterizations of the interference statistics to receiver design. A new design for nonlinear receivers is proposed that can significantly outperform the state of the art in multi-carrier IoT systems. When receivers are restricted to be linear, the optimal structure is identified and the bit error rate characterized. Numerical results also illustrate how the average quantity of data interfering devices are required to transmit affects the receiver performance.

Index terms —— NB-IoT, SCMA, α-stable, t-copula, linear combining, impulsive interference, receiver design.

Résumé

Title: *Interférences impulsives et dépendantes dans les réseaux IoT*

Le nombre de dispositifs dans l'Internet des objets (IoT) communiquant sans fil est en rapide augmentation et devrait continuer à croître dans les années à venir. Pour soutenir cette connectivité massive, un certain nombre de nouvelles technologies, collectivement connu sous le nom de Low Power Wide Area Network (LPWAN), ont été développées. Le nombre de transmission des objets dans les LPWANs est limitée par les contraintes de duty cycle qui fixe la proportion de temps d'occupation d'une ressource radio. Pour des réseaux sans fil coexistant dans une même zone géographique et utilisant les mêmes ressources fréquentielles, le nombre croissant d'appareils entraîne la présence fréquente de signaux non désirés par le récepteur et connus sous le nom d'interférences.

Dans cette thèse, nous caractérisons les statistiques d'interférence dans des LPWANs, avec un accent particulier mis sur le NB-IoT et les approches émergentes telles que le Sparse Code Multiple Access (SCMA). Une telle caractérisation est essentielle pour améliorer le traitement du signal au niveau du récepteur afin d'atténuer l'impact de l'interférence.

Plusieurs facteurs influent sur les propriétés statistiques de l'interférence : l'emplacement des dispositifs, l'atténuation des signaux, les protocoles d'accès à la ressource radio. De nombreux travaux récents développent des modèles d'interférence mais beaucoup se limitent à la puissance ce qui n'est pas suffisant pour la conception des récepteurs. Nous proposons dans cette thèse un modèle de l'amplitude (complexe) de l'interférence en le liant aux principaux paramètres du réseau.

La première contribution est de réexaminer l'interférence dans une seule dimension (par exemple une sous-porteuse), un cas largement rencontré dans les solutions actuelles de l'IoT. Dans ce scénario, l'hypothèse de départ est de distribuer les dispositifs interférents selon un processus de Poisson homogène. Il est connu depuis longtemps que l'interférence résultante est bien approximée par un modèle α-stable, plutôt qu'un modèle gaussien. Ce modèle est étendu au cas complexe (sous-Gaussien) et confronté à des hypothèses plus réalistes, notamment la présence de zones de garde, un réseau de rayon fini et des processus non homogènes régissant l'emplacement des appareils.

La deuxième contribution est l'étude, pour la première fois, des statistiques sur les interférences dans les réseaux IoT multi-porteuses, par exemple le NB-IoT ou le SCMA. Motivé par les résultats obtenus dans le cas

d'une seule sous-porteuse, un modèle multivarié basé sur des parginales α-stable et des relations de dépendance modélisées par des copules est proposé. Ce modèle est vérifié par simulation et justifié par un nouvel algorithme d'estimation des paramètres qui se révèle très proche de l'optimal mais avec une très faible complexité.

Dans la troisième partie, les modèles d'interférence sont utilisées pour améliorer la conception des récepteurs. Les récepteurs non linéaires améliorent de manière significative les performances des systèmes. Si l'on se limité à des récepteurs linéaires, il est possible d'obtenir le système optimal et le taux d'erreurs binaires. Les résultats illustrent également comment la charge du réseau et la quantité moyenne d'information que chaque noeud essaie de transmettre affecte les performances du récepteur.

Contents

List of Figures

Acronym

BER Bit Error Rate

BPP Binomial Point Process

BPSK Binary Phase Shift Keying

BSS Blind source separation

CCA Copula Component Analysis

CDF Cumulative Distribution Function

CF Characteristic Function

CLT Central Limit Theorem

CSI Channel State Information

CSMA Carrier-sense Multiple Access

CSMA/CD Carrier-sense Multiple Access with Collision Avoidance

CSS Chirp Spread Spectrum

EGC Equal Gain Combining

eRB elementary Resource Blocks

GCLT Generalized Central Limit Theorem

HPPP homogeneous Poisson point process

ICA Independent Component Analysis

IFM Inference-Functions-for-Margins

IoT Internet of Things

ISM Industrial, Scientific and Medical

i.i.d. independent and identically distributed

KL divergence Kullback-Leibler divergence

LDPC Low-Density Parity-Check

LLR Log-Likelihood Ratio

LPWAN Low Power Wide Area Network

LTE Long Term Evolution

MAC Media Access Control

MIMO Multiple-Input and Multiple-Output

ML Maximum Likelihood

MRC Maximum Ratio Combining

MTC Machine Type Communication

msB minimum size Block

NB-IoT Narrowband IoT

NOMA non-orthogonal multiple access

NPUSCH Narrowband Physical Uplink Shared Channel

OLC Optimal linear combining

OFDM orthogonal frequency-division multiplexing

PDF probability density function

PRB physical resource blocks

PPP Poisson point process

P-P plot Probability-Probability plot

QPSK Quadrature Phase-shift Keying

Q-Q plot Quantile-Quantile plot

RB Resource Block

SαS symmetric α-stable

SC Selection Combining

SCMA Sparse Code Multiple Access

SC-FDMA Single Carrier Frequency-Division multiple access

SISO Single-Input and Single-Output

SNR Signal-to-Noise Ratio

URLLC Ultra-Reliable Low-Latency Communication

UWB Ultra Wide Band

3GPP 3rd Generation Partnership Project

Notation

Vectors or matrices are denoted by bold lowercase letters and random vectors or matrices by bold uppercase letters, respectively (e.g., $\mathbf{x}$, $\mathbf{X}$).

Symbol	Description
$\mathbf{I}$	Identity matrix
$\sim$	has the distribution of
$\approx$	approximate
$\stackrel{d}{=}$	Both sides of the equality have the same distribution
Φ	Point process
$\mathcal{R}^n$	The n-dimensional space
$\mathbb{R}^n$	The n-dimensional real vector space
$|\mathbf{x}|$	Euclidean norm
$|\cdot|$	Lebesgue measure
$(\cdot)^T$	Matrix transpose
$\mathbb{E}[\cdot]$	Expectation
$\xrightarrow{a.s.}$	converges almost surely to
$\mathbb{1}(\cdot)$	Indicator function
$\Gamma(\cdot)$	Gamma distribution
$\{r_j\}$	The sequence
$\|\cdot\|$	The 2 norm
S^{d-1}	Unit sphere in d dimensions
$\mathcal{O}(d)$	d-dimenional orthogonal matrix
$\mathrm{Re}(\cdot)$	take the real part of
$\mathrm{Im}(\cdot)$	take the imaginary part of
$\Phi_{\mathbf{x}}(\cdot)$	Characteristic function
$\psi_{\mathbf{x}}(\cdot)$	Log characteristic function
$N(B)$	Number of points in the area B
$\mathrm{sign}(\cdot)$	Sign function
$\exp\{\cdot\}$	Exponential function
$\mathcal{CN}(\mu, \sigma^2)$	Complex symmetric normal distribution with mean μ and variance σ^2
$S_\alpha(\gamma, \beta, \delta)$	α-stable distribution with characteristic exponent α, scale parameter γ, symmetry parameter β and location parameter δ
$\mathbb{P}(\cdot)$	The probability of
$\Gamma(r_{\min}, r_{\max})$	An annulus with $r_{\min}$ and $r_{\max}$
$\mathrm{Unif}\{+1, -1\}$	distributed on $+1$ and -1 with equal probability

Introduction

1.1 Background

The IoT is a network where large numbers of devices are deployed, connected to the internet and transmit and receive data without necessarily human intervention. According to [Ala18], the number of IoT devices will reach over 75 billion by the year 2025. The performance of a receiver is degraded by undesired signals from other devices (in the form of interference) and thermal noise. This huge amount of devices, without doubt, will lead to a severe **interference** problem.

The massive scale of IoT networks means that individual devices must be cheap, resulting in constraints on transmit power and computational resources. As such, devices are more likely to employ simple modulation and access schemes. In addition, the proliferation of these IoT devices means that centralized scheduling is unfeasible; and thus, it is unrealistic for them to work together. As a consequence, random access schemes based on either Aloha (duty cycle), e.g., Sigfox and LoRa or carrier sensing (Listen before talk) are favored. In the Long Term Evolution (LTE) network, the channel bandwidth has been divided into physical resource blocks (PRB), which is the smallest unit of resources with 180 kHz wide in frequency and 1 slot long in time. And orthogonal frequency-division multiplexing (OFDM) is employed.

Previous studies have been focused on the LTE network where each device is allocated with at least one Resource Block (RB) and transmits on OFDM subcarriers, which does not capture the features of IoT networks, especially for the NB-IoT. In NB-IoT, a single resource block is divided into 12 subcarriers in the uplink, and a device can transmit on 1, 3, 6 or 12 of theses subcarriers. Due to this access protocol of NB-IoT, devices are more likely to transmit on the same subcarriers which thus leads to severe co-channel interference. This problem also arises when non-orthogonal multiple access (NOMA) schemes are employed.

That is, when a large number of devices operate in an uncoordinated fashion in the IoT networks, they will occupy and transmit on the same channel resources. In this case, the accumulative undesired signals from other devices—i.e., the interference—is difficult to characterize. It is even more challenging when signal processing (e.g., OFDM) is used to reduce the impact of variations in the wireless channel or in the Sparse Code Multiple Access (SCMA) schemes, where interfering devices utilise non-orthogonal

time-frequency resources.

The recent Aalborg measurements [Lau+17a; Cla+20] also suggest that the interference is non-Gaussian and exhibits impulsiveness. That is, the probability density function (PDF) of its distribution has heavier tails, and it is more likely to have large values. Therefore, an appropriate model for the interference is desired.

The non-Gaussian interference impacts the system design in two aspects: *1)* At the network level, it changes the optimization of the network parameters such as density of devices or power allocation. This is due to the fact that most analyses of the average throughput and coverage probability rely on the Gaussian noise assumption. As a consequence, the capacity has to be revisited [DF+17], as well as the network throughput. *2)* At the device level, the receiver has to be redesigned. The performance of the receiver depends on the interference statistics as the interference changes the PDF of the received signal and thus impacts the detection methods such as Maximum Likelihood (ML) or linear combining. What is more, because the devices transmit on common subcarriers as in the case of NB-IoT or NOMA, the interference is on different subcarriers is statistically dependent. Consequently, standard detection algorithms based on independent and identically distributed (*i.i.d.*) Gaussian interference have degraded performance. Therefore, to improve the design of signal processing in the receiver, it is essential to characterize the interference statistics.

1.2   Motivation and challenges

The goal of our thesis is to **characterize the statistics of interference and study its impact on the receiver performance** in the IoT networks. This work is initially motivated by networks exploiting NB-IoT or SCMA but we expect that it can be extended to more general settings. To achieve this aim, we address the following challenges:

Interference modeling on a single subcarrier

Previous studies have proposed several models to capture the impulsive or non-Gaussian behavior of the interference, such as Middleton Model [Mid77; Mid99], ϵ-contaminated [Pha+03; AB07; Alh+17] or Gaussian-mixture [GDK06]. However, those models are either complex for analytical derivation of the receiver or lack accuracy. Therefore, a more tractable characterization of the interference is required which is of simple form and accurate.

Interference modeling on multiple subcarriers

As we mentioned, devices overlap on multiple subcarriers in networks employing NB-IoT or SCMA. Consequently, the sets of interferers on different

subcarriers overlap as well, which leads to statistical dependence between interference on different subcarriers. It is difficult to derive the exact characterization of the interference vector and model such dependence.

Receiver performance

Existing receiver designs tailored to Gaussian interference may have degraded performance in IoT networks. As a result, it is required to have new receiver designs tailored to interference arising from IoT networks. Besides, to study the performance, characterization of metrics such as Bit Error Rate (BER) is necessary.

1.3 Contribution

The contribution of this thesis is described as follows.

In Chapter 2, we develop a general mathematical formalization for the physical layer and access policy:

- The framework takes into consideration the interferers' location following point processes;

- Although it is developed based on NB-IoT, this formalization is quite generic for other IoT networks.

In Chapter 3, we focus on modeling the interference on single subcarrier with α-stable model:

- We consider the impact of the guard-zone on the validity of α-stable model;

- In addition to homogeneous Poisson point process (HPPP), the validity of α-stable model is also checked under quite general point processes.

In Chapter 4, we focus on modeling the interference on multiple subcarriers:

- We first derive the exact joint distribution of the interference vector under special cases;

- For the general case, we proposed a t-copula model combined with α-stable distribution, motivated by the results in Chapter 3;

- Tailor to this model, a low complexity estimation algorithm is proposed.

In Chapter 5, we study the impact of the interference on the receiver performance.

- Based on the results in Chapter 4, optimal linear receiver is obtained for certain scenarios and accurate approximations for BER are derived;

- Performance of different receivers are studied and compared.

1.4   Scientific publications

This section summarizes the publications, conferences and collaborations based on work that was done during the period of Ph.D. candidature.

Journal papers

- **Ce Zheng**, Malcolm Egan, Laurent Clavier, Gareth W. Peters and Jean-Marie Gorce. "A Tractable Characterization of Multivariate Heavy-Tailed Interference Arising from Nearly Poisson Spatial Point Processes" In: *IEEE Transactions on Communications* (2020-under review)

- Malcolm Egan, Laurent Clavier, **Ce Zheng**, Mauro Lopes de Freitas, Jean-Marie Gorce. "Dynamic Interference in Uplink SCMA for Large-Scale Wireless Networks without Coordination," In: *EURASIP Journal on Wireless Communications and Networking*, vol. 2018, no. 1, p. 213, 2018.

International conference papers

- **Ce Zheng**, Malcolm Egan, Troels Pedersen, and Jean-Marie Gorce, "Linear Combining in Dependent α-stable Interference", In *Proc. IEEE International Conference on Communications (ICC)*, pp. 1-6, 2020.

- **Ce Zheng**, Malcolm Egan, Troels Pedersen, and Jean-Marie Gorce, "Copula-based interference models for iot wireless networks", In *ICC 2019-53rd IEEE International Conference on Communications*, pp. 16, 2019.

French national conference papers

- **Ce Zheng**, Malcolm Egan, Laurent Clavier, Gareth W. Peters and Jean-Marie Gorce. "On the Validity of Isotropic Complex α-stable Interference Models for Interference in the IoT," *Gretsi, 2019*

Chapter 2

A Mathematical Formulation of IoT Networks

2.1 General context

While the number of IoT devices is continuously increasing, communication paradigms are changing. Energy consumption and cost have to remain low and a centralized network architecture, as it was the case in cellular networks up to the 4th generation, is no longer an option. This results in networks with a very limited coordination, if any. In such cases, orthogonal multiple access schemes are too complex to implement and interference becomes a crucial issue.

Let us consider an area where a large number of devices are attempting to transmit some information. Among all these devices, one will be considered as the one we want to decode, the one that transmits useful information. This specific device will be designed as the **desired user**. It uses a specific time-frequency resource to transmit its information. This resource is composed of one or several **physical resource blocks (PRB)**. In a general setting, the transmission of the information can require several PRBs, either separated in time or in frequency. The quantity of information transmitted on each PRB is also dependent on the way the system is defined. It can be very few bits in the frequency hopping strategy used by Bluetooth [Haa98; Mor02] or Time-Hopping Ultra Wideband communications [BY09] or a complete packet as in LoRa [Mek+19], Sigfox [Sig17; LPP19] or NB-IoT [OS16].

We define **interference** as the accumulation of all undesired signals transmitted, at least partially, on the same PRBs as the desired user. A fundamental question—and the focus of this thesis— is then how to characterize the statistics of the interference. This is a non-trivial question due to the asynchronous nature of IoT communications, the range of applications that IoT is intended to support, and also the variety of protocols that have been adopted.

Many works have already addressed this question, from the early works

from Middleton [Mid77; Mid99] to more recent works dealing with stochastic geometry [Sou92; IH98; Gul+10; Pin+06; PW10a; PW10b]. The detailed state of the art is left for the following chapters. We first want to set the right framework for the study and the underlying assumptions. These assumptions must be sufficiently precise to allow for analytical studies that will be useful in defining the systems and flexible enough to apply to many contexts. They will form the basis for the interference characterization in the following chapters.

Communication System
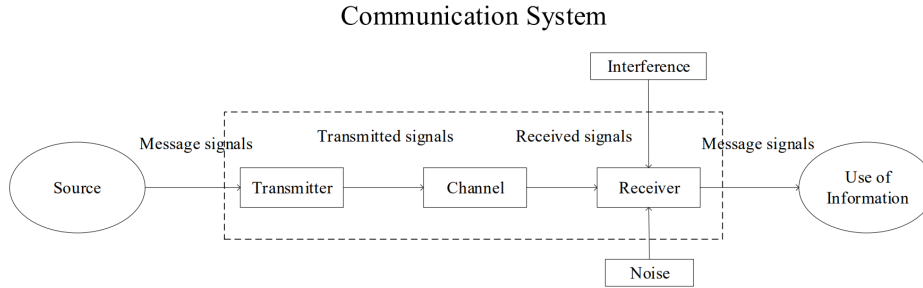
FIGURE 2.1: Structure of communication system.

The physical structure of a communication system (in IoT networks) is illustrated in Fig. 2.1. Several aspects will impact the interference properties and have to be considered to build a significant model:

1. *The physical layer of communication.* Interfering devices can belong to the same network as the desired device (intra-network interference) or to another network (inter-network interference). This latter case is particularly significant in Industrial, Scientific and Medical (ISM) bands. For instance the co-existence of SigFox and LoRa is an open question.

2. *The locations of interfering devices.* Indeed, the received signal strength from an interfering device is dependent on this distance. When studying the efficiency of a cellular network, a regular (hexagonal) structure was used [Gil+91; ZD97; The+02; Gol05; SC09; XZA11], this is no longer valid with IoT networks. Indeed, in many situations devices will be randomly located and this randomness has to be accounted for. Even in cellular networks, when more accurate evaluations are needed, the hexagonal structure is no longer sufficient [Gil+91; ABG11; NJ15]. We will choose modeling approaches that have recently been proposed for location modeling, coming from the large literature on networks and stochastic geometry [HG09; Hae+09; ABG11; Hae13; Car10; WA12; BB10b; Bła+18].

3. *The access protocol adopted by the interfering devices.* For instance, the first networks deployed in ISM bands like Bluetooth or WIFI are using

a listen before talk strategy [Fre02; SSH15]. On the contrary, more recent LPWAN are using a duty-cycle based protocol. That is, they do not listen to the channel before transmission but are limited in the percentage of time they can access the channel [ZZ17].

Based on these three components, we detail the input-output relationship for the desired communication link in the presence of interference induced by other IoT devices, either from the same network or from another network. We attempted to have both a general framework but simple enough to allow tractable results. As much as possible, we constrained this work by protocols that have been either standardized (NB-IoT) or channel access strategies that have been proposed in the literature (SCMA). We kept the physical layer and channel model as general as possible. Given known statistics for the interference derived in Chapter 3 and Chapter 4, this input-output relationship provides a means of designing improved receiver architectures and analyzing metrics such as the area spectral efficiency.

2.2 Existing technologies

The main concern of this work is the Low Power Wide Area Network (LPWAN) technology. The LPWAN is a type of wireless telecommunication wide area network designed to allow long-range communications at a low bit rate among things. In LPWAN, scalability is a bottleneck as interference becomes the main limitation with the low-cost, long-life devices that are deployed. Sigfox, Lora and NB-IoT are the three leading technologies. We are going to give their main features that justify the assumptions we make for the communication technologies.

2.2.1 Narrowband IoT

The NB-IoT is a LPWAN standard developed by the 3rd Generation Partnership Project (3GPP) to support the Machine Type Communication (MTC) in the LTE networks. It operates and coexists on both licensed and unlicensed frequency bands in the LTE network. As opposed to other LTE technologies, where the whole physical resource (frequency band) is allocated to a single user, the NB-IoT is working over only on limited frequency bands, i.e., 180 kHz. This 180 kHz bandwidth is divided equally into 12 or 48 sub-carriers or subbands, as shown in Fig. 2.2 from [MZW17]. In the single-tone mode, each user is allocated with one sub-carrier. In the multi-tone mode, each user is allocated with either 3, 6 or 12 sub-carriers.

To be flexibly deployed and compatible with the LTE network, NB-IoT keeps many LTE design features. In the uplink, it uses the Single Carrier Frequency-Division multiple access (SC-FDMA) scheme with each tone of

a) Bandwidth of each sub-carrier is 3.75 kHz. There are 48 sub-carriers in total.

b) Bandwidth of each sub-carrier is 15 kHz. There are 12 sub-carriers in total.
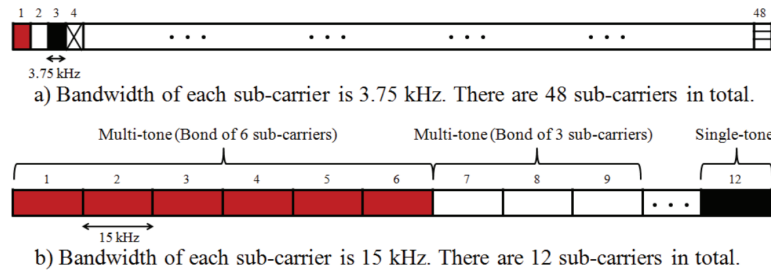
FIGURE 2.2: NB-IoT transmission modes [MZW17]: (a)
single-tone mode; (b) single-tone and multi-tone mode.
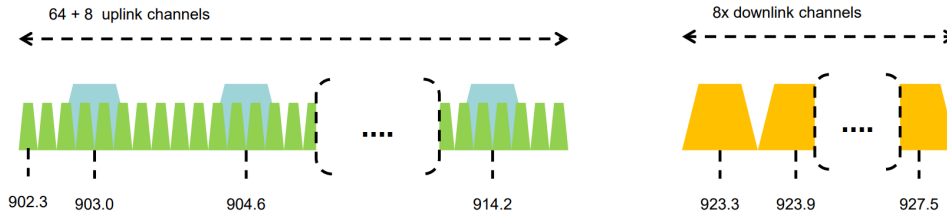
FIGURE 2.3: LoRa channel frequencies [All17].

either 3.75kHz or 15 kHz. In the downlink, it keeps the OFDM scheme with
each tone of 15 kHz. However, with 12 or 48 sub-carriers, it is impossible to
meet the increase in the number of devices since NB-IoT adopts an orthog-
onal multiple access approach. What is more, the subsequent access delay
may also become a big issue for Ultra-Reliable Low-Latency Communica-
tion (URLLC) in a burst communication scenario due to the limited num-
ber of channel resources. To tackle such a problem, a promising solution is
the NOMA where devices can partially or fully share the same sub-carriers
[Sai+13; Sha+20], such as SCMA.

2.2.2   Sigfox and LoRa

Unlike NB-IoT working on licensed LTE frequency band, Sigfox and LoRa
are working on unlicensed bands. In Europe, they both operate on ISM 868
MHz band. For Sigfox, the band is divided into 400 channels of 100 Hz
starting at 868.180 MHz and ending at 868.220 MHz, though channel 181-
219 are reserved and not used [Mar+15]. In the United States, Canada and
South America, LoRa works on ISM 915 MHz band starting at 902 MHz
and ending at 928 MHz, shown in Fig. 2.3 [All17]. For the uplink, LoRa de-
fines 64 channels numbered 0 to 63, starting at 902.3 MHz and incrementing
linearly by 200 kHz to 914.9 MHz, and 8 channels numbered 64 to 71 start-
ing at 903.0 MHz and incrementing linearly by 1.6 MHz to 914.2 MHz. In
the downlink, 8 different channels will be used, starting at 923.3MHz and
incrementing linearly by 600 kHz to 927.5MHz.

The cost of the end-device is less than 2 euros for Sigfox and between 3
to 5 euros for LoRa, much lower comparative of NB-IoT (more than 20 eu-
ros) [Mek+19]. Such low-cost devices can not afford excessive signaling and

control overhead. As such, simple random access schemes are favored. Sigfox and LoRa resort to Aloha, the first and simplest multiple access scheme, which is categorized into the grant-free systems where channel resources are accessed without undergoing assignment [WM19]. Nevertheless, Aloha rapidly becomes inefficient when device density increases and the collision probability is extremely high for the massive number of devices occupy scarce radio resources.

2.3 Physical layer

Existing LPWAN technologies face the challenge of massive connectivity caused by the increasing number of devices with the constraint of the limited frequency resources but also, in some use cases, low latency. To address these issues, new access schemes are required, complying with existing standards if possible but not necessary. A promising strategy, which can both increase the number of connected devices and keep a reduced complexity, is NOMA where devices can transmit concurrently utilizing non-orthogonal resources. However, because devices partially or fully share the same sub-carriers, NOMA yields more severe interference. Besides, the level of interference is not necessarily independent on different sub-carriers (illustrated further in the sequel). To design the network, it is necessary to predict what the interference will look like. This requires some assumptions on the different components influencing its distribution.

Any communication system can break down into three components: the transmitter, the receiver and the channel as illustrated in Fig. 2.1. We will keep the physical layer description as generic as possible so that our approach can be used for very different systems and conditions.

The transmitter is a device that has a set of information to transmit. It transforms this set into a signal that will be transmitted according to the channel access protocol. In this work, the information source has no impact, only the waveform that is transmitted, even though a very wide range of modulation schemes can be considered.

In its discrete baseband representation, it is a complex vector that we will denote by $X_{n,k}$. Indexes n and k allow identifying the resource blocks that are used as will be described in Section 2.6. In NB-IoT and Sigfox, devices employ Quadrature Phase-shift Keying (QPSK) modulation and Binary Phase Shift Keying (BPSK) modulation respectively, while LoRa uses the Chirp Spread Spectrum (CSS) modulation that spreads a narrow-band signal over a wider channel bandwidth.

Remark 2.3.1. *In the rest of the work, we will assume that all interfering devices employ the same linear modulation scheme. However, this could be extended to*

heterogeneous networks quite easily, either by separating the contribution of each network in a first step or by considering a weighted mixture for the statistical properties of the source resulting from the combination of the properties of each network contributing to the interference.

Furthermore, we will assume that each device is using the same transmission power. Indeed, power control is a complicated process, difficult to implement for IoT networks. Besides, if power is adjusted, this can be taken into account in the channel model or as a variation in the user location; and it does not modify the framework of the study.

2.4   Channel

Three main factors are to be considered that impact the channel attenuation: path loss, large-scale fading and small-scale fading. We use a simple and generic expression for a given radio link from a device to a receiver located at a distance r:

$$l(r) = r^{-\frac{\eta}{2}} h = r^{-\frac{\eta}{2}} A e^{j\theta}, \tag{2.1}$$

where $l(r)$ denotes the channel gain (in amplitude) at the distance r, η is the path-loss exponent, and $h = A e^{j\theta}$ is the fading.

This model has a significant drawback due to $l(r)$ tending to infinity as r tends to 0. However, this will be addressed by defining a guard zone around the receiver where no interfering devices can occupy (see Section 2.5.4).

Remark 2.4.1. *In the rest of the work, we will consider Rayleigh fading, i.e., $h \sim \mathcal{CN}(0,1)$. The Rayleigh fading affects the received signal with a uniformly distributed phase $\theta \sim \mathrm{U}[0, 2\pi]$ and Rayleigh distributed amplitude. Other models can be used instead with limited modifications in most of the results. Large scale fading (shadowing) can impact the choice of the statistical properties of h but can also be accounted for in the spatial process of the device locations. Non-homogeneous Poisson processes like the doubly Poisson cluster process or Matérn hard-core process of type II (see Section 2.5.2 and Section 2.5.3) can indeed account for the presence of some obstacles by grouping users or suppressing the presence of them in some areas.*

2.5   Interferer locations

The dependence on the distance in the signal observed by a receiving device implies that the locations of interfering devices have a large impact on interference statistics and thus the system performance. On the other hand, the location of IoT devices is largely unstructured. As a consequence, it

has become increasingly popular to model the locations of IoT devices via stochastic processes, in particular the theory of point processes [Gha+16].

In this section, we introduce models for the locations of devices known as *point processes*, i.e., the mathematical models of a discrete set of points with random locations. Specifically, we introduce three point process models that we will consider in this work: homogeneous Poisson point process, doubly Poisson cluster point process and Matérn hard-core process of type II. The supplementary background is provided in Appendix A.

Point process models provide a flexible means of accounting for a variety of applications; for example, the family of homogeneous Poisson point process (HPPP)s induces device locations that are roughly independent of each other. On the other hand, devices may exhibit similar behaviors and group together due to human activity or network deployment. In heterogeneous networks, devices gather around their common access points and are more "cohesive" in space. Therefore, point processes with attraction are more favored such as the family of Poisson cluster processes. Besides, devices also interact with each other due to access schemes. For example, in Carrier-sense Multiple Access (CSMA) network, two devices close by are usually forbidden to transmit simultaneously, which requires point processes with repulsion. A typical model is the Matérn hard-core process of type II where a minimum distance between two points is forced, and thus points are more regular. In the extreme case, a lattice is obtained.

Snapshots of the aforementioned three point processes are given in Fig. 2.4.

(A) homogeneous Poisson point process (B) Doubly Poisson cluster process (C) Matérn hard-core process of type II
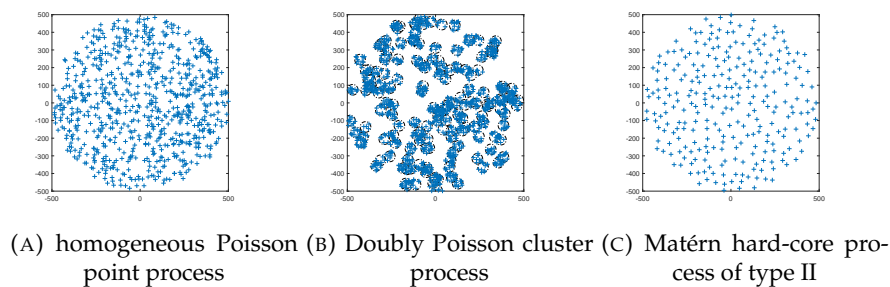
FIGURE 2.4: Snapshots of three point processes over a circle with radius of 500 m.

2.5.1 Homogeneous Poisson point process

The HPPP is the most common point process in wireless system models. It was used to replace the regular hexagonal lattice model in cellular networks [ABG11]. In the IoT networks, devices are more randomly and densely distributed. What is more, many of the devices may be moving instead of being installed in a fixed place. As such, the HPPP with the feature of spatial randomness serves as a good model. Formally, a HPPP is defined as follows:

Definition 2.5.1. *(**Homogeneous Poisson point process**) A point process is homogeneous Poisson point process with density λ in $\mathcal{R}^2$ if*

- *Let $N(B)$ denotes the number of points located within the bounded set B, $N(B)$ follows a Poisson distribution with mean $\lambda|B|$, i.e.,*

$$P[N(B) = k] = \frac{(\lambda|B|)^k}{k!}e^{-\lambda|B|};\qquad(2.2)$$

- *If regions $B_1, \cdots, B_n$ are non-overlapping, then $N(B_i)$ are independent random variables.*

The HPPP exhibits complete spatial randomness due to this independent property. That is there is no interaction between the points. A snapshot of the realization of HPPP is plotted in Fig. 2.4a.

2.5.2   Doubly Poisson cluster process

The hypothesis of HPPP may lead to inaccurate analysis. Indeed, many causes of heterogeneity may occur. For instance, devices tend to gather together and be more clustered to some extent due to human activities. A large amount of IoT devices can exist in hot-spot zones formed by humans, such as business buildings and shopping malls. While outside these buildings, fewer devices are deployed, or in areas that are obstructed, the devices will not be visible by a given receiver, creating some empty regions. Within hospital complexes where patients may be grouped together, wireless wearables also form clusters and send messages and medical data to the medical personnel via a gateway at the cluster center. These networks and similar scenarios, such as smart home or e-health, can be modeled with the Poisson cluster process [AC18; Mek+17], which is a particular case of Neyman-Scott cluster process [Hae+09]:

Definition 2.5.2. *A Neyman-Scott cluster process is a cluster process where the parent points form a HPPP with intensity λ_p and the daughter processes are i.i.d. point processes.*

If each cluster is itself a Poisson point process, the resulting process is also called a doubly Poisson cluster process.

Definition 2.5.3. *(**Doubly Poisson cluster process**) The doubly Poisson cluster process is a cluster process where the parent points form a HPPP with density λ_p, and each daughter cluster is an i.i.d. finite Poisson point process with density λ_d.*

For the ease of analysis, in this thesis, we assume that each daughter process is a HPPP with density λ_d restricted to a disc of radius r_c. Points from the parent HPPP are included into the daughter process. A similar approach is also utilized in modeling heterogeneous networks where the

parent points are kept as the base stations from the upper layer [SAD17]. Hence, the average number of points in each cluster is $c = \lambda_d \pi r_c^2 + 1$. That is

$$\Phi = \bigcup_{\mathbf{z} \in \Phi_P} [\mathbf{z} + \Phi_{\mathbf{z}}], \tag{2.3}$$

where Φ_P denotes the parent process following HPPP with intensity λ_p, and $\Phi_{\mathbf{z}}$ denotes the daughter point process following HPPP over the disc of radius r_c around the cluster center $\mathbf{z}$ with intensity λ_d.

Although the standard formulation of the doubly Poisson cluster process studied in [Gul+10] does not include the parent process points, doing so does not significantly change the interference statistics and enables the rigorous approximation theorems in Section 3.3.

A snapshot of the realization of the doubly Poisson cluster process is plotted in Fig. 2.4b. Compared with HPPP, points are more clustered and grouped together.

2.5.3 Matérn hard-core process of type II

Carrier-sense Multiple Access (CSMA) is a Media Access Control (MAC) protocol whereby a device detects the presence of the signal from another device on the same carrier before it transmits. If there are no other signals, a transmission occurs. Otherwise, it postpones the transmission. This guarantees that two devices close by do not transmit simultaneously, and it reduces the collision risk. The feasibility of applications of CSMA in a IoT network has been widely studied in recent works [Pha18; EA+19; LWK19]. The CSMA network is better modeled by Matérn hard-core process of type II [Hae11; BBM06] where a distance of two nodes larger than a carrier-sense range is forced.

As opposed to the cluster point process which exhibits attraction, hard-core processes are point processes where points are forbidden to be closer than a certain minimum distance, i.e., points repulse each other and are less clustered compared with the Poisson point process. One significant hard-core process is the Matérn hard-core process of type II, where the starting locations of users are drawn from a HPPP, and points that violate the minimum-distance condition are then removed. The definition of Matérn hard-core process of type II is given as follows.

Definition 2.5.4. *Starting with an underlying HPPP Φ_p with density λ_p, add to each point x an independent random variable $m(x)$ uniformly distributed on $[0, 1]$, called a mark. Flag for removal all points that have a neighbor within distance r that has a smaller mark. Then remove all flagged points. That is*

$$\Phi \overset{\triangle}{=} \{x \in \Phi_p : \ m(x) < m(y), \ for \ all \ y \in \Phi_p \cap b(x, r_h) \setminus \{x\}\},$$

where r_h is the hard-core distance.

All points are removed simultaneously, so even points that are thinned out can eliminate other points. According to [HG09], the density of Matérn hard-core process of type II is

$$\lambda = \frac{1 - e^{-\lambda_p \pi r_h^2}}{\pi r_h^2}. \tag{2.4}$$

The maximum density is achieved as $\lambda_p \to \infty$: $\lambda = \frac{1}{\pi r_h^2}$.

A snapshot of the realization of Matérn hard-core process of type II is plotted in Fig.2.4c. Compared with HPPP, points are more repulsive, and a minimum distance is ensured.

2.5.4 Spatial region

The spatial region where devices are located is usually assumed to be $\mathcal{R}^2$. However, practical considerations make it difficult to have a transmitter with a very small distance from the desired receiver. This is even more unrealistic if a CSMA approach is used because when close to the receiver, a device should not transmit signals if its neighboring devices are active. Consequently, it is essential to include a guard zone, i.e., a region around a receiver where no active interferers can be located [HA07]. By setting up a guard zone, the nearby interference is avoided to some extent. It also suppresses the problem induced by the channel model (see Section 2.4) where the received power would tend to infinity if the interferer-receiver distance is tending to zero.

The assumption of an infinite network radius is also not realistic. Nevertheless, we can expect this assumption to have less impact because far users contribute less to the cumulative interference.However, in personal or local area network, e.g. within buildings such as shopping mall or hospital complex, the transmission range is in the order of magnitude of 100 meters or 1 Km for NB-IoT networks [SZ08]. Thus, devices are grouped within limited regions, and receivers actually experience interference from finite-area regions. Consequently, we will include in our model the fact that interfering devices are constrained over an annulus.

Let us consider a network of devices located according to a general point process, denoted by Φ. These devices form interferers for a receiver located at the origin. We introduce

- the radius of the network, $r_{\max}$, the maximum distance at which an interferer can be located, and

- the guard zone radius $r_{\min}$, the minimum distance at which an interferer can be located.

We define the annulus (see Fig. 2.5b)

$$\Gamma(r_{\min}, r_{\max}) = \{\mathbf{x} \in \mathbb{R}^2 : r_{\min} \leq \|\mathbf{x}\| \leq r_{\max}\}. \tag{2.5}$$
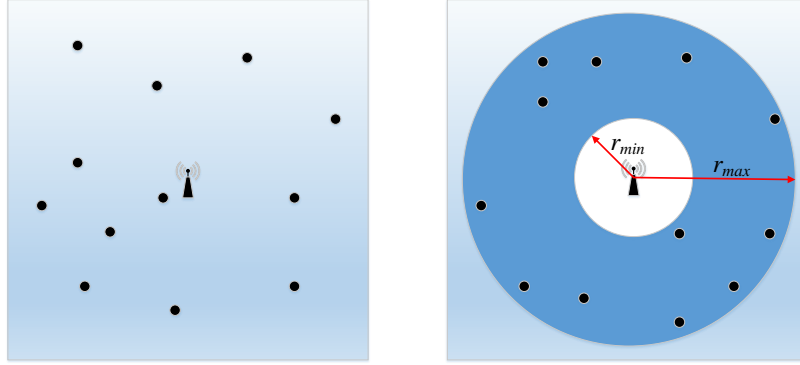
(A) Case 1: $r_{\min} = 0$ and $r_{\max} \to \infty$ (B) Case 2: $0 < r_{\min} < \infty$ and $r_{\max} < \infty$

FIGURE 2.5: Two cases for the interference in a field of general point process distributed interferers.

We restrict the original process Φ to this annulus, yielding a new point process, which is denoted by

$$\Phi_{\Gamma(r_{\min}, r_{\max})} = \Phi \cap \Gamma(r_{\min}, r_{\max}). \tag{2.6}$$

The interferers are restricted on $\Phi_{\Gamma(r_{\min}, r_{\max})}$ with guard-zone radius $r_{\min}$ and finite network radius $r_{\max}$. This annular model of device locations will be used in the remainder of the thesis.

2.6 Interferer access protocol

2.6.1 General model

Access policies in LPWAN systems are constrained by two key factors: First, due to the low cost and low power budget of the LPWAN, the devices can not employ complex control schemes or overloaded signaling overhead. Therefore, the grant-free access scheme is a feasible approach whereby users independently access channel resources without undergoing any scheduling. Associated to this access scheme is a parameter p, which stands for the simplest strategy that devices access the channel and transmit immediately when they need to: a device, when it needs to send data, transmits on any given resource block with probability p as will be explained below. Second, the access probability p can also be interpreted in terms of the service rate, i.e., the average quantity of data that each device is required to transmit. For instance, in a system based on OFDM, the value of

p is related to the amount of data to be transmitted and therefore the mean number of subbands occupied by a user.

Note that some other properties of the channel access can be taken into account by the spatial process modeling the position of interferers. For instance, CSMA leads to the repulsion property, which can be captured by Matérn hard-core process of type II described in Section 2.5.3.

Let us consider the time-frequency space $\mathcal{S}$ that the desired user can access, represented in Fig. 2.6. $\mathcal{S}$ is divided into segments, each called a time-frequency RB, and each RB is divided into elementary Resource Blocks (eRB) which are the smallest units that a device can access.
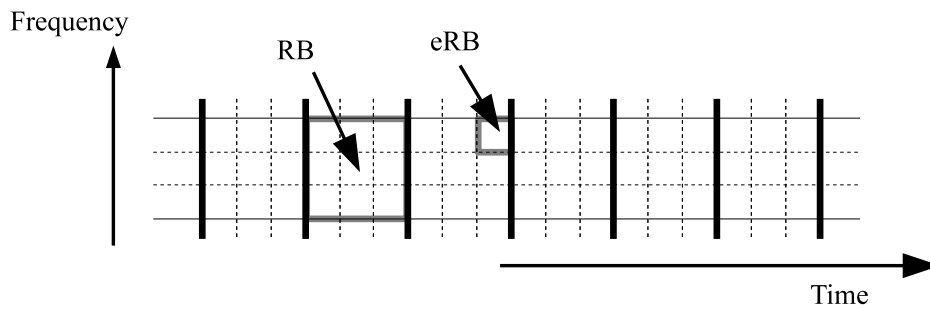
FIGURE 2.6: Illustration of the channel access with six consecutive RBs, each containing $N = 9$ eRBs.

We consider a constant number N of eRBs per RB. The channel access policy consists in attributing the required number of eRBs to each device so that they can transmit a sufficient amount of information. Our objective is to have a general formulation that can result in tractable interference models and can be applied to as many practical situations as possible. One important access policy that inspires our model is certainly SCMA.

To do so, we introduce the general process as follows:

- We consider a RB.

- We group N eRBs into a minimum size Block (msB) and force that a user uses all eRBs in the msB or none of them. We denote a msB by $B_u = \{b_{u,1}, \ldots, b_{u,N}\}$. Moreover, we assume that the eRBs in B_u are disjoint from the eRBs in any other msB $B_{u'}$ for $u' \neq u$. This step can be useful if some specific codes are used at the transmitter.

- The total RB is divided into K msBs, denoted by $\mathcal{B} = \{B_1, \ldots, B_K\}$, so that the total number of eRBs in a RB is NK.

- On a given RB, each interfering device transmits on a set of msBs in $\mathcal{B}$. The decision is distributed and made by the devices without any knowledge of other devices. To do so, the interfering device scans all

msBs in $\mathcal{B}$, selecting each msB B_u randomly and independently with probability p. As a consequence, the probability that a given device transmits on k msBs in $\mathcal{B}$ is given by $\binom{K}{k}p^k(1-p)^{K-k}$. In fact, p is related to the needs of the transmitting device: the higher required rate, the higher the value of p. The access probability p is decided by the devices or the IoT network according to the demands of data transmission. For the ease of analysis, we assume that p is the same for each device in this work. Based on the choices of p, we identify three scenarios in this section:

– Heavily loaded networks, corresponding to $p \approx 1$;

– Moderately loaded networks, corresponding to $0 < p < 1$;

– Lightly loaded networks, corresponding to $p \approx 0$.

• In IoT networks, devices are of various types and have different unpredictable traffic patterns. As such, the uncoordinated cooperation is preferred to simplify the hardware in order to reduce the cost and energy consumption and prolong the battery life. Therefore, we assume devices working uncoordinatedly. Specifically, we assume that each of the msBs selected by any device $k \in \Phi_{\Gamma(r_{\min},r_{\max})}$ is independent of the msBs selected by any other device k'. The set of devices transmitting on the msB B_u is denoted by Φ_{B_u}.

• Finally the interference on each eRB results from the contributions of all interfering devices that do transmit on this eRB (devices in Φ_{B_u}). The model is illustrated in Fig. 2.7 with $K = 5$ and $N = 2$.

2.6.2 Specific contexts

In the practical LPWAN protocols, the grouping of eRBs is not relevant yet. In that case, eRB and msB are the same, and $N = 1$. For Sigfox and LoRa, the RB could be a time frame that covers the whole packet duration and the band of the desired signal in the ISM 868 or 915 MHz bands. The eRB could cover the same frequency band but be reduced to the duration of the symbol. Our approach would fit this environment with special attention to the fact that some interferers can start or stop their transmission in the duration of the RB so that p could not be drawn independently from one eRB to another eRB. On the other hand, if the full packet length is considered for the eRB, the model could fit with a p value close to zero.

In the NB-IoT protocol for the uplink transmissions — i.e., the Narrowband Physical Uplink Shared Channel (NPUSCH) — each block can contain $N = 1, 3, 6, 12$ subbands with a 15 kHz spacing [Bey+17], which justifies the grouping. The RB would be a time slot and the eRBs be the subbands in this time slot.
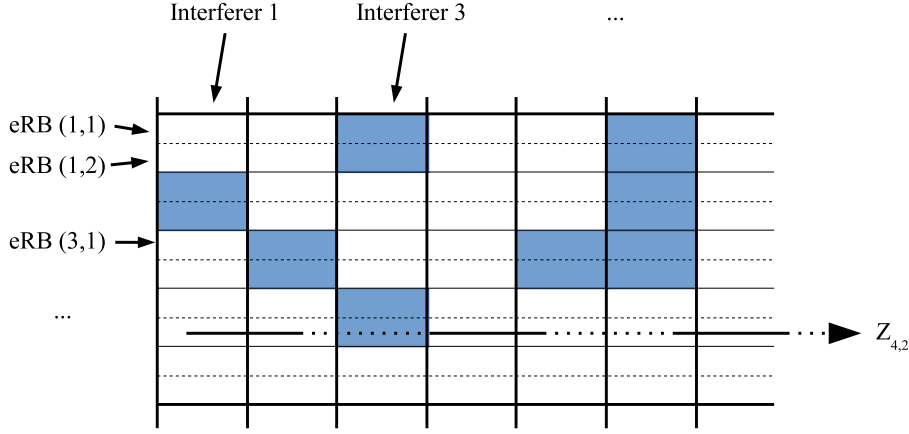
FIGURE 2.7: Illustration of the channel access; only one RB is considered, containing 10 eRBs grouped 5 by 2 ($K = 5$, $N = 2$). eRB (u, i) is the i-th eRB from the u-th msB. We represent the contribution of each interferer: blue indicates that the device is active. The resulting interference is a complex vector with NK elements. The element $Z_{u,i}$ corresponds to the sum of all contributions falling in the i-th eRB from the u-th msB.

In this thesis, we focus on the case of a single time slot and multiple subbands.

2.6.3   Complex baseband representation of the interference

Consider an eRB $b_{u,i}, i \in \{1, \ldots, N\}$ associated with the block B_u. If used by the desired user, the cumulative signal received is

$$Y(t) = h_0 r_0^{-\frac{\eta}{2}} \sqrt{\frac{2E_0}{T}} X(t) + Z(t) + N(t), \quad t \in [0, T], \tag{2.7}$$

where

- $h_0 = A_0 e^{j\phi_0}$ is the complex channel fading with amplitude A_0 and phase ϕ_0;

- r_0 is the link distance;

- η is the path-loss exponent;

- E_0 is the transmitted energy per symbol;

- T is the symbol duration;

- $X(t)$ is the baseband representation of the transmitted signal;

- $N(t)$ is the thermal noise;

- $Z(t)$ is the interference.

The interference term can be written as:

$$Z(t) = \sum_{j \in \Phi} h_j r_j^{-\frac{\eta}{2}} \sqrt{\frac{2E_j}{T_j}} X_j(t), \tag{2.8}$$

where

- Φ is the set of active interferers;

- $h_j = A_j e^{j\phi_j}$ is the complex channel fading with amplitude A_j and phase ϕ_j for device j;

- r_j is the distance between device j and the receiver;

- E_j is the transmitted energy per symbol;

- T_j is the user j symbol duration;

- $X_j(t)$ is the modulated transmitted signal.

Hence, the baseband representation of the interference is

$$Z = \sum_{j \in \Phi} h_j r_j^{-\frac{\eta}{2}} x_j, \tag{2.9}$$

where $x_j(t)$ is the counterpart of $\sqrt{\frac{2E_j}{T_j}} X_j(t)$ in (2.7) after demodulation. In a M-ary phase shift keying system modulation for instance, if $X_j(t) = cos(2\pi f_c t + \theta_j)$ where f_c is the carrier frequency, and θ_j is the phase of the transmitted signal of device j, then $x_j = \sqrt{\frac{2}{T}} \int_0^T X_j(t) \cos(2\pi f_c t) \mathrm{d}t$.

Considering the interference on multiple eRBs with the access scheme defined in Section 2.6, the interference on the i-th eRB in the msB B_u is given as

$$Z_{b_{u,i}} = \sum_{j \in \Phi_{b_{u,i}}} r_j^{-\frac{\eta}{2}} h_{j,b_{u,i}} x_{j,b_{u,i}}, \tag{2.10}$$

where $x_{j,b_{u,i}}$ is the transmitted baseband signal.

Remark 2.6.1. *For most of the results in this work, aside from weak technical conditions detailed in the sequel, very few restrictions are placed on the distributions of $h_{j,i}$ and $x_{j,i}$ with the exception that $h_{j,i}$ and $x_{j,i}$ are independent for all $j \in \Phi_{B_u}$ and $i \in \{1, \ldots, N\}$. Concretely, the conditions are often satisfied when $h_{j,b_{u,i}} \sim \mathcal{CN}(0, 1)$ (i.e., Rayleigh fading) and $x_{j,b_{u,i}} \sim \mathrm{Unif}(\{+1, -1\})$.*

Finally, we give a vector representation in $\mathbb{R}^{2NK}$ of the received interference consisting in stacking the interference on each eRB:

$$\mathbf{Z} = \left[\mathrm{Re}(Z_{b_{1,1}}), \mathrm{Im}(Z_{b_{1,1}}), \ldots, \mathrm{Re}(Z_{b_{K,N}}), \mathrm{Im}(Z_{b_{K,N}})\right]^T. \tag{2.11}$$

2.7   Maximum likelihood receiver

In the interference-limited regime, where we neglect the thermal noise, if the desired user is using K msBs, we have

$$\mathbf{Y} = \mathbf{g}\mathbf{X} + \mathbf{Z}, \tag{2.12}$$

where $\mathbf{X}$ is the transmitted vector in $\mathbb{R}^{2NK_0}$, $\mathbf{g} = [g_1, \cdots, g_{2NK_0}]$ is the channel of the desired user, and $\mathbf{z} = [z_1, \cdots, z_{2NK_0}]$ is the interference vector.

The distribution of channel coefficient g_i depends on the considered channel model (see Section 2.4, e.g. $r^{-\eta/2}$ and Rayleigh fading). We assume perfect Channel State Information (CSI) at the receiver.

Given the observation $\mathbf{Y}$ and equally likely sequences $\mathbf{X}$, the error probability is minimized through the maximization of the likelihood. That is

$$\max_{\mathbf{X}} f(\mathbf{Y}|\mathbf{X}, \mathbf{g}), \tag{2.13}$$

where $f(\cdot|\mathbf{X}, \mathbf{g})$ is the PDF of the received signal given that the symbol $\mathbf{X}$ is transmitted, and the channel coefficient is $\mathbf{g}$. From (2.12), we have

$$f(\mathbf{Y}|\mathbf{X}, \mathbf{g}) = f_{\mathbf{Z}}(\mathbf{Y} - \mathbf{g}\mathbf{X}). \tag{2.14}$$

As such, the statistics of the interference vector $\mathbf{Z}$ is essential to optimal decoding.

Chapter 3

Impulsive Interference in IoT Networks

A great amount of work has focused on modeling interference in IoT Networks. In different kinds of settings, it has been shown that non-Gaussian models naturally arises. Specifically, due to the large deployment of devices and fast varying active transmitter set, the interference exhibits impulsive behavior. A recent empirical study from Aalborg university suggests that the interference power is heavy-tailed [Lau+17b; Cla+20].

We are going to quickly survey this literature, giving significant results but not in an exhaustive manner. The main result we will be interested in is that the interference follows an α-stable distribution under the Poisson field network over the whole plane [Sou92; IH98; PW10a; Gul+10], under some specific assumptions (HPPP, infinite area, no guard zone with the channel gain going to infinity when transmission distance goes to 0). But in practical systems, they are not necessarily verified. The interferers are actually distributed over the finite area instead of the infinite plane. In [Sou92], considering the effect of guard zone, the author set a threshold on the amplitude path-loss function, i.e., $a(r) = \min\{s, r^{-\frac{\eta}{2}}\}$ and the analytical expression for the Characteristic Function (CF) was derived. Nonetheless, the effect of guard zone is not further studied. In [SZ08], the author studied the interference over finite area and gave the exact closed-form expressions for the moments. In [Gul+09; Gul+10], the author derived the closed-form approximation of the interference distribution from the field of Poisson and Poisson cluster distributed interferers. It shows that the interference can be modeled as Middleton Class A over the finite-area annular region. Nevertheless, the Middleton seems not the best option for modeling the interference due to that it is of complicated form and thus difficult to be used for analysis. Consequently, we resort to α-stable distribution of which the characterization is simpler and more tractable.

Despite it is necessarily an approximation of the interference distribution, we will use α-stable distributions to model interference on a subband. Indeed they are a powerful family of distribution, very well suited to model rare events, so impulsive interference in our case. They do exhibit a lot of properties that make them attractive, although their PDF is not known in

closed form. But before addressing the multivariate case, it is necessary to validate the accuracy of the α-stable model in more practical settings. As opposed to the HPPP over the infinite plane, the system model is revisited in two aspects: first, we restrict the distribution of the HPPP within an annular $\Gamma(r_{\min}, r_{\max})$ with the guard-zone radius $r_{\min}$ and the finite network radius $r_{\max}$; second, the HPPP is extended with more general point processes, i.e., Poisson cluster process for attraction and Matérn hard-core process of type II for repulsion. This is the contribution presented in this chapter.

To be self-contained, preliminaries on α-stable distribution is provided in Appendix B along with references for further details.

3.1 Interference modeling

In many previous papers, it has been shown that the interference term is not adequately modeled with a simple Gaussian distribution assumption. We present here some of the key results in this regard.

3.1.1 Middleton model and extensions

We can trace back some works on non-Gaussian noise to 1960 [FI60] and 1972 [GH72] about atmospheric noise. Assuming Poisson distributed sources, the CF of the impulsive noise can be obtained. Furthermore, appropriate assumptions on the transmission medium and source waveforms allow one to obtain the interference PDF. A similar approach based on the CF was used by Middleton [Mid77; Mid99], who obtained more general expressions based on series expansions. He classified interference in two main categories depending on whether the noise bandwidth is less than the useful signal (class A) or greater (class B). Class C is a sum of class A and B. Expressions of the distribution functions, involving infinite series, are obtained.

Middleton models have been widely used in different contexts (MIMO [Cho+09], OFDM [III07] or power line communications [AP10]). It is clear, however, that this popular model is challenging to work with since the PDF is a doubly-infinite sum. Consequently, several approximation models have been proposed. The main approach is to consider only the most significant terms. For instance, it is claimed in [Vas84] that, in many situations for the class A, two or three terms can be sufficient to obtain a good approximation leading to a Gaussian mixture [GDK06]. The two terms case is often denoted as the ϵ-contaminated noise, see [Pha+03; AB07; Alh+17]. In this case, the interference PDF is

$$\mathbb{P}(x) = (1-p)\mathcal{N}\left(0, \sigma^2\right) + p\mathcal{N}\left(0, \kappa\sigma^2\right), \tag{3.1}$$

where p denotes the probability to have an impulse, distributed from a Normal with variance $\kappa\sigma^2$, while $(1-p)$ gives the probability to only have the Gaussian noise with variance σ^2. Usually, p is small ($p = 0.01$) and κ large ($\kappa = 50, 100$).

In [AB07; Pha+03; SZ01], an ϵ-contaminated channel is used but with a different approach: pulses are generated in time according to a Poisson distribution, and the shape of the pulse can be chosen. Some performance metrics are studied showing, for instance, that an impulsive environment can offer more capacity than a Gaussian situation. The ϵ-contaminated model can also be expressed in the form of a Bernoulli-Gaussian noise [dc12; Vu+14]. Noise plus interference is expressed as $n + bi$, where n is the Gaussian noise, always present, and b is a Bernoulli random variable with parameter $p = \mathbb{P}(b = 1)$ representing the frequency of impulsive noise i occurrence. Usually, i is represented by a Gaussian random variable with a larger variance than n.

In [FC09; NAHV14; Axe+17], the class A model is represented by a Markov process: the noise distribution depends on the state of the process. It reduces to the ϵ-contaminated case when only two states are present but with an additional feature of time dependence structure, see [FC09].

The popular Class B model can be approximated by an α-stable distribution [Mid99].

3.1.2 Empirical approaches

If the Gaussian model is not appropriate, a solution is to make an empirical choice that allows analytical analysis of the receiver and can be justified by simulations, observations of the estimated PDF and/or gains in performance. The main solutions that have been proposed include Gaussian-Laplace mixture [BN10], generalized Gaussian [Fio06; BSF08; KKLMC09], Gaussian mixtures [HB08] or Cauchy-Gaussian mixture [Mei+17]. In this last paper [Mei+17], it is mentioned that the heavier tail of the Gaussian Mixture allows better performance than the Laplace approach. Some surveys can be found in [BY09; Sha12].

The class of models of direct relevance to interference modeling we are interested in this work is the α-stable and has often been used in the Ultra Wide Band (UWB) context [Pin+06; Win+06; Rab+07; NB08; BY09; Gha+10]. But contrary to the previously discussed approaches, it relies (when no power control is done) on a theoretical derivation (that can be related to a physical interpretation), closely linked to the Middleton's work and finding its foundation in stochastic geometry [WA12; BB10b; BB10a].

3.1.3 Stochastic geometry and α-stable model

Although the first papers were published in the 1990s [Sou92; TNS95; IH98], the analysis of networks has recently attracted a lot of works relying on stochastic geometry. As in Middleton's work, interferers are assumed spatially distributed according to a Poisson field. In this context, the distribution of interference is expressed as

$$Z = \sum_{i \in \Omega} a(r_i).Q_i, \tag{3.2}$$

where r_i is the distance between interferer i and the destination, and $a(d)$ is the attenuation as a function of the distance; a classical model is $a_{\eta,\epsilon}(d) = d^{-\frac{\eta}{2}} \mathbb{1}_{r \geq \epsilon}, r \in \mathbb{R}^+$, where η is the channel attenuation coefficient; ϵ accounts for a minimum distance between the receiver and the transmitter for physical reasons or due to some MAC layer protocol like carrier sensing; Q_i accommodates various propagation effects, such as multipath fading and shadowing as well as the physical layer of the transmitters and the receiver; and Ω is the set of interferers.

If applied in an *ad hoc* network, an unbounded received power assumption makes the interference fall in the attraction domain of a stable law. This unbounded assumption means taking the limit as $\epsilon \to 0$; in that case, the received power tends to infinity when d tends towards zero. The accuracy of the approximation has been questioned in [Ina+09; Car10], but working without the unbounded received power assumption does allow an analytical derivation of the CF [WA12; DRG14]. A truncated α-stable distribution is proposed in [Rab+11; Ega+17] to solve the infinite variance problem at the cost of reduced tractability.

This result can be seen as a consequence of the Generalized Central Limit Theorem (GCLT) [ST94; NS95]. The main advantage of the heavy-tailed stable distributions is their ability to represent rare events. In many communication situations, these events are in fact those that will limit the system performance. The traditional Gaussian distribution ignores them leading to poor results.

The proof of this result is generally done considering the log-CF of the total interference, see for instance [Sou92; WPS09; Gha+10], which can be written as:

$$\psi_{\mathbf{Z}}(\boldsymbol{\omega}) = \log\left(\mathbb{E}\left[e^{j\boldsymbol{\omega}^T \mathbf{Z}}\right]\right) = -\delta^\alpha |\boldsymbol{\omega}|^\alpha, \tag{3.3}$$

where $\mathbf{Z}$ is the total interference and T denotes the transpose. The right term is the log-CF of a sub-Gaussian α-stable vector, defined in Appendix B, where the marginals are symmetric α-stable (**SαS**) random variables with dispersion δ. Another solution for the proof, based on the LePage series, was proposed in [IH98]. This result will be further analyzed in the next section.

Stochastic geometry has explored more complex situations. For instance, problems concerning the non-homogeneous position of users are studied, for instance based on the cluster point process [Gul+10; GBA12] for general *ad hoc* networks or Poisson hole process for cognitive radio [LH12].

3.2 Isotropic complex α-stable model under HPPP

Consider a network of devices located according to a HPPP on the plane with density λ, denoted by Φ. As a first step, for the ease of derivation and analytical analysis, we relax the condition of finite network radius in Section 2.5.4. That is, we take $r_{\max}$ as infinite. What is more, we keep a minimum distance between the receiver and the closest interferer, $r_{\min}$.

The interference observed at the origin for a given time slot is given by

$$Z = \sum_{j \in \Phi} a(r_j) h_j x_j, \tag{3.4}$$

where r_j is the distance from device j to the origin, $h_j \sim \mathcal{CN}(0,1)$ is a Rayleigh fading coefficient, and x_j is the baseband emission.

Previous studies assume that Φ is over the whole plane as shown in Fig. 2.5a. Besides, the amplitude path-loss function is

$$a(r) = r^{-\frac{\eta}{2}}, \tag{3.5}$$

where η is the path-loss exponent.

However, (3.5) is an approximation only valid in the far field. It does not fit for small values of r. In fact, as $r \to 0$, due to (3.5), the power of the received signal tends to infinity. This obviously cannot happen. When a transmitter comes too close to the receiver, the model is no longer valid.

To solve this issue, a widely used solution, as in [Sou92], is to model the path loss as a truncated function:

$$a(r) = \min \left\{ r^{-\frac{\eta}{2}}, s \right\}. \tag{3.6}$$

Another frequent way to address this issue is to consider physical reasons. We will assume that two devices cannot be that close so that r cannot tend to zero. One way to explain such a situation is in the case of a CSMA based protocol. If a receiver is active, the protocol should avoid a transmitter to be active close to it. In both cases, introducing a guard zone, i.e., an area around the receiver where no active devices can be located, seems the right thing to do.

To capture the effect of guard zones, the signal attenuation is governed by

$$a(r) = \begin{cases} r^{-\frac{\eta}{2}}, & r \geq r_{\min} \\ 0, & r < r_{\min}. \end{cases} \tag{3.7}$$

That is, all interfering devices within $r_{\min}$ are inhibited as in [WA12; HA07; LVK10].

3.2.1 Infinite plane

Denote Z in (3.4) with

$$Z = Z_1 + iZ_2, \tag{3.8}$$

where $Z_1 = \mathrm{Re}(Z)$, and $Z_2 = \mathrm{Im}(Z)$.

For $r_{\min} = 0$, i.e., the interferers are distributed over the whole plane, we have the following theorem [Ega+17]:

Theorem 3.2.1. *Consider the interference Z in (3.4), and Φ is over the whole plane. Suppose that $h_j x_j$ in (3.4) is an isotropic complex random variable, and*

$$\mathbb{E}[|\mathrm{Re}(h_j x_j)|^{\frac{4}{\eta}}] < \infty \tag{3.9}$$

with $\eta > 2$, Then, Z in (3.4) converges almost surely to an isotropic $4/\eta$-stable random variable.

Moreover, if the fading coefficients h_j are i.i.d., and baseband emissions x_j are also i.i.d., then the scale parameters of real and imaginary components are equal, given by

$$\gamma = \left(\pi \lambda C_{\frac{4}{\eta}}^{-1} \mathbb{E}[|\mathrm{Re}(h_j x_j)|^{\frac{4}{\eta}}] \right)^{\frac{\eta}{4}}, \tag{3.10}$$

where

$$C_\alpha = \begin{cases} \frac{1-\alpha}{\Gamma(2-\alpha)\cos\left(\frac{\pi}{2}\alpha\right)}, & \text{if } \alpha \neq 1 \\ \frac{2}{\pi}, & \text{if } \alpha = 1. \end{cases} \tag{3.11}$$

Proof. We first prove that the marginal distribution follows the α-stable distribution first:

Let $X_j = h_j x_j$ in (3.4), and denote X_j as

$$X_j = X_{j,r} + iX_{j,i}, \tag{3.12}$$

Then, (3.4) is rephrased as

$$Z = \sum_{j \in \Phi} r_j^{-\frac{\eta}{2}} (X_{j,r} + iX_{j,i}). \tag{3.13}$$

And hence,

$$Z_1 = \sum_{j \in \Phi} r_j^{-\frac{\eta}{2}} X_{j,r},$$

$$Z_2 = \sum_{j \in \Phi} r_j^{-\frac{\eta}{2}} X_{j,i} \tag{3.14}$$

According to Proposition A.3.2, $\{r_j^2\}$ is the one-dimensional HPPP with intensity $\lambda\pi$. As such, according to Theorem B.2.14, Z_1 and Z_2 are α-stable distributed with $\alpha = \frac{4}{\eta}$ and scale parameter γ given in (3.10).

As $X_j = h_j x_j$ is isotropic, i.e.,

$$e^{j\phi} X_j \overset{d}{=} X_j, \qquad \forall \phi \in [0, 2\pi), \tag{3.15}$$

we have

$$e^{j\phi} Z \overset{d}{=} Z. \tag{3.16}$$

Therefore, Z is isotropic α-stable. $\qquad\square$

3.2.2 Guard zone

Although $Z = Z_1 + iZ_2$ is isotropic α-stable when $r_{\min} = 0$, the resulting models are not analytically tractable for $r_{\min} \neq 0$.

In [Sou92], the CF was derived with the truncated path-loss model of (3.6). Similarly, we have the following proposition which follows the same argument as in [Sou92].

Proposition 3.2.2. *Consider the interference $Z = Z_1 + iZ_2$ in (3.4) with the path-loss function given in (3.7). The CF of $\mathbf{Z} = (Z_1, Z_2)$ can be obtained as follows:*

$$\mathbb{E}[e^{i\boldsymbol{\theta} \cdot \mathbf{Z}}] = \exp\left\{ \lambda\pi|\boldsymbol{\theta}|^\alpha \int_0^{|\boldsymbol{\theta}| r_{\min}^{-\eta/2}} \frac{\Phi_0'(x)}{x^\alpha} \mathrm{d}x - \lambda\pi r_{\min}^2 \Phi_0\left(r_{\min}^{-\eta/2} |\boldsymbol{\theta}| \right) \right\}, \tag{3.17}$$

where $\alpha = 4/\eta$.

Proof. Recall that $Z = Z_1 + iZ_2 = \sum_{j \in \Phi} a(r_j) h_j x_j$.

Denote $X_j = X_{j,1} + iX_{j,2} = h_j x_j$, we have

$$\mathbf{Z} = \sum_{j \in \Phi} a(r_j) \mathbf{X}_j, \tag{3.18}$$

where $\mathbf{Z} = [Z_1, Z_2]$ and $\mathbf{X}_j = [X_{j,1}, X_{j,2}]$.

The CF of $\mathbf{Z}$ can be written as

$$
\begin{aligned}
\phi_{\mathbf{Z}}(\boldsymbol{\theta}) &= \mathbb{E}[\exp\{i\boldsymbol{\theta}\cdot\mathbf{Z}\}] \\
&= \mathbb{E}\left[\exp\left\{\sum_{j\in\Phi}ia(r_j)\boldsymbol{\theta}\cdot\mathbf{X}_j\right\}\right] \\
&= \mathbb{E}\left[\prod_{j\in\Phi}\exp\{ia(r_j)\boldsymbol{\theta}\cdot\mathbf{X}_j\}\right].
\end{aligned}
\tag{3.19}
$$

Since $h_j \sim \mathcal{CN}(0,1)$, h_j is isotropic, i.e.,

$$
e^{i\phi}h_j \overset{d}{=} h_j, \qquad \forall\phi\in(0,2\pi].
\tag{3.20}
$$

Hence, X_j and Z are also isotropic. And the vectors $\mathbf{Z}$ and $\mathbf{X}_j$ are spherically symmetric, i.e., its distribution only depends on $|\mathbf{X}_j|$. The CF is also spherically symmetric and can be written as $\Phi_{\mathbf{X}}(\boldsymbol{\theta}) = \Phi_0(|\boldsymbol{\theta}|)$.

To derive the CF, we first restrict all interferers within an annulus with radius from $r_{\min}$ to b, denoted as $D_{(r_{\min},b)}$. Then let $b\to\infty$,

$$
\begin{aligned}
&\phi_{\mathbf{Z}}(\boldsymbol{\theta}) \\
&\overset{(1)}{=} \lim_{b\to\infty}\sum_{k=0}^{\infty}\mathbb{P}[N_D=k]\cdot\mathbb{E}\left[\prod_{i=1}^{k}\exp\{ja(r_i)\boldsymbol{\theta}\cdot\mathbf{X}\}\right] \\
&\overset{(2)}{=} \lim_{b\to\infty}\sum_{k=0}^{\infty}\mathbb{P}[N_D=k]\cdot(\mathbb{E}[\exp\{ja(r)\boldsymbol{\theta}\cdot\mathbf{X}\}])^k \\
&\overset{(3)}{=} \lim_{b\to\infty}\sum_{k=0}^{\infty}\frac{(\lambda\pi(b^2-r_{\min}^2))^k}{k!}e^{-\lambda\pi(b^2-r_{\min}^2)}\cdot\left(\mathbb{E}[\exp\{jr^{-\frac{\eta}{2}}\boldsymbol{\theta}\cdot\mathbf{X}\}]\right)^k \\
&\overset{(4)}{=} \lim_{b\to\infty}e^{-\lambda\pi(b^2-r_{\min}^2)}\sum_{k=0}^{\infty}\frac{1}{k!}\left(\lambda\pi(b^2-r_{\min}^2)\mathbb{E}[\exp\{jr^{-\frac{\eta}{2}}\boldsymbol{\theta}\cdot\mathbf{X}\}]\right)^k \\
&\overset{(5)}{=} \lim_{b\to\infty}e^{-\lambda\pi(b^2-r_{\min}^2)(1-\mathbb{E}[\exp\{jr^{-\frac{\eta}{2}}\boldsymbol{\theta}\cdot\mathbf{X}\}])},
\end{aligned}
\tag{3.21}
$$

where

(1) N_D is the number of devices within the annulus $D_{(r_{\min},b)}$;

(2) According to Theorem A.2.2, each device is independent once N_D is fixed;

(3) N_D follows Poisson distribution;

(4) Rephrase (3), we have (4);

(5) According to

$$
\sum_{k=0}^{\infty}\frac{1}{k!}\left(\lambda\pi(b^2-r_{\min}^2)\mathbb{E}[\exp\{jr^{-\frac{\eta}{2}}\boldsymbol{\theta}\cdot\mathbf{X}\}]\right)^k\cdot e^{-\lambda\pi(b^2-r_{\min}^2)\mathbb{E}[\exp\{jr^{-\frac{\eta}{2}}\boldsymbol{\theta}\cdot\mathbf{X}\}]} = 1,
\tag{3.22}
$$

we get (5).

We take logarithm on both sides and have the log-CF, where we use the PDF of the distance between an interferer and the receiver $f_r(r) = \frac{2r}{b^2 - r_{\min}^2}$ if $r \in [r_{\min}, b]$, and $f_r(r) = 0$ if $r < r_{\min}$ and $r > b$.

$$
\begin{aligned}
&\psi_{\mathbf{Z}}(\boldsymbol{\theta}) \\
&= \log \Phi_{\mathbf{Z}}(\boldsymbol{\theta}) \\
&= \lim_{b \to \infty} \lambda \pi (b^2 - r_{\min}^2)[\mathbb{E}(\exp(jr^{-\frac{\eta}{2}}\boldsymbol{\theta} \cdot \mathbf{X})) - 1] \\
&= \lim_{b \to \infty} \lambda \pi (b^2 - r_{\min}^2)\left[\int_{r_{\min}}^{b} \exp(jr^{-\frac{\eta}{2}}\boldsymbol{\theta} \cdot \mathbf{X})\frac{2r}{b^2 - r_{\min}^2}\mathrm{d}r - 1\right] \\
&= \lim_{b \to \infty} \lambda \pi (b^2 - r_{\min}^2)\left[\int_{r_{\min}}^{b} \Phi_{\mathbf{X}}(r^{-\frac{\eta}{2}}\boldsymbol{\theta})\frac{2r}{b^2 - r_{\min}^2}\mathrm{d}r - 1\right] \\
&= \lim_{b \to \infty} \lambda \pi \left[\int_{r_{\min}}^{b} \Phi_{\mathbf{X}}(r^{-\frac{\eta}{2}}\boldsymbol{\theta})\mathrm{d}r^2 - (b^2 - r_{\min}^2)\right] \\
&= \lim_{b \to \infty} \lambda \pi \left[\int_{r_{\min}}^{b} \Phi_{\mathbf{X}}(r^{-\frac{\eta}{2}}\boldsymbol{\theta})\mathrm{d}r^2 - (b^2 - r_{\min}^2)\right] \\
&= \lim_{b \to \infty} \lambda \pi \left[\underbrace{r^2\Phi_{\mathbf{X}}(r^{-\frac{\eta}{2}}\boldsymbol{\theta})\big|_{r_{\min}}^{b} - (b^2 - r_{\min}^2)}_{T_1} - \underbrace{\int_{r_{\min}}^{b} r^2\mathrm{d}(\Phi_{\mathbf{X}}(r^{-\frac{\eta}{2}}\boldsymbol{\theta}))}_{T_2}\right]. \quad (3.23)
\end{aligned}
$$

And for T_1, we have

$$
\begin{aligned}
T_1 &= \lim_{b \to \infty} \lambda \pi \left[r^2\Phi_{\mathbf{X}}(r^{-\frac{\eta}{2}}\boldsymbol{\theta})\big|_{r_{\min}}^{b} - (b^2 - r_{\min}^2)\right] \\
&= \lim_{b \to \infty} \lambda \pi \left[b^2\Phi_{\mathbf{X}}(b^{-\frac{\eta}{2}}\boldsymbol{\theta}) - r_{\min}^2\Phi_{\mathbf{X}}(r_{\min}^{-\frac{\eta}{2}}\boldsymbol{\theta}) - (b^2 - r_{\min}^2)\right] \\
&\stackrel{(a)}{=} \lim_{b \to \infty} \lambda \pi b^2 \left[\Phi_{\mathbf{X}}(b^{-\frac{\eta}{2}}\boldsymbol{\theta}) - 1\right] - \lambda \pi r_{\min}^2 \left[\Phi_{\mathbf{X}}(r_{\min}^{-\frac{\eta}{2}}\boldsymbol{\theta}) - 1\right] \\
&= -\lambda \pi r_{\min}^2 \left[\Phi_{\mathbf{X}}(r_{\min}^{-\frac{\eta}{2}}\boldsymbol{\theta}) - 1\right] \\
&= -\lambda \pi r_{\min}^2 \left[\Phi_0(r_{\min}^{-\frac{\eta}{2}}|\boldsymbol{\theta}|) - 1\right], \quad (3.24)
\end{aligned}
$$

where step (a) is based on L'Hopital's rule and equivalent to

$$
\begin{aligned}
&\lim_{x \to 0} \frac{\Phi_0(x^{\frac{\gamma}{2}}|\boldsymbol{\theta}|) - 1}{x^2} \\
&= \lim_{x \to 0} \frac{\frac{\gamma}{2}x^{\frac{\gamma}{2}-1}\Phi_0'(x^{\frac{\gamma}{2}}|\boldsymbol{\theta}|)}{2x} \\
&= \lim_{x \to 0} \frac{\gamma \Phi_0'(x^{\frac{\gamma}{2}}|\boldsymbol{\theta}|)}{4x^{2-\frac{\gamma}{2}}} \\
&= \lim_{x \to 0} \frac{\frac{\gamma^2}{2}x^{\frac{\gamma}{2}-1}\Phi_0''(x^{\frac{\gamma}{2}}|\boldsymbol{\theta}|)}{4(2-\frac{\gamma}{2})x^{1-\frac{\gamma}{2}}} \\
&= \lim_{x \to 0} \frac{\gamma^2}{4(4-\gamma)}x^{\gamma-2}\Phi_0''(x^{\frac{\gamma}{2}}|\boldsymbol{\theta}|) \\
&= 0. \quad (3.25)
\end{aligned}
$$

For T_2, we have

$$
\begin{aligned}
T_2 &= -\lambda\pi\int_0^\infty r^2 \mathrm{d}(\Phi_{\mathbf{X}}(\mathrm{a}(\mathrm{r})\boldsymbol{\theta})) \\
&= -\lambda\pi\int_{r_{\min}}^\infty r^2 \mathrm{d}(\Phi_{\mathbf{X}}(\mathrm{r}^{-\frac{\eta}{2}}\boldsymbol{\theta})) \\
&\overset{(b)}{=} \lambda\pi\int_0^{r_{\min}^{-\frac{\eta}{2}}} t^{-\alpha}\mathrm{d}(\Phi_{\mathbf{X}}(\mathrm{t}\boldsymbol{\theta})) \\
&\overset{(c)}{=} \lambda\pi|\boldsymbol{\theta}|^\alpha\int_0^{|\boldsymbol{\theta}|r_{\min}^{-\frac{\eta}{2}}} x^{-\alpha}\mathrm{d}(\Phi_0(x)) \\
&= \lambda\pi|\boldsymbol{\theta}|^\alpha\int_0^{|\boldsymbol{\theta}|r_{\min}^{-\frac{\eta}{2}}} \frac{\Phi_0'(x)}{x^\alpha}\mathrm{d}x,
\end{aligned}
\tag{3.26}
$$

where step (b) takes $t = r^{-\frac{\eta}{2}}$, and step (c) takes $\Phi_{\mathbf{X}}(\boldsymbol{\theta}) = \Phi_0(|\boldsymbol{\theta}|)$ and $x = t|\boldsymbol{\theta}|$.

Hence, taking (3.24) and (3.26) into (3.23), we get

$$
\psi_{\mathbf{Z}}(\boldsymbol{\theta}) = \lambda\pi|\boldsymbol{\theta}|^\alpha\int_0^{|\boldsymbol{\theta}|r_{\min}^{-\frac{\eta}{2}}} \frac{\Phi_0'(x)}{x^\alpha}\mathrm{d}x - \lambda\pi r_{\min}^2\left[\Phi_0(r_{\min}^{-\frac{\eta}{2}}|\boldsymbol{\theta}|) - 1\right].
\tag{3.27}
$$

$\square$

We can easily check that when $r_{\min} \to 0$, the CF becomes:

$$
\mathbb{E}[e^{i\boldsymbol{\theta}\cdot\mathbf{Z}}] = \exp\left\{\lambda\pi\int_0^\infty \frac{\Phi_0'(x)}{x^\alpha}\mathrm{d}x|\boldsymbol{\theta}|^\alpha\right\}.
\tag{3.28}
$$

According to (B.41) in Proposition B.2.27, $\mathbf{Z}$ is sub-Gaussian α-stable with an underlying independent Gaussian vector. And the scale parameter is [IH98]:

$$
\gamma = \left(\lambda\pi\int_0^\infty \frac{\Phi_0'(x)}{x^\alpha}\mathrm{d}x\right)^{\frac{1}{\alpha}} = \left(\lambda\pi C_\alpha^{-1}\mathbb{E}[|\mathrm{Re}(h_jx_j)|^\alpha]\right)^{\frac{1}{\alpha}},
\tag{3.29}
$$

which is consistent with Theorem 3.2.1.

3.2.3 Validity of the α-stable model

Assuming that the location of users is modeled with a HPPP over the whole plane, the aggregated interference at the receiver follows an α-stable distribution, as shown in Theorem 3.2.1. However, very limited works study the impact of more realistic situations. Indeed, the infinite channel gain that arises when the transmitter - receiver distance r tends to 0 with a path loss proportional to $r^{-\frac{\eta}{2}}$ is unrealistic, and we have seen in Proposition 3.2.2 that the α-stable model is no longer valid. The key question that we address in

this section is under which conditions (the value of $r_{\min}$) is the isotropic α-stable model a good approximation of the interference arising in the system model detailed in Section 3.2.

To do so, we will compare the α-stable model with interference simulated in a network of finite radius and with the presence of a guard-zone around the receiver. Our comparison will be based on two features of the interference models:

- *the marginal distributions*: to study them we will consider two steps. First, we will estimate the characteristic exponent $\hat{\alpha}$ [Sta]; theoretical analysis gives a value of α, which only depends on the channel attenuation coefficient. We evaluate if this parameter is modified or not by more realistic assumptions without compromising the accuracy of the α-stable model; Secondly, we will study the Cumulative Distribution Function (CDF) and quantiles of the marginals, i.e., Probability-Probability plot (P-P plot) and Quantile-Quantile plot (Q-Q plot). P-P plot is better for the central values of the distribution, while Q-Q plot focuses more on the tails. They allow assessing the goodness-of-fit of the model for the marginals as in previous works [Zhe+19b; Gul+10; MC20; Cla+20];

- *the dependence structure*: between the real and imaginary part of the received signal. Note that unlike isotropic Gaussian distribution, the isotropic α-stable model exhibits dependence between its real and imaginary components. As such, we will study this dependence structure via copula.

In our tests, we simulate the data based on the system model in Section 3.2 (simulated data set) and compare it with the data generated from the theoretical isotropic α-stable model ($\alpha = \frac{4}{\eta}$) (theoretical data set), the fitted α-stable model ($\hat{\alpha}$) (fitted model data set) and the Gaussian model with $\alpha = 2$ (Gaussian data set).

The density is set as $\lambda = 0.001 \, \text{devices/m}^2$, and the path-loss exponent is $\eta = 5$, which corresponds to an average of one device in a disc of the radius of approximately $18 \, \text{m}$ and a non-line of sight path-loss environment (e.g., indoor or urban).

Let $Z(r_{\min})$ denote the interference with a guard-zone radius $r_{\min}$. Then the void probability can be treated as a measure of how close $Z(r_{\min})$ is to $Z(0)$. That is

$$
\begin{aligned}
P_{Void} &= \mathbb{P}[\text{No interfers within } r_{\min}] \\
&= \mathbb{P}[Z(r_{\min}) - Z(0) = 0] \\
&= e^{-\lambda \pi r_{\min}^2}.
\end{aligned}
\tag{3.30}
$$

We will show, for realistic device densities, that when the guard-zone radii do not exceed 5 meters, the α-stable model with theoretical characteristic exponent $\alpha = \frac{4}{\eta}$ is a good approximation. The estimated stable model with $\hat{\alpha}$ keeps as a good approximation for different choices of guard-zone radii, tending to the Gaussian case ($\alpha = 2$) when the guard-zone radii become very large.

Marginal distributions

We first examine the distributions of real and imaginary parts of the interference. In the isotropic α-stable model, the real and imaginary parts are **SαS** random variables.
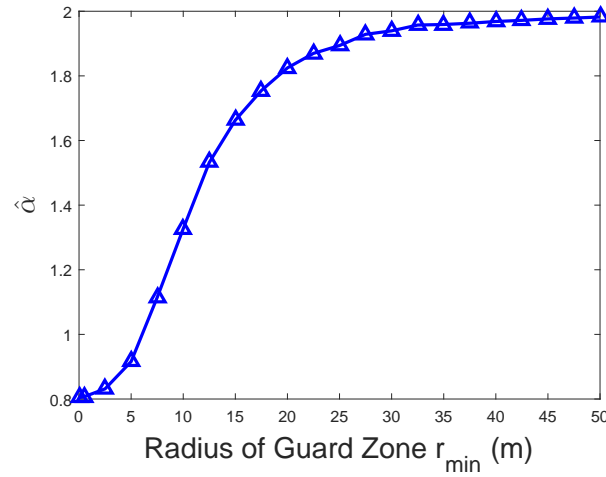
FIGURE 3.1: Estimated $\hat{\alpha}$ under different guard-zone radii $r_{\min}$.
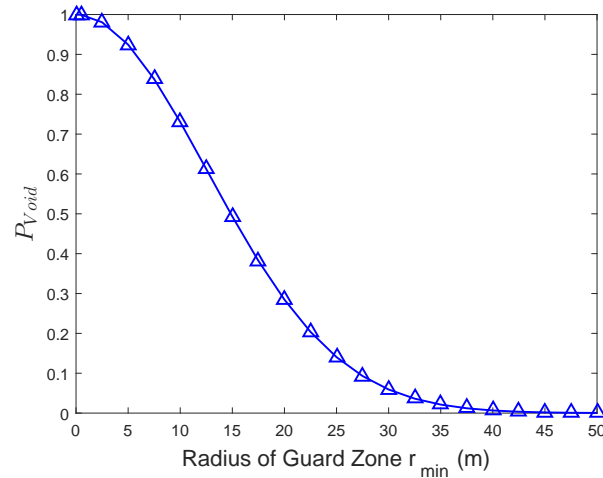
FIGURE 3.2: Void probability under different guard-zone radii $r_{\min}$.

Fig. 3.1 and Fig. 3.2 show the effect of increasing the guard-zone radius $r_{\min}$. We vary $r_{\min}$ between 0 and 50 m. From the simulated dataset, we estimate the parameter $\hat{\alpha}$ of the marginals. It is to be mentioned that both marginals (real and imaginary parts) give the same result, and we will only present the results from one of them.

Observe that for small guard-zone radii, the estimated parameter $\hat{\alpha}$ is approximately 0.8. This is expected from the theoretical model, which gives $\alpha = \frac{4}{\eta} = 0.8$.

On the other hand, as $r_{\min}$ goes beyond 5 m, $\hat{\alpha}$ increases rapidly and gets larger than 0.9 up to 2 when $r_{\min}$ reaches 30 m. This can be related to the void probability which decreases in this region, from $P_{Void} = 0.92$ for $r_{\min} = 5$. The increase in $\hat{\alpha}$ indicates that the interference becomes less impulsive.

For $r_{\min} > 30$ m, $\hat{\alpha}$ reaches approximately 2. This implies that for very large values of $r_{\min}$, a Gaussian model is the best fit, which is consistent with the Gaussian assumption of interference in previous literature [GC05].

Nevertheless, for a guard zone such that 5 m $< r_{\min} < 30$ m, neither the theoretical α-stable model nor the Gaussian model is a good choice. Hence, it requires a new model. An intuitive approach is to keep the stable model but replacing $\alpha = \frac{4}{\eta}$ with the fitted $\hat{\alpha}$.

To obtain further insights into the behavior of the distributions of the real or imaginary parts of the interference Z, we study P-P plot and Q-Q plot. They are two graphical tools for comparing two probability distributions, defined as follows:

Definition 3.2.3. *A P-P plot plots two CDFs against each other: given two probability distributions, with CDFs F and G, it plots $(F(z), G(z))$.*

Definition 3.2.4. *A Q-Q plot plots the quantiles of two distributions against each other.*

Remark 3.2.5. *According to [GK90], the P-P plot is good for the light-tailed and moderate-tailed distributions, whereas the Q-Q plot is more powerful to the heavy-tailed distributions.*

We first compare the simulated data set to the theoretical one. We transform the data set into the domain $[0,1] \times [0,1]$ via the CDF. In P-P plot, if the two distributions being compared are similar, the points will approximately lie on the line $y = x$.

Fig. 3.3 shows the P-P plots between the CDFs from the simulated data set with $r_{\min} = 5$, 10 and 30 m, denoted by P_I, against the CDF from the theoretical data set with $r_{\min} = 0$, denoted by P_0. As expected from Fig. 3.1, when $r_{\min} \leq 5$ m, the theoretical model is in good agreement with the simulated data. In particular, the curve exhibit straight lines. For $r_{\min} > 5$

m, the CDFs begin to significantly differ, suggesting that the theoretical model is no longer suitable. Indeed, as $r_{\min}$ increases, the curves become steeper, implying that the theoretical data set, giving P_0, is more dispersed than the simulated one giving P_I. The "S" shaped curve indicates that the P_0 is more skewed and thus has heavier tails than P_I.
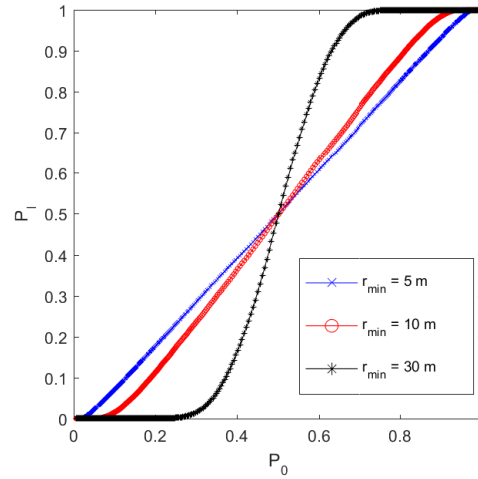
FIGURE 3.3: P-P plots, the system model ($r_{\min} > 0$) against the theoretical model ($r_{\min} = 0$).

To confirm the tendency, Fig. 3.4 shows the Q-Q plots. The quantiles estimated from the simulated data set with $r_{\min} > 0$ are denoted by X_I, and the ones estimated from the theoretical data set with $r_{\min} = 0$ are denoted by X_0.
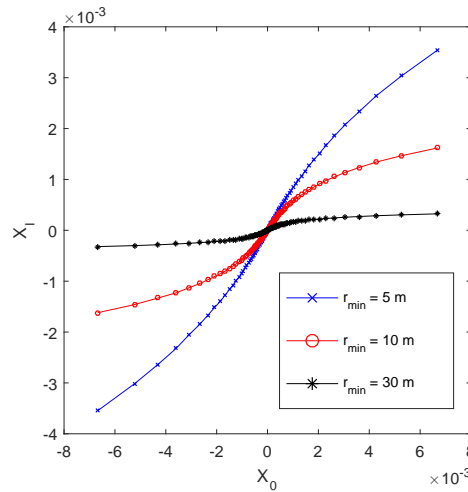
FIGURE 3.4: Q-Q plots, the system model ($r_{\min} > 0$) against the theoretical model ($r_{\min} = 0$).

The curve for $r_{\min} = 5$ m is slightly 'S' shaped. The Q-Q plot has a very better resolution in the tails than the P-P plot; thus, the slight deviation due to the limitation of the very strong impulses can be observed. This further implies that even for small values of $r_{\min}$, the theoretical data set (giving X_0) is more "impulsive" than the simulated one (giving X_I). Indeed, X_I is

(A) $r_{\min} = 2.5m$, $\hat{\alpha} = 0.83$

(B) $r_{\min} = 5m$, $\hat{\alpha} = 0.93$

(C) $r_{\min} = 10m$, $\hat{\alpha} = 1.33$

(D) $r_{\min} = 30m$, $\hat{\alpha} = 1.93$
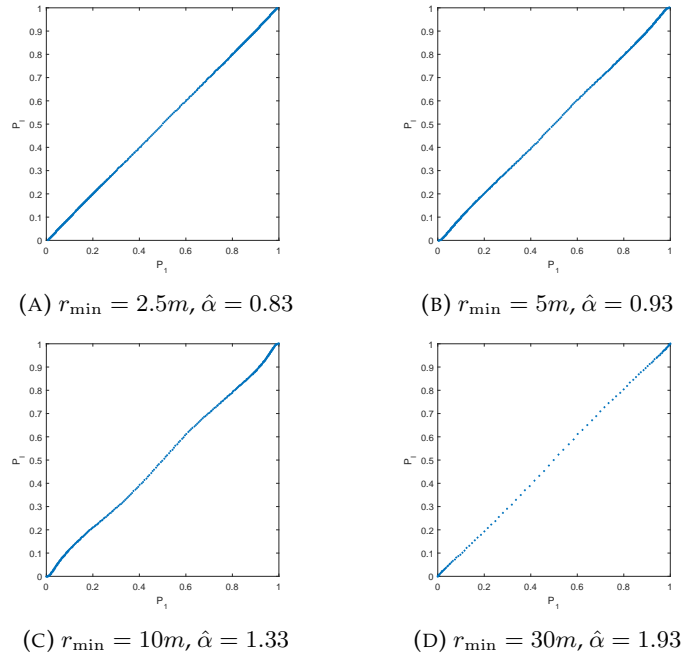
FIGURE 3.5: P-P plots, the system model ($r_{\min} > 0$) against the fitted model ($\hat{\alpha}$).

a bit less "impulsive" compared with X_0. This is consistent with $\hat{\alpha} = 0.9$ observed in Fig. 3.1. Nevertheless, we can expect that the α-stable model can still be a good approximation for $r_{\min} \leq 5$ m.

As with the P-P plots, we see a larger distortion for $r_{\min} > 5$ m. This confirms that the theoretical data set does not represent the simulated data set for larger $r_{\min}$.

In a second step, we are going to compare the simulated data set with the fitted model data set. We keep P_I and replace P_0 with the CDFs obtained from the fitted model data set, using $\hat{\alpha}$, denoted as P_1. We represent the P-P plots in Fig. 3.5. We also keep the quantiles X_I from the simulated data set and plot them against the quantiles from the fitted model data set X_1 to make the Q-Q plots in Fig. 3.6.

In both Fig. 3.5 and Fig. 3.6, for the different values of $r_{\min}$, the fitted model data set is in good agreement with the simulated data set. For values of $r_{\min} \leq 5$ m, those results are consistent with Fig. 3.4, and $\hat{\alpha}$ is close to 0.8 as shown in Fig. 3.1.

For $r_{\min} > 5$ m, the P-P plots and Q-Q plots are still very close to the line $y = x$, even if they start to slightly differ. In that case, the α-stable marginal distribution still seems to be a good approximation, but the theoretical result without guard zone can no longer be used directly, and the parameters $\hat{\alpha}$ have to be modified.

When $r_{\min} > 30$ m, the fit becomes even better than when 5 m $< r_{\min} <$ 30 m. In that case, as observed in Fig. 3.1, $\hat{\alpha}$ is very close to 2. In fact, interference in such cases exhibits a Gaussian behavior.

(A) $r_{\min} = 2.5m$, $\hat{\alpha} = 0.83$ (B) $r_{\min} = 5m$, $\hat{\alpha} = 0.93$

(C) $r_{\min} = 10m$, $\hat{\alpha} = 1.33$ (D) $r_{\min} = 30m$, $\hat{\alpha} = 1.93$
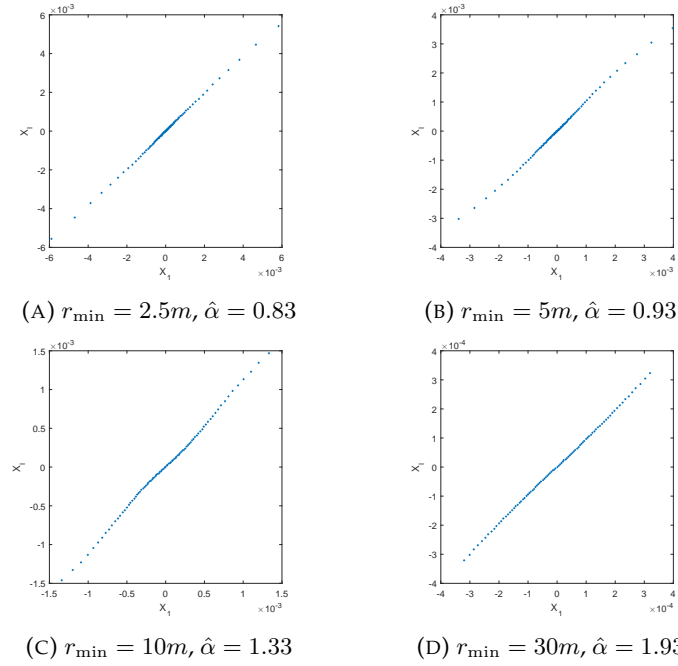
FIGURE 3.6: Q-Q plots, the system model ($r_{\min} > 0$) against the fitted model ($\hat{\alpha}$).

In conclusion, α-stable models are a good approximation for different $r_{\min}$. Even if the theoretical values of the parameters cannot be used in all cases, generalizing the Gaussian models to the family of stable distributions (which includes the Gaussian one) is a good option for an accurate interference model.

Dependence structure

While the real and imaginary parts of isotropic Gaussian random variable are independent, the isotropic α-stable random vector contains some dependency according to Remark B.2.28. The correlation function is traditionally used to study dependence but it is not an option when working with stable distributions. Indeed, covariances are infinite and the Pearson correlation coefficient does not exist for α-stable random variables [Nel99; ST94]. A large number of tools have been developed to replace the correlation such as the covariation [GK09].

A more popular method for studying such a dependence structure is based on copulas. The definition of copula is given in Appendix C. In copula theory, the dependence structure is investigated by transforming a random vector $\mathbf{X}$ in $\mathbb{R}^n$ to the *copula space* via the transformation $(x_1, \ldots, x_n) \mapsto (F_1(x_1), \ldots, F_n(x_n))$ where F_i, $i = 1, \ldots, n$ are the marginal distribution functions. It is well known that the marginal distribution of the transformed vector follows a uniform distribution on $[0, 1]$. For independent x_i and x_j, the joint vector $(F_i(x_i), F_j(x_j))$ is uniformly distributed on $[0, 1] \times [0, 1]$.

The perspective of studying the dependence in copula space is attractive as it reveals the full dependence structure, and especially the non-linear dependencies in data, often more important than linear dependencies in heavy-tailed data (e.g., in α-stable models ($\alpha < 2$)).

Fig. 3.7a and Fig. 3.7b are histograms of the simulated data set—from the theoretical α-stable model with $\alpha = 0.8$ and $\alpha = 1.99$, respectively—in the copula space corresponding to the pair of real and imaginary components for the interference. By Theorem 3.2.1, the pair is sub-Gaussian

(A) $\alpha = 0.8$ (B) $\alpha = 1.99$
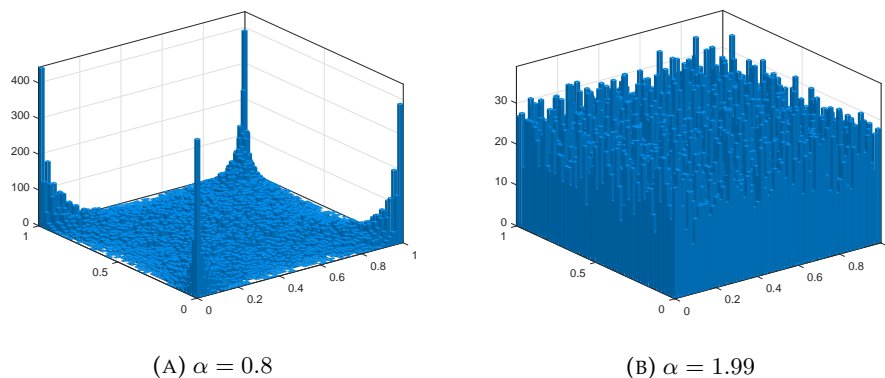
FIGURE 3.7: Histogram for the samples of the real and imaginary components of interference.

α-stable. In Fig. 3.7a, the key feature is the peaks present in the corners, corresponding to large amplitude interference on both the real and imaginary components. This means that even if the probability to have a large sample is rare, the probability to have one large sample on one dimension, conditioned on the fact that a large sample is present on the other dimension, gets higher. This can be understood because when a transmitter, close to the receiver, strongly contributes to the interference, it is likely it does it on both the real and the imaginary parts. This demonstrates a strong dependence in the tails of the distribution for each component. However, in Fig. 3.7b, the feature is less obvious as the distribution becomes more Gaussian.

Figure. 3.8 shows the scatter plots for the data set simulated from the system model corresponding to different $r_{\min}$ in the copula space.

First, in Fig. 3.8a, the scatter points concentrate in the diagonals as well as in the four corners. It clearly shows the strong dependence arising in the interference vector (despite the isotropic distribution).

When $r_{\min} < 5$ m, the same behavior is observed. In this regime, we have already seen that the distributions for the real and imaginary parts of the interference are approximately **SαS**. For $\alpha < 2$, isotropic complex α-stable random variables do not have independent real and imaginary parts and this is particularly evident by the concentration of points in the corners of the scatter plot, i.e., strong tail dependence. What is more, the central part

(A) $r_{\min} = 0$

(B) $r_{\min} = 2.5m$

(C) $r_{\min} = 5m$

(D) $r_{\min} = 7.5m$

(E) $r_{\min} = 10m$

(F) $r_{\min} = 30m$
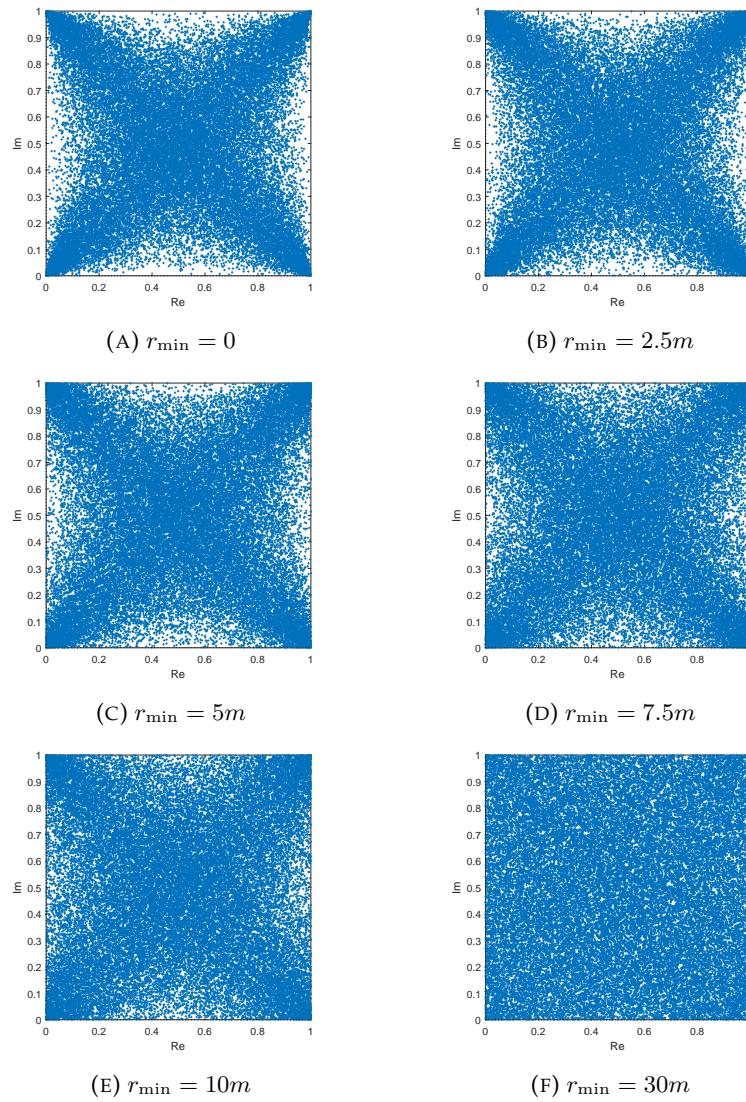
FIGURE 3.8: Samples in copula space under different guard-zone radii $r_{\min}$.

of each figure remains approximately uniform. An implicit explanation is that for $r_{\min}$, the distribution of $(\text{Re}(Z), \text{Im}(Z))$ follows a sub-Gaussian α-stable distribution where $(\text{Re}(Z), \text{Im}(Z)) = \sqrt{A}(G_1, G_2)$, A is skewed stable, and G_1 and G_2 are independent Gaussian. When the absolute values of $\text{Re}(Z)$ and $\text{Im}(Z)$ are small, the vector (G_1, G_2) takes dominance and results in the more uniform behavior that can be observed in the central part.

Those plots confirm that the simulated interference behaves like an α-stable random vector.

Fig. 3.8c, Fig. 3.8d and Fig. 3.8e show the impact of further increasing $r_{\min}$. In these cases, the scatter plot is again non-uniform but points are less concentrated, which means that the Gaussian model is not an appropriate choice. Nonetheless, tail dependence is necessary to include in the model and the stable approach is a good way to do it.

Finally, observe in Fig. 3.8f that the scatter plot becomes approximately uniform. It implies that the real and imaginary parts of the interference are independent. This is expected because the interference Z is isotropic and when $r_{\min}$ gets large, it becomes approximately Gaussian. Then, for a complex Gaussian random variable, isotropic means that its real and imaginary parts are independent.

In conclusion, the dependence structure arising in our simulated data set is well aligned with the α-stable and sub-Gaussian α-stable models. Again, the increase in the guard-zone radius will make the model go from the theoretical stable one with $\alpha = 4/\eta$ to the Gaussian model. But it seems relevant to remain in the stable family, adapting the value of α.

3.3 α-stable Interference under general point processes

Although the HPPP model enables analytical expression and tractable analysis of the interference, it also imposes strong constraints over the universal settings. The locations of devices are perfectly modeled with HPPP when the network is of complete randomness. However, devices are not independent and may interact with each other due to a list of reasons, e.g, access schemes or human activity. Therefore, the homogeneous assumption is often not realistic, and there exists attraction or repulsion between devices, which requires more general point processes. Toward this end, two general point processes — the doubly Poisson cluster process and Matérn hardcore process of type II— are considered, along with HPPP which captures full randomness. The general family of doubly Poisson cluster processes is able to account for clustering or attraction due to human activity in certain regions, such as smart home devices or e-health devices in hospitals. On

the other hand, devices exploiting Carrier-sense Multiple Access with Collision Avoidance (CSMA/CD) induces repulsion of device locations, which is better modeled by Matérn hard-core processes [BBM06]. In addition, we further limit the interferers within an annular region as the assumption of infinite plane in Section 3.2.3 is unrealistic.

We validate the α-stable approximation by first observing that each of the more general families of point processes induce interference that converges in distribution to interference induced by a HPPP. We then verify via simulation that the Kullback-Leibler divergence (KL divergence) between the α-stable interference model and the interference arising from the general point process models is indeed small for practical parameter choices, e.g., the guard-zone radius.

3.3.1 System model

Consider a network of devices located according to a general point process, denoted by Φ. We consider the three point processes defined in Section 2.5:

(i) *Homogeneous Poisson point process* with intensity λ devices/m^2;

(ii) *Doubly Poisson cluster process*: the parent point process is a HPPP with intensity λ_p devices/m^2, and each daughter process, centered on its parent's position is also a HPPP with intensity λ_d devices/m^2 restricted to a disc of radius r_c. Points from the parent HPPP are included. Hence, the average number of points in each cluster is $c = \lambda_d \pi r_c^2 + 1$ devices;

(iii) *Matérn hard-core process of type II*: the underlying HPPP is with intensity λ_p devices/m^2, and the hard-core distance is r_h.

In each case, the intensity — e.g., λ in the case of the HPPP — corresponds to the intensity of active devices with data to transmit. In 5G, a common target is one device per square meter; however, the density of active devices with a given protocol, in a given time-frame and spectrum band, may be significantly lower. We will often set $\lambda \in [0.001, 0.01]$ devices/m^2.

We still keep the guard-zone radii as we did in Section 3.2.3. What is more, we consider the network radius $r_{\max}$ as finite. That is we consider the model $\Phi_{\Gamma(r_{\min}, r_{\max})}$ defined in (2.6) in Section 2.5.4.

The interference in (3.4) is rewritten as

$$Z = \sum_{j \in \Phi_{\Gamma(r_{\min}, r_{\max})}} r_j^{-\frac{\eta}{2}} h_j x_j. \tag{3.31}$$

3.3.2 Approximations of the interference distribution induced by general point processes

As defined in Section 2.5, a key feature of doubly Poisson cluster process and Matérn hard-core process of type II is that they are constructed from HPPP. The limiting case where cluster radius $\lambda_d \to 0$ for doubly Poisson cluster processes or hard-core radius $r_h \to 0$ for Matérn hard-core process of type II is a HPPP. As such, it may be expected that for certain choices of parameters, the process is well approximated by a HPPP.

Moreover, the resulting distribution of the interference may be well approximated by the distribution of the interference arising from the HPPP. We can then expect that the interference statistics arising from the HPPP forms a unifying approximation for more general families of point processes.

In Theorem 3.3.1, we make these assertions precise. We establish that under a range of fading models, the interference induced by $\Phi_{\Gamma(r_{\min},r_{\max})}$ for the point processes in Section 3.2 converges in distribution to the interference induced by a HPPP restricted to the annulus $\Gamma(r_{\min},r_{\max})$. This is achieved by introducing a sequence of point processes parameterized by a sequence of parameters $(\kappa_n)_{n=1}^{\infty}$, which converges to a parameter κ_0 corresponding to a HPPP.

To present our approximation result, let $\Phi_{\Gamma(r_{\min},r_{\max})}^{\kappa_n}$ be a doubly Poisson cluster process or a Matérn hard-core process of type II with intensity λ and parameter κ_n. In the case of the doubly Poisson cluster process, κ_n corresponds to the intensity λ_d of the daughter process, and $\kappa_0 = 0$. On the other hand, for the Matérn hard-core process of type II, κ_n corresponds to the hard-core distance r_h, and $\kappa_0 = 0$. We denote the interference induced by $\Phi_{\Gamma(r_{\min},r_{\max})}^{\kappa_n}$ by $\mathbf{Z}_n$, where $\mathbf{Z}_n$ corresponds to the interference random vector in (2.11).

Theorem 3.3.1. *Let $\Phi_{\Gamma(r_{\min},r_{\max})}^{\kappa_n}$ be a doubly Poisson cluster process or a Matérn hard-core process of type II with intensity λ and parameter κ_n such that $\kappa_0 = \lim_{n\to\infty}\kappa_n$. Suppose that $\Phi_{\Gamma(0,\infty)}^{\kappa_0}$ is a homogeneous Poisson point process with intensity λ and $\mathrm{supp}(h_{j,i}x_{j,i})$ in (3.31) is compact for all $i = 1,\ldots,N$, $j \in \Phi_{\Gamma(r_{\min},r_{\max})}^{\kappa_n}$ and $n \in \mathbb{N}$. Then, $\mathbf{Z}_n \overset{d}{\to} \mathbf{Z}_0$ as $n \to \infty$.*

Proof. Let $N_1, N_2, \ldots$ be point processes on $\mathbb{R}^2$.

Then, the sequence $(N_n)_{n=1}^{\infty}$ converges in distribution to a point process N on $\mathbb{R}^2$; i.e., $N_n \overset{d}{\to} N$ if and only if $\mathbb{E}[h(N_n)] \to \mathbb{E}[h(N)]$ for every bounded continuous function h on the space $\mathcal{N}$ of all counting measures on $\mathbb{R}^2$.

Let $\mathcal{B}_N = \{B \in \mathcal{B} : N(\partial B) = 0 \ a.s.\}$ and $\mathcal{C}_c^+$ be the set of all continuous functions $f : \mathbb{R}^2 \to \mathbb{R}_+$ with compact support. Convergence in distribution

is characterized in the following theorem, which will provide the link between convergence in distribution of a point process and the convergence of the interference distribution it induces.

Theorem 3.3.2 (Theorem 6.1, [Ser90])**.** *The following statements are equivalent:*

(i) $N_n \overset{d}{\to} N$;

(ii) $\int_{\mathbb{R}^2} f(x) N_n(dx) \overset{d}{\to} \int_{\mathbb{R}^2} f(x) N(dx)$ *for all* $f \in \mathcal{C}_c^+$.

In particular, consider the interference random vector in (2.11). The real or imaginary component of the interference on a single subband can be written in the form

$$Z^{\kappa_n} = \sum_{j \in \Phi^{\kappa_n}_{\Gamma(r_{\min}, r_{\max})}} w_j \|\mathbf{x}_j\|^{-\eta/2}, \tag{3.32}$$

where $\Phi^{\kappa_n}_{\Gamma(r_{\min}, r_{\max})}$ is the point process inducing the interference, and w_j represents the real or imaginary part of a term $h_{j,i} x_{j,i}$ in (2.10). Under the hypotheses of Theorem 3.3.1, each w_j has compact support.

Let $f(\mathbf{x}, w) = w\|\mathbf{x}\|^{-\eta/2}$ which is bounded and continuous since $\Phi^{\kappa_n}_{\Gamma(r_{\min}, r_{\max})}$ and each w_j lie in compact sets. As such, we immediately obtain convergence of distribution for $\mathbf{Z}^{\kappa_n}$ as $n \to \infty$ if (i) in Theorem 3.3.2 holds.

To establish that (i) in Theorem 3.3.2 holds, we require the following result.

Theorem 3.3.3 (Theorem 6.2, [Ser90])**.** *Suppose N is simple and*

$$\lim_{m \to \infty} \limsup_{n \to \infty} P(N_n(B) > m) = 0, \ B \in \mathcal{B}. \tag{3.33}$$

Then, $N_n \overset{d}{\to} N$ *if and only if*

$$\lim_{n \to \infty} P(N_n(B) = 0) = P(N(B) = 0), \ B \in \mathcal{B}_N. \tag{3.34}$$

A sufficient condition for (3.34) *to hold is given by*

$$\limsup_{n \to \infty} \mathbb{E}[N_n(I)] \le \mathbb{E}[N(I)] < \infty, \ I \in \mathcal{I}_N, \tag{3.35}$$

where $\mathcal{I}_N$ *is the set of all intervals in* $\mathcal{B}_N$.

To apply Theorem 3.3.3, we note that the point process inducing the interference in (2.11) can be viewed as an independently marked point process with points in $\mathbb{R}^2$ and marks in $\mathbb{C}^{KN}$, where KN is the total number of subbands. As $\Phi^{\kappa_n}_{\Gamma(r_{\min}, r_{\max})}$ is simple, the resulting marked process is simple as well.

We now establish that (3.35) holds for the point processes identified in Theorem 3.3.1. For the doubly Poisson cluster process, we have for all $I \in \mathcal{B}_{\Phi^{\kappa_n}_{\Gamma(r_{\min}, r_{\max})}}$ that

$$\mathbb{E}\left[\Phi^{\kappa_n}_{\Gamma(r_{\min}, r_{\max})}(I)\right] = \mathbb{E}\left[\Phi^{\kappa_0}_{\Gamma(r_{\min}, r_{\max})}(I)\right] + \mathbb{E}\left[\sum_{j \in \Phi^{\kappa_0}_{\Gamma(r_{\min}, r_{\max})}} \Phi^{\kappa_n}_{d,j}(I)\right],$$
(3.36)

where $\Phi^{\kappa_n}_{d,j}$ is the daughter point process corresponding to the jth point in $\Phi^{\kappa_0}_{\Gamma(r_{\min}, r_{\max})}$. Therefore by (3.35), we only need to show that

$$\limsup_{n \to \infty} \mathbb{E}\left[\sum_{j \in \Phi^{\kappa_0}_{\Gamma(r_{\min}, r_{\max})}} \Phi^{\kappa_n}_{d,j}(I)\right] = 0.$$
(3.37)

Since each $\Phi^{\kappa_n}_{d,j}$ is a HPPP restricted to a particular region, it follows that the number of points in each I does not exceed that of the unrestricted HPPP. Since the expected number of points for a HPPP tends to zero as the intensity tends to zero, it follows that (3.37) holds. For the Matérn hard-core process of type II, (3.35) holds immediately since $\Phi^{\kappa_n}_{\Gamma(r_{\min}, r_{\max})}$ is a thinned version of $\Phi^{\kappa_0}_{\Gamma(r_{\min}, r_{\max})}$. $\square$

Theorem 3.3.1 provides a justification for approximating the interference statistics induced by a doubly Poisson cluster process or a Matérn hard-core process of type II by the interference from HPPP. As such, we verify via a simulation study that for practical choices of parameters, the HPPP approximation is in fact valid.

3.3.3 Model verification

Theorem 3.2.1 and Theorem 3.3.1 suggest that the α-stable distribution is a good approximation for interference induced by homogeneous Poisson point processes, doubly Poisson cluster processes and Matérn hard-core process of type II restricted to a finite annulus. In the sequel, we validate this approximation in terms of KL divergence through simulations.

Definition 3.3.4 (Kullback-Leibler divergence)**.** *For distributions P and Q of a continuous random variable, the KL divergence is defined to be the integral:*

$$D_{KL}(P||Q) = \int_{-\infty}^{\infty} p(x) \log\left(\frac{p(x)}{q(x)}\right) x.$$
(3.38)

Remark 3.3.5. *The KL divergence is a measure of how close one distribution is to another. The value of D_{KL} is always greater than 0. The smaller of D_{KL}, the closer $p(x)$ is to $q(x)$. And $D_{KL} = 0$ if and only if p and q are the same distribution, i.e., $p(x) = q(x)$.*

Homogeneous Poisson point process

We consider a set of interferers governed by the point process $\Phi_{\Gamma(r_{\min},500)}$ with path-loss exponent $\eta = 5$, where Φ is a HPPP with intensity $\lambda = 0.001$ devices/m^2. Fig. 3.9a plots the impact of varying $r_{\min}$ on the KL divergence between the simulated interference over the annulus $\Gamma(r_{\min}, r_{\max})$ and three different models:

   (i) the α-stable model that assumes Φ over the whole plane (theoretical stable);

  (ii) an α-stable model with parameters estimated from a set of simulated data;

 (iii) a fitted Gaussian model.

Fig. 3.9b shows the estimated $\hat{\alpha}$ of the fitted stable model for different guard-zone radii.
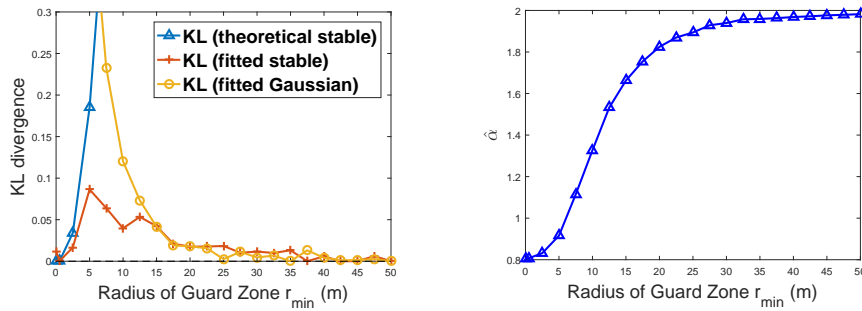
(A) KL divergence between the simulated data set and three statistical models: the theoretical stable model ($\alpha = \frac{4}{\eta}$); the fitted stable model ($\hat{\alpha}$); and the fitted Gaussian model.

(B) Fitted stable parameter — $\hat{\alpha}$ under different $r_{\min}$.

FIGURE 3.9: Homogeneous Poisson point process under different guard-zone radii $r_{\min}$.

We can observe that for a very small guard-zone radius $r_{\min} < 5$ m, the theoretical model ($\alpha = \frac{4}{\eta}$) exhibits a good fit as interference follows a stable distribution with $\alpha = \frac{4}{\eta}$ when $r_{\min} \to 0$. We also verify that the estimated $\hat{\alpha}$ in Fig. 3.9b is approximately $\hat{\alpha} \approx \frac{4}{\eta} = 0.8$, which further validates the theoretical model.

For a large guard zone ($r_{\min} > 15$ m in our set-up), the Gaussian model becomes a good fit. Although the existence of interferers in proximity to the receiver is rare, it has a large contribution in $\mathbf{Z}^{\kappa_n}$. The absence of them reduce the impulsive behavior of the interference and explains the good fit of the Gaussian model.

In the medium-range area (5 m $< r_{\min} <$ 15 m in our set-up), neither the theoretical α-stable approach nor the Gaussian one fits. However, when
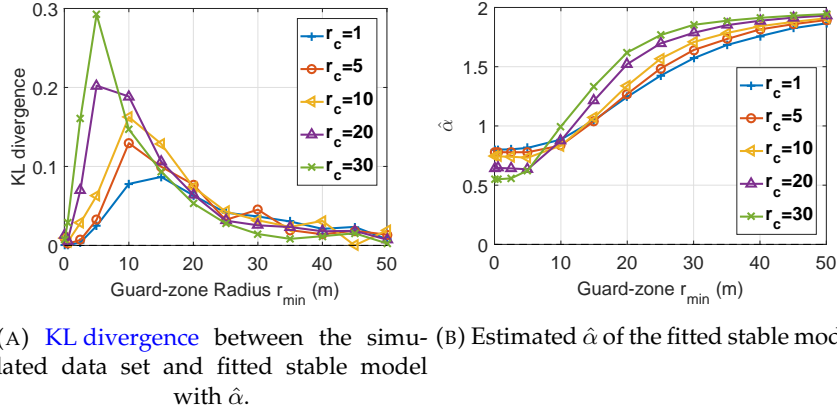
(A) KL divergence between the simu-
lated data set and fitted stable model
with $\hat{\alpha}$.

(B) Estimated $\hat{\alpha}$ of the fitted stable model.

FIGURE 3.10: Doubly Poisson cluster process under differ-
ent guard-zone radii $r_{\min}$.

estimating the value of α, using the estimated $\hat{\alpha}$, the fitted stable model
yields a low KL divergence.

The values of the fitted parameter $\hat{\alpha}$ as a function of $r_{\min}$ ranging from
0.5 m to 50 m are shown in Fig. 3.9b. This value increases from approxi-
mately 0.8 (expected from the α-stable theoretical model since $\frac{4}{\eta} = 0.8$) to
nearly 2.

The low KL divergence when using $\hat{\alpha}$ shows that the $\hat{\alpha}$-stable models
are robust to changes in $r_{\min}$—implying that the techniques in this paper
hold rather generally, but the best choice of α may be larger than $\frac{4}{\eta}$ as pre-
dicted by Theorem 3.2.1.

Doubly Poisson cluster process

We now consider that the point process $\Phi_{\Gamma(r_{\min},500)}$ governing the set of in-
terferers is a doubly Poisson cluster process with the following parameters:

- density of parent process $\lambda_p = 2 \times 10^{-4} \text{ /m}^2$;

- average number of devices for each cluster $c = \lambda_d \pi r_c^2 + 1 = 11$ devices,
  thus the density of the process is $\lambda_d = \frac{1}{\pi r_c^2}(c-1)$;

- path-loss exponent $\eta = 3$.

Fig. 3.10 and Fig. 3.11 plot the impact of varying the guard-zone radius $r_{\min}$
and the cluster radius r_c. Since the doubly Poisson cluster process con-

verges to the HPPP, the interference with small r_c is very similar to that
illustrated in Fig. 3.9. However, with an increase of the cluster radius r_c,
the KL divergence between the data from simulation and the $\hat{\alpha}$-stable inter-
ference model approximation increases for $r_{\min} \leq 20$. Values remain low
but the accuracy of the model has to be questioned, implying that neither
the fitted α stable nor the Gaussian is a good model. Nevertheless, as ex-
pected from Theorem 3.3.1, the α-stable model remains valid. Indeed, for
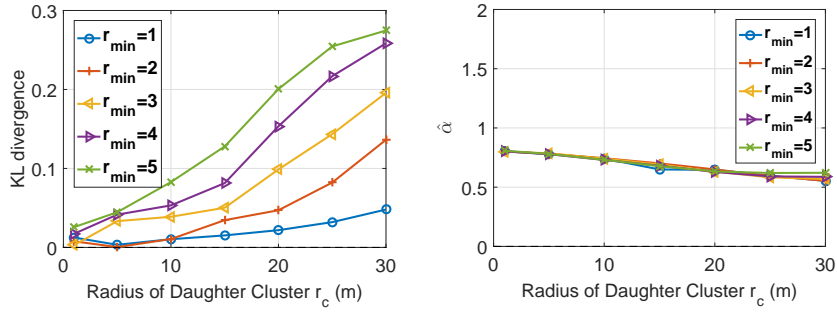
(A) KL divergence between the simulated data set and fitted stable model with $\hat{\alpha}$

(B) Estimated $\hat{\alpha}$ of the fitted stable model

FIGURE 3.11: Doubly Poisson cluster process under different cluster radii $r_{\min}$.
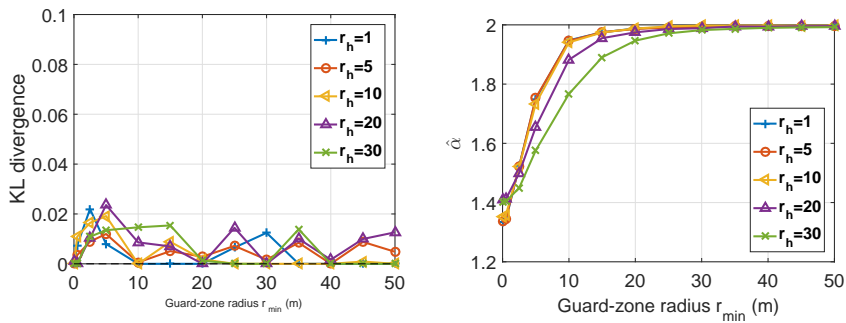
(A) KL divergence between the simulated data set and fitted stable model with $\hat{\alpha}$

(B) Estimated $\hat{\alpha}$ of the fitted stable model

FIGURE 3.12: Matérn hard-core process of type II under different guard-zone radii $r_{\min}$.

a cluster radius $r_c = 1$ m, the KL divergence keeps small for all values of $r_{\min}$. Fig. 3.11 also verifies that the $\hat{\alpha}$-stable model is valid for a large set of cluster radius when the guard-zone radius is small enough (less than 5 m in our setup), consistent with Theorem 3.3.1.

Matérn hard-core process of type II

We finally consider that the point process $\Phi_{\Gamma(r_{\min},500)}$ governing the set of interferers is Matérn hard-core process of type II with the following parameters:

- $\lambda_p = 0.002$ devices/m^2;

- $\eta = 3$.

Fig. 3.12 shows the impact of varying $r_{\min}$ under different hard-core radius r_h. We observe that unlike the doubly Poisson cluster process, the fitted α-stable model is robust to changes in $r_{\min}$. Similar to HPPP, the estimated $\hat{\alpha}$ increases from a certain value — still be approximately $\frac{4}{\eta}$ for $r_h < 10$ but not for large values of r_h — to nearly 2 as the guard-zone radius

(A) KL divergence between the simulated data set and fitted stable model with $\hat{\alpha}$

(B) Estimated $\hat{\alpha}$ of the fitted stable model
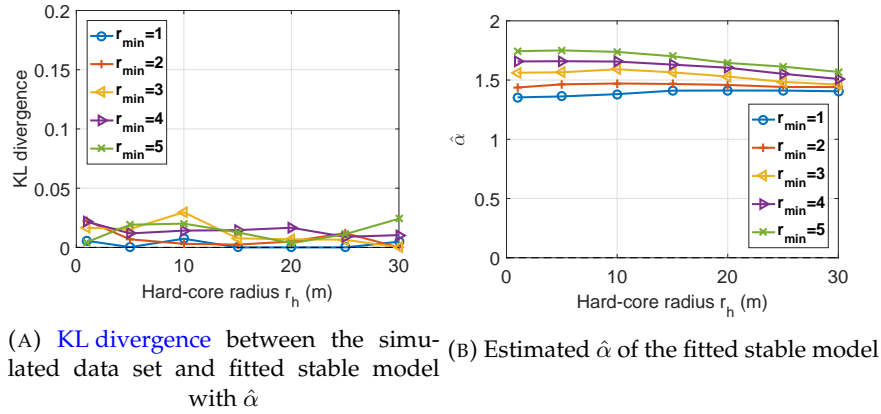
FIGURE 3.13: Matérn hard-core process of type II under different hard-core radii r_h.

increases. This is because the Matérn hard-core process of type II can be well approximated by the HPPP. The accuracy of such an approximation is proved in [Hae11; CKJ13]. Fig. 3.13 illustrates the impact of r_h under different guard-zone radii $r_{\min}$. Again, we observe that for a wide range of r_h, the KL divergence remains uniformly small, implying the HPPP a good approximation for Matérn hard-core process of type II once more in Fig. 3.13a. In Fig. 3.13b, the estimated $\hat{\alpha}$ decreases with the increase of r_h, this can be explained this way: The density of Matérn hard-core process of type II is a decreasing function of r_h as given in (2.4). As HPPP is a good approximation of Matérn hard-core process of type II, the void probability, given in (3.30), becomes smaller with the larger value of r_h, which therefore increases the impulsiveness.

3.4 Chapter conclusion

It is challenging to model interference in IoT networks due to its impulsiveness and non-Gaussian behavior. Although many distributions have been studied, for instance Middleton class A and B, α-stable distribution proved to be a promising model. Indeed they are a broad family of distribution, including the Gaussian one, which allows modeling rare but large events that will be critical in a communication. They have a large set of significant properties that have been well studied and can be used to characterize the behavior of interference.

While there were several works investigating the validity of α-stable model for interference, the impact of the guard-zone radius is generally neglected. In this chapter, this is the first aspect we consider, under the HPPP. Although the theoretical stable model (with $\alpha = \frac{4}{\eta}$) has degraded performance as the guard-zone radius increases, the fitted stable model (with $\hat{\alpha}$) is a good approximation for the interference. By checking the estimated $\hat{\alpha}$, P-P plot, Q-Q plot and copula space, we validate our conclusion.

We then further extend this work to more general point processes, i.e., the doubly Poisson cluster process for attraction and the Matérn hard-core process of type II for repulsion. They generally allow a better model for the spatial location of interferers. First, we proved that the interference induced these two aforementioned point processes converges in distribution to the interference induced by HPPP. This provides the intuition that α-stable model could be a good approximation for the general point processes in theory. Then we verify it via KL divergence with practical parameters.

The α-stable distribution is obtained for interference making three main assumptions: no guard zone and an infinite plane, HPPP and a path loss $r^{-\frac{\eta}{2}}$ that tends to infinity when r tends to zero. We have shown in this chapter that these assumptions can be relaxed and the α-stable family provides a good fit for interference models in a wide variety of contexts.

Chapter 4

Dependent Interference in IoT Networks

In the IoT networks, devices transmit over non-orthogonal channel resources to improve the spectral efficiency and support the demand of a large number of transmissions over limited channel resources. In the NB-IoT standard with multi-tone mode or the SCMA where devices get access to the channels based on their own codebooks, devices operate on multiple overlapping resource blocks. As a consequence, a statistical dependence between interference on each subband arises. In the case of impulsive interference, this dependence structure is tricky to characterize.

Although it has been shown that the marginal interference can be well approximated as α-stable in Chapter 3, the joint distribution of the interference vector still remains unknown. We can expect however that the gap between the joint distribution and the marginals — i.e., the dependence structure of the interference vector — has a significant impact on the design of the receivers.

The dependence of interference exists in many different settings and in different dimensions: space, time and frequency. In a multiple receiving antenna system, two or more antennas may receive strong interference at the same time if there is a strong interferer in the vicinity of the receiver. What is more, devices are usually active and transmitting signals for some time, and thus, the assumption of independent interference in time is not valid. In addition to the spatial and temporal dependence, the interference exhibits dependence in frequency as devices transmit over multiple bands. Empirical evidence is also shown in [Pet+14].

Although it is an important feature for the network analysis, the dependence of interference has often been neglected in previous studies, essentially because it is difficult to handle. Nevertheless, it is attracting many works [GES12; Yan+15; MC17; Sor+17; Zhe+20]. Mahmood *et al.* studied the dependence structure at the baseband between two α-stable interference samples [MCA12b; MCA12a] and showed that with proper sampling they could be made independent. In [YP03], the author studied the temporal dependence structure of interference. By assuming the holding time of

interferers is a random variable under an infinite Poisson field, the CF and joint CF are obtained. It showed that the interference vector is not necessarily α-stable even if the marginals are α-stable. [GES12] further extends the work of [YP03] with a bounded path loss and shows that the joint interference follows a multivariate Gaussian mixture distribution. Recently, some works are focusing on modeling the dependence structure separately from modeling the marginals of the interference using copula functions[Yan+15; Sor+17; Zhe+19a].

The *Copula* function is a powerful mathematical tool for modeling dependence. It recently found a few applications in communication contexts. In Multiple-Input and Multiple-Output (MIMO) system, the channel estimation requires the density of the received signal composed of several components, i.e., different signals from channels and the noise. These components are dependent, and copulas are applied to model such dependence. In [GAR13], a signal-dependent noise (SDN) channel is considered, in which the noise characteristics depend highly on the transmitted signal. Under the assumption of dependence between faded signal and noise, it estimates the parameters of the Nakagami-m fading channels by determining the analytical PDF of the received signal using Gaussian copula and Clayton copula. Similarly, a 2×2 MIMO system with correlated Nakagami channels is studied with Gaussian, t and Clayton copulas in [GAR15]. In terms of information theory, it has been proved that the mutual information is actually the copula entropy [MS11]. Hence, copula can be used for the estimation of mutual information [ZD11]. In signal processing, the copula was used for Blind source separation (BSS). In [MS07; KM09], a copula-based BSS method named Copula Component Analysis (CCA) is suggested as an alternative as opposed to the popular Independent Component Analysis (ICA) method. In [SJ15; SJL16], the concept of cumulative capacity was brought in, and bounds on the CDF of the cumulative capacity are derived based on the copula theory. In [Lin+17; Lin+19], copulas are used to characterize the channel orders for the capacity regions.

In this thesis, the copula will be mainly applied to modeling the dependence structure of the interference. It will allow studying the impact of dependence on the receiver performance, which is a continuation to previous works in [Yan+15; Sor+17].

In this chapter, we characterize the multivariate statistics of the interference in IoT networks. Based on the model introduced in Chapter 2, we derive the joint distribution of the interference vector for certain limiting cases ($p \to 0$ and $p \to 1$). The general case ($0 < p < 1$) is not analytically tractable or would require to use a multivariate stable vector which is nontrivial. As a consequence, we develop a new model based on t-copula. A low-complexity estimation algorithm tailored to our interference model is

proposed based on an approximation of the tail dependence and Kendall's τ. The proposed model is validated using the KL divergence.

4.1 System model

We keep the model introduced in Chapter 2. That is, we consider a receiver at the origin and the interferers' locations following one of the three point processes over the annular $\Phi_{\Gamma(r_{\min}, r_{\max})}$. Moreover, we keep the access protocol with service rate p over a RB consisting of K msB $\mathcal{B} = \{B_1, \cdots, B_K\}$. Each msB contains N eRB $B_u = \{b_{u,1}, \ldots, b_{u,N}\}$. As such, the different eRBs see sets of interferers that partially overlap [EP18].

Consider an eRB $i \in \{1, \ldots, N\}$ associated with the msB B_u, denoted as $b_{u,i}$. The interference observed by the receiver at the origin on this eRB is given by

$$Z_{b_{u,i}} = \sum_{j \in \Phi_{b_{u,i}}} r_j^{-\frac{\eta}{2}} h_{j,b_{u,i}} x_{j,b_{u,i}}, \tag{4.1}$$

where r_j is the distance from device j to the origin, $\eta > 2$ is the path-loss exponent, $h_{j,b_{u,i}}$ is the fading coefficient for device j on the eRB $b_{u,i}$, and $x_{j,b_{u,i}}$ is the baseband emission.

After stacking the interference on each eRB for each msB, the resulting interference random vector is given by

$$\mathbf{Z} = \left[\text{Re}(Z_{b_{1,1}}), \text{Im}(Z_{b_{1,1}}), \ldots, \text{Re}(Z_{b_{K,N}}), \text{Im}(Z_{b_{K,N}})\right]^T. \tag{4.2}$$

The distribution of each pair $\left[\text{Re}(Z_{b_{u,i}}), \text{Im}(Z_{b_{u,i}})\right]$ has been analyzed and proved to be sub-Gaussian α-stable in Chapter 3. However, this representation is not amenable to the study of the interference vector $\mathbf{Z}$ in (4.2) since $Z_{b_{u,i}}$ and $Z_{b_{u',i'}}$ are not independent. As such, we investigate the joint distribution of the $\mathbf{Z}$ in the following section.

4.2 Interference random vector characterization

It is difficult to derive or characterize the joint distribution of $\mathbf{Z}$ directly as the dependence structure between msBs and that within msBs are different, which need to be treated separately. Therefore, we first study the interference vector for a single msB.

4.2.1 Interference over a minimum size block

In this section, we study the interference statistics on a msB, $B_u \in \mathcal{B}$ consisting of N eRBs. Recall that if a device transmits on an eRB within a msB

B_u, then it transmits on all eRBs in B_u so that the set of interferers remains unchanged on all eRBs: $\Phi_{b_{u,i}} = \Phi_{B_u}$ for all eRBs in B_u.

For a given msB B_u, let $\mathbf{Z}_{B_u}$ denote the interference on all eRBs within B_u; that is,

$$
\begin{aligned}
\mathbf{Z}_{B_u} &= [z_{b_{u,1},1}, z_{b_{u,1},2}, \cdots, z_{b_{u,N},1}, z_{b_{u,N},2}]^T \\
&= [\mathrm{Re}(Z_{b_{u,1}}), \mathrm{Im}(Z_{b_{u,1}}), \ldots, \mathrm{Re}(Z_{b_{u,N}}), \mathrm{Im}(Z_{b_{u,N}})]^T.
\end{aligned}
\tag{4.3}
$$

In this special case, the interference random vector in (4.3) can be characterized exactly as shown in the following theorem.

Theorem 4.2.1. *Let $j \in \Phi_{B_u}$ denote an active interferer in the msB B_u. Suppose that $h_{j,b_{u,i}} \sim \mathcal{CN}(0,1)$(Rayleigh fading), $\mathrm{Re}(x_{j,b_{u,i}}) \sim \mathrm{Unif}(\{+1,-1\})$, $\mathrm{Im}(x_{j,b_{u,i}}) \sim \mathrm{Unif}(\{+1,-1\})$, and that the conditions in Theorem 3.2.1 hold. Then, the interference random vector $\mathbf{Z}_{B_u}$ follows the sub-Gaussian α-stable distribution with an underlying Gaussian vector having i.i.d. $\mathcal{N}(0, \sigma^2_{\mathbf{Z}_{B_u}})$ components, $\alpha = \frac{4}{\eta}$ and scale parameter*

$$
\gamma_{\mathbf{Z}_{B_u}} = \left(\pi \lambda p C_{\frac{4}{\eta}}^{-1} \mathbb{E}[|\mathrm{Re}(h_{j,b_{u,1}} x_{j,b_{u,1}})|^{\frac{4}{\eta}}] \right)^{\frac{\eta}{4}},
\tag{4.4}
$$

where $C_{\frac{4}{\eta}}$ is given in (B.22), and $\gamma_{\mathbf{Z}_{B_u}} = \frac{1}{\sqrt{2}} \sigma_{\mathbf{Z}_{B_u}}$.

Proof. We fist rephrase the interference in (4.1) as

$$
Z_{b_{u,i}} = \sum_{j \in \Phi_{B_u}} Z_{b_{u,i}}^j,
\tag{4.5}
$$

where $Z_{b_{u,i}}^j = r_j^{-\frac{\eta}{2}} h_{j,b_{u,i}} x_{j,b_{u,i}}$ corresponds to the contribution of device $j \in \Phi_{B_u}$ on the eRB $b_{u,i}$.

The vector $\mathbf{Z}_{B_u}$ in (4.3) is rewritten as

$$
\mathbf{Z}_{B_u} = \sum_{j \in \Phi_{B_u}} \mathbf{Z}_{B_u}^j,
\tag{4.6}
$$

where

$$
\begin{aligned}
\mathbf{Z}_{B_u}^j &= [z_{b_{u,1},1}^j, z_{b_{u,1},2}^j, \cdots, z_{b_{u,N},1}^j, z_{b_{u,N},2}^j]^T \\
&= [\mathrm{Re}(Z_{b_{u,1}}^j), \mathrm{Im}(Z_{b_{u,1}}^j), \cdots, \mathrm{Re}(Z_{b_{u,N}}^j), \mathrm{Im}(Z_{b_{u,N}}^j)]^T.
\end{aligned}
\tag{4.7}
$$

By Theorem 3.2.1, the elements of $\mathbf{Z}_{B_u}$ are $\frac{4}{\eta}$-stable random variables with parameter $\gamma_{\mathbf{Z}_{B_u}}$. Consider the first and second components of $\mathbf{Z}_{B_u}$, corresponding to the real and imaginary parts of the interference on the

first subcarrier associated to msB B_u. These elements can be written as

$$z_{b_u,1,1} = \sum_{j \in \Phi_b} r_j^{-\frac{\eta}{2}} \left[\text{Re}(h_{j,b_u,1})\text{Re}(x_{j,b_u,1}) - \text{Im}(h_{j,b_u,1})\text{Im}(x_{j,b_u,1}) \right],$$

$$z_{b_u,1,2} = \sum_{j \in \Phi_b} r_j^{-\frac{\eta}{2}} \left[\text{Re}(h_{j,b_u,1})\text{Im}(x_{j,b_u,1}) + \text{Im}(h_{j,b_u,1})\text{Re}(x_{j,b_u,1}) \right]. \qquad (4.8)$$

Assume that $h_{j,b_u,1} \sim \mathcal{CN}(0,1)$, $\text{Re}(x_{j,b_u,1}) \sim \text{Unif}(\{+1,-1\})$, and $\text{Im}(x_{j,b_u,1}) \sim \text{Unif}(\{+1,-1\})$. Consider the random vector $\mathbf{Z}_{B_u}^j$, corresponding to the contribution of device $j \in \Phi_{B_u}$ on each eRB associated to the msB B_u. This can be written as

$$\mathbf{Z}_{B_u}^j = r_j^{-\eta/2} \left(\mathbf{f} \odot \text{Re}(\mathbf{x}_{j,B_u}) + \mathbf{g} \odot \text{Im}(\mathbf{x}_{j,B_u}) \right), \qquad (4.9)$$

where

$$\mathbf{f} = [\text{Re}(h_{j,b_u,1}), \text{Im}(h_{j,b_u,1}), \cdots, \text{Re}(h_{j,b_u,N}), \text{Im}(h_{j,b_u,N})]^T,$$
$$\mathbf{g} = [-\text{Im}(h_{j,b_u,1}), \text{Re}(h_{j,b_u,1}), \cdots, -\text{Im}(h_{j,b_u,N}), \text{Re}(h_{j,b_u,N})]^T,$$
$$\mathbf{x}_{j,B_u} = [x_{j,b_u,1}, x_{j,b_u,1}, \cdots, x_{j,b_u,N}, x_{j,b_u,N}]^T, \qquad (4.10)$$

and $\odot$ is the Hadamard (element-wise) product.

Since $h_{j,b_u,i} \sim \mathcal{CN}(0,1)$, it follows that $\mathbf{f}$ and $\mathbf{g}$ are Gaussian random vectors with independent components with the same variance. It then follows that for any orthogonal matrix $\mathbf{U}$ in the set of real orthogonal matrices $\mathcal{O}(2N)$ of dimension $2N \times 2N$,

$$\mathbf{f} \odot \text{Re}(\mathbf{x}_{j,B_u}) \overset{d}{=} \mathbf{U} \left(\mathbf{f} \odot \text{Re}(\mathbf{x}_{j,B_u}) \right),$$
$$\mathbf{g} \odot \text{Im}(\mathbf{x}_{j,B_u}) \overset{d}{=} \mathbf{U} \left(\mathbf{g} \odot \text{Im}(\mathbf{x}_{j,B_u}) \right). \qquad (4.11)$$

This in turn implies that $\mathbf{Z}_{B_u}^j \overset{d}{=} \mathbf{U}\mathbf{Z}_{B_u}^j$ and hence $\mathbf{Z}_{B_u} \overset{d}{=} \mathbf{U}\mathbf{Z}_{B_u}$.

To complete the proof, we apply the following lemma which is a straightforward generalization of [ST94, Theorem 2.6.3].

Lemma 4.2.2. *Let $\mathcal{O}(d)$ be the set of real orthogonal matrices and $\mathbf{U} \in \mathcal{O}(d)$. Let $\mathbf{Z}$ be an α-stable random vector on $\mathbb{R}^d$. Then, $\mathbf{Z} \overset{d}{=} \mathbf{U}\mathbf{Z}$ if and only if $\mathbf{Z}$ is a sub-Gaussian α-stable random vector with an underlying Gaussian vector having i.i.d. $\mathcal{N}(0,\sigma^2)$ components.*

$\square$

This section mainly shows that if the set of interferers is the same on each eRB, the resulting interference vector belongs to the sub-Gaussian α-stable family, a particular case of α-stable random vectors that allow an easier representation and can consequently be more easily used for instance

in receiver design. However, when the set of interferers change (analyzing different msBs), this result does not hold any longer.

4.2.2 Interference vector in the limiting cases ($p \to 0$ or 1)

Recall that the resource allocation strategy is defined by the probability p that each device chooses to transmit on a msB. The choice is made for all available msBs one by one and independently. The value of p ranges from 0 to 1, and we will start with two particular cases: lightly loaded networks for $p \to 0$ and heavily loaded network corresponding for $p \to 0$. We will then address the more complex cases of any p value.

Lightly loaded scenario ($p \to 0$)

In the IoT networks, a common phenomenon is that many IoT devices only transmit small amounts of data over a long period of time. This is especially the case in the LPWAN, which very often requires low data rates. In that context, devices transmit intermittent data packets; for example, sensors in trash bins only transmit signals every one or two hours with a small amount of information "empty/full". Although the number of devices in the IoT networks is large, many of them may be in "sleep" mode most of the time. As a consequence, the network is lightly loaded, which can be represented with the scenario $p \to 0$ in our model.

In the regime $p \to 0$, when considering a full RB, the probability that a device transmits on more than one msB becomes very small. Indeed few users need to be served, and they do not need a significant amount of resources. In such a scenario, the probability that the same two or more users or devices transmit on different msBs is nearly zero. Since there are no common interferers on different msBs with high probability, it follows from the independent thinning theorem of HPPP—detailed in Appendix. A— that the interference on each msB is approximately independent. By Theorem 4.2.1, the interference on each msB $\mathbf{Z}_{B_1}, \cdots, \mathbf{Z}_{B_K}$ are independent sub-Gaussian α-stable vector. As such, the full interference vector in (4.2) can be rephrased as

$$\mathbf{Z} = [\mathbf{Z}_{B_1}^T, \cdots, \mathbf{Z}_{B_K}^T]^T \tag{4.12}$$

and consists of K independent sub-Gaussian α-stable random vectors.

In particular, the joint density for $\mathbf{Z}$ factorizes as

$$p_{\mathbf{Z}}(\mathbf{Z}) = \prod_{u=1}^{K} p_{\mathbf{Z}_{B_u}}(\mathbf{Z}_{B_u}), \tag{4.13}$$

where $p_{\mathbf{Z}_{B_u}}(\mathbf{Z}_{B_u})$ is the joint density of a $2N$-dimensional sub-Gaussian α-stable random vector $\mathbf{Z}_{B_u}$.

We call such a model **independent sub-Gaussian α-stable model**.

Heavily loaded scenario ($p \to 1$)

In addition to the lightly loaded case, we can imagine a scenario where users need to transmit a large amount of data in a limited time. This could be similar to a scarce resource, i.e. a limited number of eRBs per RB. Under such situations, each device needs to use most of the msBs, and the network becomes heavily loaded. This is translated in our model by $p \to 1$.

In this regime, if a device transmits on one msB, it transmits on all msBs within the RB, $\mathcal{B}$. The set of interferers on each subband is almost the same on each msB and, consequently, on each eRB. As was shown in Theorem 4.2.1, the interference vector $\mathbf{Z}$, in that case, is a $2KN$-dimensional sub-Gaussian α-stable random vector.

We call such a model **2KN sub-Gaussian α-stable model**.

4.2.3 Interference vector in the general case ($0 < p < 1$)

We now turn to the general case ($0 < p < 1$), where devices may neither necessarily transmit on all msBs simultaneously nor on a single msB.

In this scenario, the interference on the eRBs within the same msB has the same set of interferers, while these sets are different on the eRBs from different msBs. Therefore, the multivariate statistics of interference are tricky to characterize due to the complicated dependence between different eRBs. As the distribution of marginal interference is already known (and can be approximated as α-stable), a popular approach in statistics to cope with this scenario is to exploit *copulas* to model the dependence structure separately from modeling the marginals.

Copula intuition

The preliminaries on *Copula Theory* are given in Appendix. C. According to Sklar's theorem [Nel99], any random vector $\mathbf{X} = [X_1, \cdots, X_n]^T$ has the following form

$$F(x_1, \cdots, x_n) = C\left(F_1(x_1), \cdots, F_n(x_n)\right), \tag{4.14}$$

where $F_i(\cdot), i = 1, \ldots, n$ are the marginal distribution functions, and $C : [0,1]^n \to [0,1]$ is called *copula* function. $C(\cdot)$ is unique if the marginal CDFs $F_i(\cdot)$ are continuous. When both the joint and marginal distributions admit density functions (as is the case in the interference models considered in this section), the joint PDF has the form

$$p_{\mathbf{X}}(x_1, \ldots, x_n) = c(F_1(x_1), \ldots, F_n(x_n)) \prod_{i=1}^{n} p_{X_i}(x_i). \tag{4.15}$$

From (4.15) we see that the joint PDF decomposes into the product of the marginal densities and another function $c : [0,1]^n \to \mathbb{R}_+$, which captures dependence between the different components of $\mathbf{X}$. More details on copulas are given in Appendix. C.

In our system, the marginals are proved to be approximated as α-stable. As such, we only need to model the dependence, i.e., the copula density c in (4.15) which is unique according to Sklar's Theorem [Nel99].

A highly desirable property of copula models is that they provide a parametric representation of the joint distribution for random vectors. By varying these parameters, one can reach a wide range of dependence structure with flexibility. Nevertheless, deriving the exact copula can be a very challenging problem. Besides, it also raises difficulties when we need to efficiently estimate its parameters and simulate the resulting random vector. These tasks become even more tricky in our case due to the α-stable marginals, which do not have a closed-form expression for their PDFs. Consequently, we seek copula models for the interference vector over multiple eRBs that satisfy the following properties:

1. The true distribution of the interference random vector Z is well approximated by the copula model;

2. The copula has a closed-form representation or, at least, is computationally feasible to numerically evaluate.

T-Copula inference (α-stable) model

Among the standard parametric classes of copulas, e.g., Archimedean copulas and elliptical copulas, t-copula is a good candidate to approximate the interference random vector $\mathbf{Z}$.

The t-copula function has the form

$$C_{\nu,\mathbf{\Sigma}}^t(\mathbf{u}) = F_{\nu,\mathbf{\Sigma}}\left(F_\nu^{-1}(u_1), \ldots, F_\nu^{-1}(u_n)\right). \tag{4.16}$$

where $F_\nu(\cdot)$ is the univariate t-distribution function, and $F_{\nu,\mathbf{\Sigma}}(\cdot)$ is the joint multivariate t-distribution function:

$$F_v(x) = \int_{-\infty}^x \frac{\Gamma(\frac{\nu+1}{2})}{\sqrt{v\pi}\Gamma(\frac{\nu}{2})} \left(1 + \frac{t^2}{\nu}\right)^{-\frac{\nu+1}{2}} \mathrm{d}t, \tag{4.17}$$

$$F_{v,\mathbf{\Sigma}}(\mathbf{x}) = \int_{-\infty}^{x_1} \cdots \int_{-\infty}^{x_n} \frac{\Gamma(\frac{\nu+d}{2})}{\Gamma(\frac{\nu}{2})\sqrt{(\pi\nu)^d|\mathbf{\Sigma}|}} \left(1 + \frac{\mathbf{t}^T\mathbf{\Sigma}^{-1}\mathbf{t}}{\nu}\right)^{-\frac{\nu+d}{2}} \mathrm{d}\mathbf{t}. \tag{4.18}$$

Our intuition on t-copula arises from the following properties:

1. The dependence structure of t-copula is controlled by two parameters: a scalar — the degree of freedom ν; and the scale matrix $\boldsymbol{\Sigma}$. By varying ν and $\boldsymbol{\Sigma}$, we can reach a wide range of dependence. For $\nu \to \infty$ and $\boldsymbol{\Sigma} = \mathbf{I}$, the random vector has independent components;

2. Both the sub-Gaussian α-stable distribution ($p \approx 1$) and t-distribution belong to the family of elliptical distribution and share many similar properties. For instance, t-copula has the same tail dependence as the sub-Gaussian α-stable when $\nu = \alpha$. This property will be used for parameter estimation.

Therefore, t-copula may be suitable for modeling interference and include the limiting cases — lightly loaded (independent sub-Gaussian α-stable model) and heavily loaded (**2KN** sub-Gaussian α-stable model).

As shown in (4.16), the t-copula captures the dependence structure of a multivariate t-distribution without necessarily having t-distributed marginals. In particular, (4.16) can be used in (4.14) to construct multivariate distributions with α-stable marginals. That is, the dependence structure is modeled with t-copula function, and the marginals are modeled as α-stable distributed. This t-copula inference (α-stable) model provides a basis to tractably model the interference random vectors arising from the system model in Section 4.1.

Aside from well-modeling the interference distribution, t-copula models are also tractable. That is, well-established parameter estimation and simulation methods already exist. In fact, as we will develop in Section 4.3, the system features detailed in Section 4.1 can be exploited to obtain even more efficient estimation and simulation procedures than the classical methods in [DM05].

4.3 Parameter estimation

To have practical models, it is essential to be able to estimate their parameters. Equation (4.14) implies that every marginal distribution of the underlying random vectors must be evaluated, and the data samples must be transformed onto the "copula scale" before estimating the copula parameters. Therefore, the estimation of a joint distribution based on copulas is usually comprised of two major parts: First, the estimation of the marginals; Second, the estimation of the copulas.

In our model, the process of estimating marginals is to fit the parametric (α-stable) distribution to the marginals, known as Inference-Functions-for-Margins (IFM) method. Many studies and methods have been proposed for α-stable distribution parameters estimation [Nol01]. This task is not complex because they process on a single dimension, and, in many cases, we

can even expect a similar marginal on each dimension. However, the parameters of the dependence structure are more complex to estimate, and the estimation becomes computationally demanding in large dimensions for the general t-copula model [DM05]. An alternative approach is to exploit the connections between the t-copula parameters $\boldsymbol{\Sigma}, \nu$, Kendall's τ rank correlation and tail dependence. In this section, we use these connections in order to establish a low-complexity estimation procedure tailored to the interference model in Section 4.2.3.

For *i.i.d.* vector samples $\mathbf{X}_1, \cdots, \mathbf{X}_N$ where $\mathbf{X}_i = [X_{i,1}, \cdots, X_{i,d}]^T$, we assume that the marginal distribution for each dimension is already known through the IFM method. Then, we define the pseudo-copula data as follows:

Definition 4.3.1. *The pseudo-copula data is defined as*

$$\hat{\mathbf{U}}_i = [\hat{U}_{i,1}, \cdots, \hat{U}_{i,d}]^T, \quad i = 1, \cdots, N, \tag{4.19}$$

where

$$\hat{U}_{i,j} = \hat{F}(X_{i,j}), \tag{4.20}$$

and $\hat{F}(\cdot)$ is the marginal distribution function, which can be obtained through the α-stable estimation in our model.

The t-copula parameters can be estimated by the ML method (Section 4.3.1) or based on Kendall's τ (Section 4.3.2) [DM05]. We also propose an alternative approach, suited to our context, in Section 4.3.3.

4.3.1   Maximum likelihood method

Assume that the marginal distribution has been estimated, and the pseudo-copula data has been obtained as

$$\begin{aligned}
\hat{\mathbf{U}}_i &= (\hat{U}_{i,1}, \cdots, \hat{U}_{i,d})^T \\
&= (\hat{F}(X_{i,1}), \cdots, \hat{F}(X_{i,d}))^T, \quad i = 1, \cdots, N.
\end{aligned} \tag{4.21}$$

We can estimate the parameters ν and $\boldsymbol{\Sigma}$ of t-copula through the ML method by maximizing

$$\log L(\nu, \boldsymbol{\Sigma}, \hat{\mathbf{U}}_1, \cdots, \hat{\mathbf{U}}_N) = \sum_{i=1}^{N} \log c_{\nu, \boldsymbol{\Sigma}}(\hat{\mathbf{U}}_i). \tag{4.22}$$

However, the ML method is computationally taxing, particularly for high dimensions. For this reason, an alternative method is proposed based on Kendall's τ [DM05].

4.3.2 Methods using Kendall's τ

A simpler approach for parameter estimation in t-copula models proceeds as follows. Consider a d-dimensional random vector $\mathbf{X} = [X_1, \ldots, X_d]^T$ on $\mathbb{R}^d$ governed by a t-copula with parameters $\nu, \mathbf{\Sigma}$. According to [LMS03], the elements of $\mathbf{\Sigma}$ can be obtained via Kendall's τ rank correlation $\hat{\rho}_\tau(X_j, X_k)$.

Let $\mathbf{X}_i = [X_{i,1}, \ldots, X_{i,d}]^T$, $i = 1, \ldots, n$ be n independent samples of $\mathbf{X}$. A natural estimator for $\Sigma_{j,k}$—the element of $\mathbf{\Sigma}$—is then given by [DM05]

$$\hat{\Sigma}_{jk} = \sin\left(\frac{\pi}{2}\hat{\rho}_\tau(X_j, X_k)\right), \tag{4.23}$$

where

$$\hat{\rho}_\tau(X_j, X_k) = \binom{n}{2}^{-1} \sum_{1 \le i_1 \le i_2 \le n} \text{sign}\left((X_{i_1,j} - X_{i_2,j})(X_{i_1,k} - X_{i_2,k})\right). \tag{4.24}$$

In general, there are no guarantees that this estimation solution leads to a positive definite $\hat{\mathbf{\Sigma}}$. It is then recommended to apply adjustment techniques [RM93] to ensure positive definiteness. Having estimated $\mathbf{\Sigma}$, the standard approach then obtains the degree of freedom ν via a ML estimator given $\hat{\mathbf{\Sigma}}$[DM05]:

$$\hat{\nu} = \underset{\nu}{\text{argmax}} \ \log L(\nu | \hat{\mathbf{\Sigma}}, \hat{\mathbf{U}}_1, \cdots, \hat{\mathbf{U}}_N)$$
$$= \underset{\nu}{\text{argmax}} \sum_{i=1}^{N} \log c_\nu(\hat{\mathbf{\Sigma}}, \hat{\mathbf{U}}_i). \tag{4.25}$$

This approach still suffers from the necessity to solve a likelihood maximization problem in (4.25). An alternative method relies on the tail dependence.

4.3.3 A low-complexity estimation procedure

Consider a bivariate random vector (X_1, X_2) with marginal distributions F_1, F_2, respectively. Then, the (upper) tail dependence $\lambda_{\mathbf{X}}$ is defined by

$$\lambda_{\mathbf{X}} = \lim_{u \to 1} \mathbb{P}\left(X_1 > F_1^{-1}(u) | X_2 > F_2^{-1}(u)\right). \tag{4.26}$$

In the case that (X_1, X_2) is governed by a t-copula, [DM05, Proposition 1] provides a link between the tail dependence and the degree of freedom ν.

Consider a random vector $\mathbf{X}$ governed by t-copula. If the off-diagonal elements of $\mathbf{\Sigma}$ are a constant denoted by ρ, the tail dependence is known to

be constant amongst each pair of elements in $\mathbf{X}$. It can be expressed as a function of the degrees of freedom and ρ:

$$\lambda_{\mathbf{X}} = 2F_{\nu+1}\left(\frac{\sqrt{1+\nu}\sqrt{1-\rho}}{\sqrt{1+\rho}}\right), \qquad (4.27)$$

where $F_{\nu+1}$ is defined in (4.17) with the degree of freedom $\nu+1$, and ρ is the correlation coefficient.

From (4.27), when $\lambda_{\mathbf{X}}$ and ρ are known, it is rather straightforward to obtain the degree of freedom ν [DM05]. Based on (4.27), we now develop a new low-complexity estimation procedure for the t-copula inference model proposed in Section 4.2.3. Our approach is still based on the IFM method, and we require estimates of the tail dependence $\lambda_{\mathbf{Z}}$ to obtain the degree of freedom ν, and the scale matrix $\mathbf{\Sigma}$. We first approximate the scale matrix $\mathbf{\Sigma}$ based on our specific context. We then derive the approximation for the tail dependence $\lambda_{\mathbf{Z}}$.

Scale matrix $\mathbf{\Sigma}$

To derive an estimate of $\mathbf{\Sigma}$, we recall that for $p = 1$, the interference random vector $\mathbf{Z}$ approximately forms a spherically distributed sub-Gaussian α-stable random vector (by Theorem 4.2.1). It means that the underlying Gaussian vector of $\mathbf{Z}$ has *i.i.d.* components. In this case, the Kendall's τ for each pair of $\mathbf{Z}$ is zero, and thus $\mathbf{\Sigma}$ is the identity matrix. To obtain an approximation of $\mathbf{\Sigma}$ for $p \approx 1$, we therefore base our estimate on the case $p = 1$.

For the small value of p, $\mathbf{Z}$ forms an independent sub-Gaussian α-stable vector defined in Section 4.2.2. The Kendall's τ between the pair of interference within the msB B_u is zero as the vector $\mathbf{Z}_{B_u}$ is sub-Gaussian α-stable. The pair of interference between different msBs B_u and B'_u are approximately independent. As a consequence, Kendall's τ between such a pair is again close to zero. Therefore, the scale matrix $\mathbf{\Sigma}$ can also be approximated as the identity matrix.

Fig. 4.1 shows the scale matrix $\hat{\mathbf{\Sigma}}$ estimated from Kendall's τ based on (4.23) under different values of p. It is clear from this figure that $\hat{\mathbf{\Sigma}}$ is almost the identity matrix.

We verify for other values of p that the off-diagonal values of the scale matrix are very low. This means that there is no significant linear dependence in the interference. This could probably become untrue if some dependence structure is coming from a correlation between the channel fadings on different eRBs that we did not include, only considering Rayleigh *i.i.d.* channels. This could arise if different eRBs are close subbands or coming from slightly separated antennas. However, the scale matrix should still

(A) $p = 0.2$

(B) $p = 0.4$

(C) $p = 0.6$

(D) $p = 0.8$
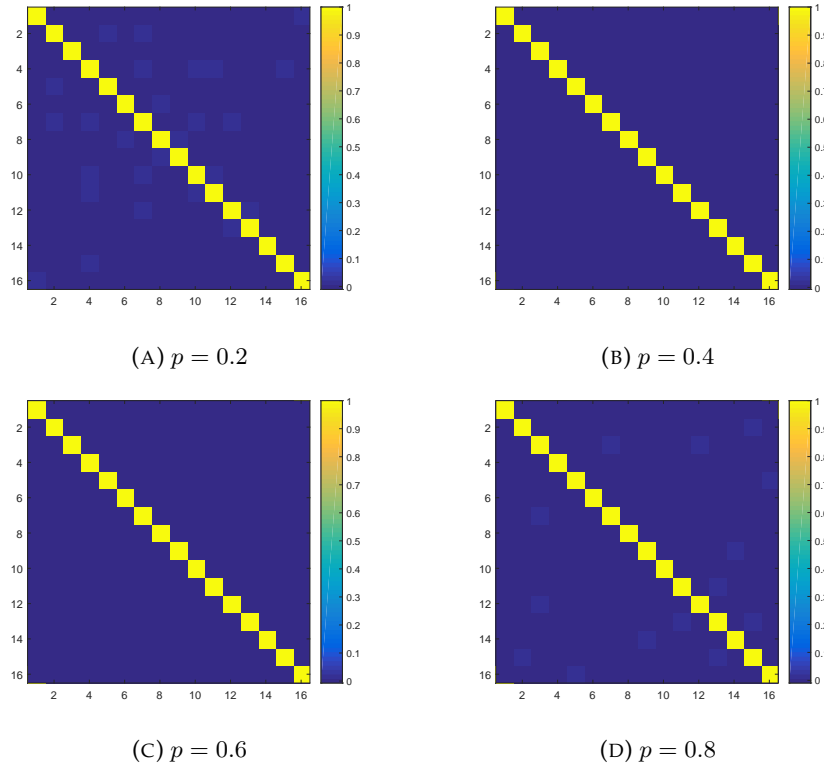
FIGURE 4.1: Estimated scale matrix $\hat{\Sigma}$ based on Kendall's τ in (4.23) for different values of p.

be able to be predicted if in the case $p = 1$, we have a sub-Gaussian α-stable random vector with some correlated underlying Gaussian random vector.

Nevertheless, for our general framework though, we can set the scale matrix as

$$\Sigma = \mathbf{I}_{2KN}, \tag{4.28}$$

where $\mathbf{I}_{2KN}$ is the $2KN$ dimensional identity matrix.

Tail dependence $\lambda_{\mathbf{Z}}$

To derive an approximation of the tail dependence in (4.27), we first observe that the tail dependence is not the same for each pair of elements in $\mathbf{Z}$. This is due to the fact that the tail dependence within a given msB B_u and that between two different msBs B_u and B'_u are not the same. In the first case, the set of interferers is the same on the different components when it is not in the second case.

- For a given msB B_u, the random vector $\mathbf{Z}_{B_u}$ is sub-Gaussian α-stable. This implies that for any pair of elements in $\mathbf{Z}_{B_u}$, the tail dependence

is given by [Kri+09]

$$\lambda_{\mathbf{Z}_{B_u}} = \frac{\int_0^{\frac{1}{\sqrt{2}}} \frac{u^\alpha}{\sqrt{1-u^2}} du}{\int_0^1 \frac{u^\alpha}{\sqrt{1-u^2}} du}, \tag{4.29}$$

where α is the stable exponent.

- For a pair of eRBs coming from different msBs B_u and $B_{u'}$, the tail dependence depends on the service rate p. For example, as $p \to 0$, elements of $\mathbf{Z}$ from different msBs are approximately independent. This means that the tail dependence for these pairs, denoted by $\lambda_{\tilde{\mathbf{Z}}}$, is approximately zero. And as $p \to 1$, $\mathbf{Z}$ is sub-Gaussian α-stable, and $\lambda_{\tilde{\mathbf{Z}}}$ is approximated in (4.29).

When the number of msBs–K is large compare to the number of eRBs in one msB, there are significantly more pairs of eRBs with tail dependence $\lambda_{\tilde{\mathbf{Z}}}$ than with $\lambda_{\mathbf{Z}_{B_u}}$. For this reason, we will base our estimate of the degree of freedom ν on $\lambda_{\tilde{\mathbf{Z}}}$ instead of $\lambda_{\mathbf{Z}_{B_u}}$ and verify that this approximation is accurate enough.

The first step is then to obtain an approximation of the tail dependence $\lambda_{\tilde{\mathbf{Z}}}$. We can show that such an approximation is given by

$$\lambda_{\tilde{\mathbf{Z}}} \approx \frac{2p}{\mathbb{E}\left[|Z_{1,1}|^\alpha\right]} \int_0^\infty [1 - F_{Z_{1,1}}(z)]^2 \alpha z^{\alpha-1} dz, \tag{4.30}$$

where $\alpha = \frac{4}{\eta}$, and $Z_{1,1} = \mathrm{Re}(h_{1,1}x_{1,1})$.

Proof. By definition,

$$\lambda_{\tilde{\mathbf{Z}}} = \lim_{u \to 1} \mathbb{P}\left(\sum_{j \in \Phi_1} r_j^{-\frac{\eta}{2}} Z_{j,1} > F^{-1}(u) \,\bigg|\, \sum_{j \in \Phi_2} r_j^{-\frac{\eta}{2}} Z_{j,2} > F^{-1}(u)\right)$$

$$= \lim_{u \to 1} \frac{\mathbb{P}\left(\sum_{j \in \Phi_1} r_j^{-\frac{\eta}{2}} Z_{j,1} > F^{-1}(u), \sum_{j \in \Phi_2} r_j^{-\frac{\eta}{2}} Z_{j,2} > F^{-1}(u)\right)}{\mathbb{P}\left(\sum_{j \in \Phi_2} r_j^{-\frac{\eta}{2}} Z_{j,2} > F^{-1}(u)\right)}. \tag{4.31}$$

By Remark B.2.15 in Appendeix B, for $l \in \{1, 2\}$, as $x \to \infty$,

$$\mathbb{P}\left(\sum_{j \in \Phi_l} r_j^{-\frac{\eta}{2}} Z_{j,l} > x\right) = \frac{1}{2} C_\alpha \gamma^\alpha x^{-\frac{4}{\eta}} + o\left(x^{-\frac{4}{\eta}}\right)$$

$$= \frac{1}{2} p\lambda\pi \mathbb{E}\left[|Z_{1,1}|^\alpha\right] x^{-\frac{4}{\eta}} + o\left(x^{-\frac{4}{\eta}}\right). \tag{4.32}$$

Moreover, the dependence is also the strongest between terms that have the same distance. For $p \approx 1$, this suggests the approximation

$$\mathbb{P}\left(\sum_{j\in\Phi_1} r_j^{-\frac{\eta}{2}} Z_{j,1} > F^{-1}(u), \sum_{j\in\Phi_2} r_j^{-\frac{\eta}{2}} Z_{j,2} > F^{-1}(u)\right)$$
$$\approx p\mathbb{P}\left(r_1^{-\frac{\eta}{2}} Z_{1,1} > F^{-1}(u), r_1^{-\frac{\eta}{2}} Z_{1,2} > F^{-1}(u)\right). \tag{4.33}$$

Since r_1 is the closest point in a [HPPP](#),

$$f_{r_1}(r) = 2p\lambda\pi r e^{-p\lambda\pi r^2}. \tag{4.34}$$

This yields

$$\mathbb{P}\left(\sum_{j\in\Phi_1} r_j^{-\frac{\eta}{2}} Z_{j,1} > F^{-1}(u), \sum_{j\in\Phi_2} r_j^{-\frac{\eta}{2}} Z_{j,2} > F^{-1}(u)\right)$$
$$\approx p\mathbb{P}\left(Z_{1,1} > F^{-1}(u)r_1^{\frac{\eta}{2}}, Z_{1,2} > F^{-1}(u)r_1^{\frac{\eta}{2}}\right)$$
$$= p\int_0^\infty \mathbb{P}\left(Z_{1,1} > F^{-1}(u)r^{\frac{\eta}{2}}, Z_{1,2} > F^{-1}(u)r^{\frac{\eta}{2}} \Big| r\right) 2p\lambda\pi r e^{-p\lambda\pi r^2} dr$$
$$= p\int_0^\infty \left[1 - F_{Z_{1,1}}\left(F^{-1}(u)r^{\eta/2}\right)\right]^2 2p\lambda\pi r e^{-p\lambda\pi r^2} dr. \tag{4.35}$$

At this point, we make the change of variables

$$z = F^{-1}(u)r^{\frac{\eta}{2}}, \tag{4.36}$$

which yields

$$\mathbb{P}\left(\sum_{j\in\Phi_1} r_j^{-\frac{\eta}{2}} Z_{j,1} > F^{-1}(u), \sum_{j\in\Phi_2} r_j^{-\frac{\eta}{2}} Z_{j,2} > F^{-1}(u)\right)$$
$$\approx \frac{4}{\eta} p^2 \lambda\pi F^{-1}(u)^{-\frac{4}{\eta}} \int_0^\infty [1 - F_{Z_{1,1}}(z)]^2 e^{-p\lambda\pi z^{\frac{4}{\eta}} F^{-1}(u)^{-\frac{4}{\eta}}} z^{\frac{4}{\eta}-1} dz. \tag{4.37}$$

Combining (4.37) and (4.32), it follows that the tail dependence is well approximated in (4.30).

Note that the validity of swapping the limit and integral can be readily justified by an application of the dominated convergence theorem. $\qquad\square$

A key observation is that the approximation of $\lambda_{\tilde{\mathbf{Z}}}$ in (4.30) scales linearly with p with a maximum value corresponding to $p = 1$, which is the sub-Gaussian α-stable scenario by Theorem 4.2.1. In this case, the tail-dependence is given by

$$\lambda_{\tilde{\mathbf{Z}}} \approx \frac{2}{\mathbb{E}\left[|Z_{1,1}|^\alpha\right]} \int_0^\infty [1 - F_{Z_{1,1}}(z)]^2 \alpha z^{\alpha-1} dz. \tag{4.38}$$

To verify the approximation in (4.38), we consider the case $p = 1$. By Theorem 4.2.1, the interference random vector is sub-Gaussian α-stable. As a consequence, the tail dependence is given by (4.29).
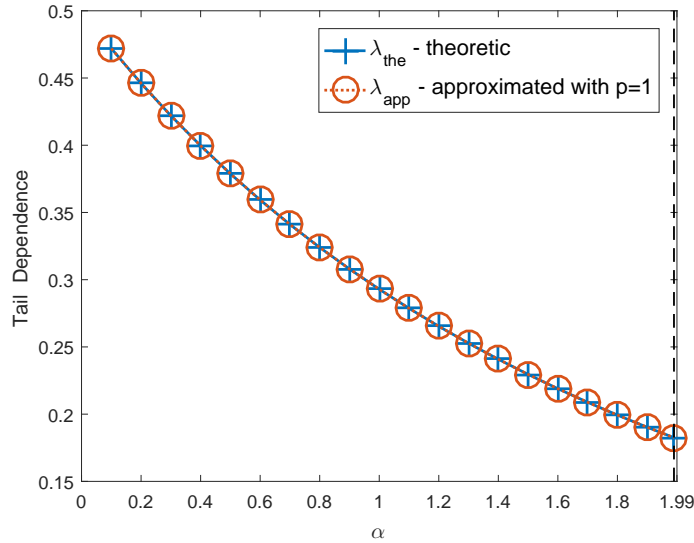
FIGURE 4.2: Theoretical and estimated tail dependence for varying α.

Fig. 4.2 plots the tail dependence under different α where we take $h_{i,j} \sim \mathcal{CN}(0,1)$ and $x_{i,j} \sim \mathrm{Unif}(\{+1,-1\})$. It shows that the approximation in (4.38) is in good agreement with the exact expression in (4.29), even as α is varied. The tail dependence is strong with small values of α, i.e., when the marginals are more impulsive. With α increases, the marginals are more "Gaussian", and the tail dependence becomes small.

The validity of the approximation will be further studied in Section 4.4. The quality of the estimation procedure will be evaluated in terms of the KL divergence between the resulting interference model and the system model in Section 4.1 for the three families of point processes.

As (4.30) exhibits a good analytical approximation for the tail dependence, the ML estimation of ν is not required, reducing the computational complexity in model calibration. As $Z_{i,j} \sim \mathcal{CN}(0,1)$, (4.30) is just a computation of integrals.

A new efficient algorithm

The observation that the tail dependence approximation in (4.38) is accurate suggests a new estimation procedure for the t-copula α-stable interference

model. We recall here the approximation of $\lambda_{\tilde{\mathbf{Z}}}$ and $\boldsymbol{\Sigma}$:

$$\boldsymbol{\Sigma} = \mathbf{I}_{2KN},$$

$$\lambda_{\tilde{\mathbf{Z}}} \approx \frac{2p}{\mathbb{E}\left[|\mathrm{Re}(Z_{1,1})|^{\alpha}\right]} \int_0^{\infty} [1 - F_{Z_{1,1}}(z)]^2 \alpha z^{\alpha-1} dz.$$

Using these two results in combination with (4.27) allows us to propose the procedure detailed in Algorithm 1.

Algorithm 1 Proposed Copula Parameter Estimation Algorithm with $\alpha = \frac{4}{\eta}$

Input: Path-loss exponent η and S independent samples of the interference random vector $\mathbf{Z}^1, \ldots, \mathbf{Z}^S$.

 1: Set $\alpha = \frac{4}{\eta}$.
 2: Estimate the dispersion of the α-stable marginals, γ;
 3: Set the scale matrix for the t-copula model $\boldsymbol{\Sigma} = \mathbf{I}_{2KN}$;
 4: Set the tail dependence for the t-copula model to be $\lambda_{\tilde{\mathbf{Z}}}$ in (4.30);
 5: Compute the degree of freedom for the t-copula model via (4.27).

In Algorithm 1, in order to perform the parameter estimation in step 1, we require independent observations of the interference random vector $\mathbf{Z}$ as the input. Assuming that the lifetime of device transmissions is not long (as it is typically the case in NB-IoT networks), these samples can be collected from consecutive frames. Following the IFM methodology, the first steps in Line 1 and 2 are then to estimate the parameters for the statistics of the in-phase and quadrature components on a single subcarrier. As these statistics are approximately symmetric α-stable by Theorem 3.2.1, only two parameters, α and γ, need to be estimated.

The second and third steps are to obtain $\boldsymbol{\Sigma}$ and $\lambda_{\tilde{\mathbf{Z}}}$ from (4.30). It is straightforward to obtain $\boldsymbol{\Sigma}$ by simply setting it as an identity matrix. For $\lambda_{\tilde{\mathbf{Z}}}$, if the fading statistics $h_{i,j}$ and the path-loss exponent η are known, $Z = \mathrm{Re}(h_{1,1}x_{1,1})$ and $\alpha = \frac{4}{\eta}$ in (4.30) are known, and $\lambda_{\tilde{\mathbf{Z}}}$ can be calculated. From $\lambda_{\tilde{\mathbf{Z}}}$, we can then numerically calculate ν based on (4.27). In fact, no samples are required in order to compute the degree of freedom ν, or $\boldsymbol{\Sigma}$. This forms a contrast with the estimation of general t-copula models (i.e., without the structure of the interference random vector $\mathbf{Z}$), where a large number of samples are required.

Note that derivation of the tail dependence in (4.30) is based on the model of HPPP over the whole plane. Nevertheless, (4.34) does not apply to the scenarios with guard-zone radius. What is more, the closest point in the doubly Poisson cluster process and the Matérn hard-core process of type II process does not follow (4.34). Thus, (4.30) may not be a good approximation.

To address this issue, we take $\hat{\alpha}$ instead of $\frac{4}{\eta}$, and all the rest remain the same. That is, we keep

$$\lambda_{\tilde{\mathbf{Z}}} \approx p\lambda_{\mathbf{Z}_{B_u}}, \tag{4.39}$$

where $\lambda_{\mathbf{Z}_{B_u}}$ is in (4.29) with the estimated $\hat{\alpha}$ and has an approximation in (4.38).

As proved in Fig. 4.5 and Fig. 4.6 in Section 4.4, the vector $\mathbf{Z}$ is approximated as sub-Gaussian α-stable for $p = 1$, and thus $\mathbf{Z}_{B_u}$ is also sub-Gaussian α-stable with estimated $\hat{\alpha}$. Therefore, instead of setting $\alpha = \frac{4}{\eta}$, we take the estimated $\hat{\alpha}$ into (4.29) and (4.39) to estimate the tail dependence.

Algorithm 2 Proposed Copula Parameter Estimation Algorithm with $\hat{\alpha}$

Input: S independent samples of the interference random vector $\mathbf{Z}^1, \dots, \mathbf{Z}^S$.

The same steps with Algorithm 1 except estimating the tail dependence using (4.39) and (4.29) with estimated $\hat{\alpha}$ in step 3.

4.4 Model verification

In this section, we compare the interference models developed in Section 4.2 with the interference arising from the scenarios detailed in Section 4.1 based on the KL divergence. We also study the dependence structure of our model and the simulated data set via transformation to the *copula space*. This provides additional insights into the behavior of the interference, particularly when multiple eRBs experience large amplitude interference.

In order to perform the model evaluation, it is necessary to calibrate and simulate the t-copula model. As such, we first detail the estimation and simulation procedures. We will then represent the dependence structure in the copula space to have an idea of the specificity of the interference random vector. Finally, we will assess the performance of the models in terms of KL divergence.

4.4.1 Estimation

Let us consider a set of samples

$$\mathbf{X}^d = [x_1^d, \cdots, x_{2KN}^d]^T, \quad d = 1, \cdots, D. \tag{4.40}$$

The estimation process of the t-copula model with α-stable marginals is decomposed into three steps:

1. Estimate the parameters of the α-stable marginals ($\hat{\alpha}$ and $\hat{\gamma}$);

2. With $\hat{\alpha}$ and $\hat{\gamma}$, translate $\mathbf{X}^d$ to the "copula space" via the $\hat{\alpha}$-stable CDF. We then obtain

$$\mathbf{U}^d = (U_1^d, \cdots, U_{2KN}^d) = \left(F_{\hat{\alpha}}(X_1^d), \cdots, F_{\hat{\alpha}}(X_{2KN}^d) \right), \qquad (4.41)$$

where $F_{\hat{\alpha}}(\cdot)$ denotes the $\hat{\alpha}$-stable CDF.

3. Estimate the degree of freedom $\hat{\nu}$ and the scale matrix $\hat{\mathbf{\Sigma}}$ of the t-copula based on $\mathbf{U}^d$.

In Step 1 and 2, the parameters of the marginals, $\hat{\alpha}$ and $\hat{\gamma}$ were estimated, and $\mathbf{X}^d$ were obtained using the stblfit and stblcdf MATLAB packages, respectively [Sta]. The estimation is based on the fitting of the four parameters to the empirical characteristic function estimated from the data proposed by Koutrouvelis [Kou80; Kou81]. Note that the parameters β and δ are set zero as the interference is symmetric.

In Step 3, the t-copula parameters can be estimated using the copulafit MATLAB package [T ca] via ML. They can also be estimated either using Algorithm 1 or Algorithm 2 from (4.39) with the estimated $\hat{\alpha}$.

4.4.2 Simulation

Knowing the parameters of the stable marginals ($\hat{\alpha}$ and $\hat{\gamma}$) and of the t-copula ($\hat{\nu}$ and $\hat{\mathbf{\Sigma}}$), we can simulate the t-copula α-stable interference with following steps:

1. Simulate data samples from the t-copula model with $\hat{\nu}$ and $\hat{\mathbf{\Sigma}}$ and get $\hat{\mathbf{U}}^d = [\hat{U}_1^d, \cdots, \hat{U}_{2KN}^d]$;

2. Do the stable inverse CDF for each marginals $\hat{U}_i^d$ based on $\hat{\alpha}$ and $\hat{\gamma}$ and get $\hat{\mathbf{X}}^d$.

In Step 1, simulation methods for t-copula models are detailed in [DM05] and can be implemented via the copularnd MATLAB package [T cb]. In Step 2, the inverse distribution function is obtained using the stblinv MATLAB package [Sta].

4.4.3 Interference random vector: Copula-space representations

The copula modeling allows to qualitatively verify that the dependence structure of our multivariate interference model is consistent with the interference arising from the simulated data. This is achieved by transforming the d-dimensional simulated data into the *copula space*, which yields a random vector on $[0, 1]^d$. In particular, for both the data simulated from the system detailed in Section 4.1 and our copula model developed in Section 4.2, we apply the transformation

$$\mathbf{Z} \mapsto [H_{\alpha,\gamma}(Z_1), \ldots, H_{\alpha,\gamma}(Z_{2KN})]^T, \qquad (4.42)$$

where $H_{\alpha,\gamma}(\cdot)$ is the CDF of the α-stable random variable Z_i with α and γ.

In Fig. 4.3 we plot the estimated density of the simulated samples arising from a HPPP with $\lambda = 0.001 \text{ devices/m}^2$ over the infinite plane with no guard zones. We consider the real components of eRBs in two different msBs transformed into the copula space drawn from the simulated data set. The case of eRBs in the same msB is similar to the real and imaginary parts studied in the paragraph "Dependence Structure" in section 3.2.3. We set $p = 0.6$, which means that the pair of real components do not have a sub-Gaussian α-stable distribution. We again observe the large probability mass in the corners of the figure, corresponding to strong dependence in the tails.
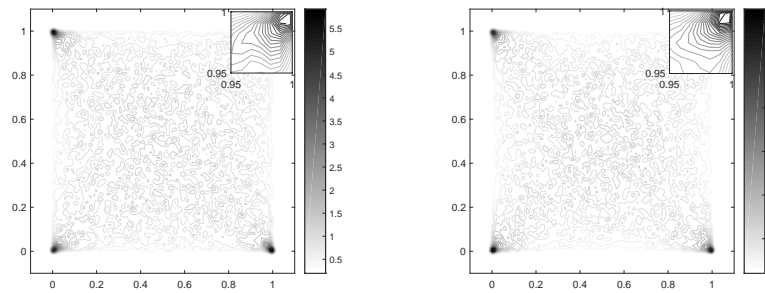
(A) The system model with $p = 0.6$.   (B) The t-copula model with $p = 0.6$.

FIGURE 4.3: Copula space transformation for real components of interference samples in different msBs with $p = 0.6$.

This fact is important and reveals why traditional second-order ways to model dependence are not sufficient. Indeed, this tail dependence can not be captured by linear dependence that is characterized through the correlation function for instance. On the contrary, this feature is well captured by the t-copula, as illustrated in Fig. 4.3b, where we represent the estimated density from the real components of eRBs in two different msBs transformed to the copula space. Samples are drawn from the proposed t-copula model. The densities are very similar and suggest that the t-copula model fits well in this scenario. This will be confirmed by the KL divergence analysis.

4.4.4   Interference random vector: KL divergence

We now turn to our model for the interference random vector developed in Section 4.2. We numerically investigate the behavior of our proposed models by evaluating the KL divergence between the interference arising from the scenario in Section 4.1 and our proposed models in Section 4.2. That is, we estimate $D_{KL}(P||Q)$ where P is the distribution corresponding to the interference from the system model, and Q is the distribution of the interference arising from our models. The interference random vector has

in general a high dimension ($2KN$ dimensions for K msBs and N eRBs in each msB as detailed in Section 4.1). This high dimension makes the numerical evaluation non-trivial.

In the sequel, all figures are generated using a simulated data set with $80,000$ samples. We use the k-nearest neighbor method [WKV06] implemented in the MATLAB package [Sza14] for the computation of the KL divergence. Due to the high dimension of the interference random vector, the k-nearest neighbor method can output very small negative values when the distributions P and Q are very close [WKV06]. In the figures, these negative values are rounded to zero.

In the experiments, we compare five models all with α-stable marginal distributions motivated by Theorem 4.2.1:

1. The t-**copula** α-**stable** model detailed in Section 4.2 with three different parameter estimation algorithms:

   a) via ML estimation, called "t-copula" in the following figures;

   b) via Algorithm 1, i.e., based on tail dependence with $\alpha = \frac{4}{\eta}$, called "Tail dependence ($\alpha = \frac{4}{\eta}$)" in the following figures;

   c) via Algorithm 2, i.e., based on tail dependence with $\hat{\alpha}$, called "Tail dependence (estimated $\hat{\alpha}$)" in the following figures.

2. The **independent sub-Gaussian** α-**stable** model consisting of independent $2N$-dimensional sub-Gaussian α-stable random vectors. In this model, the $2KN$-dimensional random interference vector $\mathbf{Z}$ is decomposed into K $2N$-dimensional random vectors (corresponding to the real and imaginary parts of N eRBs in one msB). Each $2N$-dimensional random vector is assumed to be sub-Gaussian α-stable, independent from each of the other $K - 1$ $2N$-dimensional random vectors, as detailed in Section 4.2.2. This model is exact when interfering devices only transmit on a single msB, the guard-zone radius $r_{\min} = 0$, and the network radius $r_{\max} \to \infty$.

3. The $2KN$ **sub-Gaussian** α-**stable** model consisting of a $2KN$-dimensional sub-Gaussian α-stable random vector. This model corresponds to the scenario where all devices transmit on every msB in $\mathcal{B}$, i.e., $p = 1$ (see Theorem 4.2.1).

We consider the three general point processes introduced in Section 2.5, i.e., the HPPP, doubly Poisson cluster process and Matérn hard-core process of type II. Specifically, we consider the scenarios with the following parameters:

- Number of msBs: $K = 4$;

- Number of eRBs in each msB: $N = 2$;

FIGURE 4.4: Plots of the KL divergence between the data generated from the models and interference samples simulated from a HPPP: we use the five different models and estimation methods: t-copula model (ML estimation, $\alpha = 4/\eta$ and $\hat{\alpha}$); independent sub-Gaussian α-stable model; and $4K$ sub-Gaussian α-stable model. We have $K = 4$ msBs and $N = 2$ eRBs in each msB.

- Path-loss exponent: $\eta = 3$;

- Fading: $h \sim \mathcal{CN}(0, 1)$;

- Transmitted signal: $x_{j,i}$ is uniformly drawn from $\{-1, 1\} \; \forall \; i, j$;

- Guard-zone radius: $r_{\min} = 0$;

- Network radius: $r_{\max} = 500$ m.

Homogeneous Poisson point process

We first consider the HPPP. Fig. 4.4 plots the KL divergence between the simulated data set and the three proposed interference models with the following parameters:

- Density of interferers: $\lambda = 0.001$ devices/m^2.

Observe that the $2KN$ sub-Gaussian α-stable model is in good agreement with the simulated data set as $p \to 1$. This is consistent with the characterization in Theorem 4.2.1 as when $p \to 1$ all devices transmit on all subbands with high probability. On the other hand as p decreases, the $2KN$ sub-Gaussian α-stable model is a poor fit for the simulated data set. In this lightly loaded scenario where $p \to 0$, each device transmits on more than one msB with a very low probability. By the independent thinning theorem for HPPP, it follows that the interference on each msB is independent. As a consequence, the independent sub-Gaussian α-stable model is a good
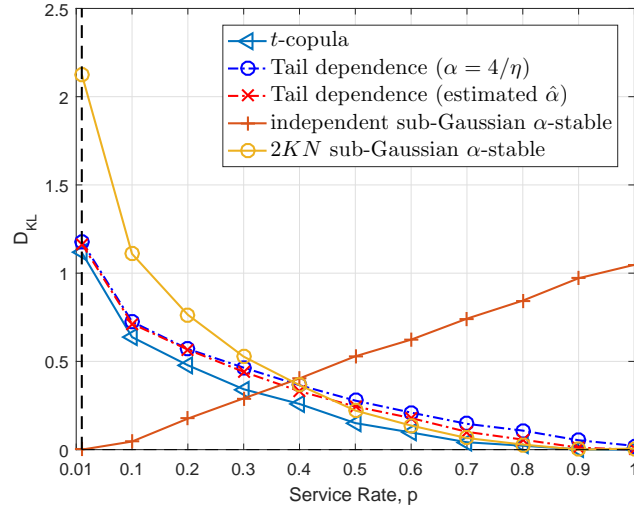
FIGURE 4.5: Plots of the KL divergence between the data generated from the models and interference samples simulated from a doubly Poisson cluster process: we use the five different models and estimation methods: t-copula model (ML estimation, $\alpha = 4/\eta$ and $\hat{\alpha}$); independent sub-Gaussian α-stable model; and $4K$ sub-Gaussian α-stable model. We have $K = 4$ msBs and $N = 2$ eRBs in each msB.

choice. This observation is verified in Fig. 4.4, where the KL divergence for this model is nearly zero for small values of p.

Fig. 4.4 also shows that the t-copula model is a good fit for a much larger range of p than the $2KN$ sub-Gaussian α-stable model. As such, it is a good choice for medium to heavily loaded IoT networks. However, for small p the t-copula model is not satisfactory. The Algorithm 1 and Algorithm 2 based on tail dependence have almost equivalent performance as the t-copula model based on the ML estimation. However, our proposed algorithms have faster runtime as we compute parameters directly, and only have the analytical expressions in (4.30) to calculate.

Doubly Poisson cluster process

Fig. 4.5 plots the KL divergence for each of the proposed models for locations governed by a doubly Poisson cluster process with parameters:

- Density of parent process: $\lambda_p = 2 \times 10^{-4}$ devices/m^2;

- Radius of the disc for daughter cluster process: $r_c = 30$ m;

- Density of daughter point process: $\lambda_d = \frac{10}{\pi r_c^2} = 0.0035$ devices/m^2, i.e., the average number of points in each cluster: $c = \lambda_d \pi r_c^2 + 1 = 11$.

Observe that the t-copula model has a very similar behavior qualitatively consistent with the HPPP case in Fig. 4.4. However, the low-complexity estimation procedures in Algorithm 1 and Algorithm 2 have
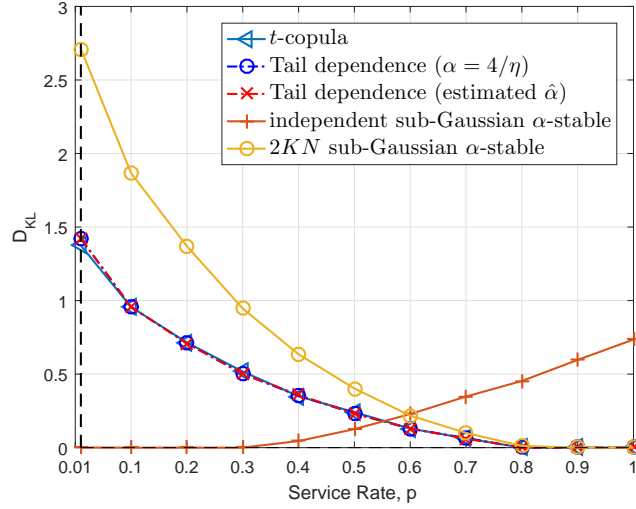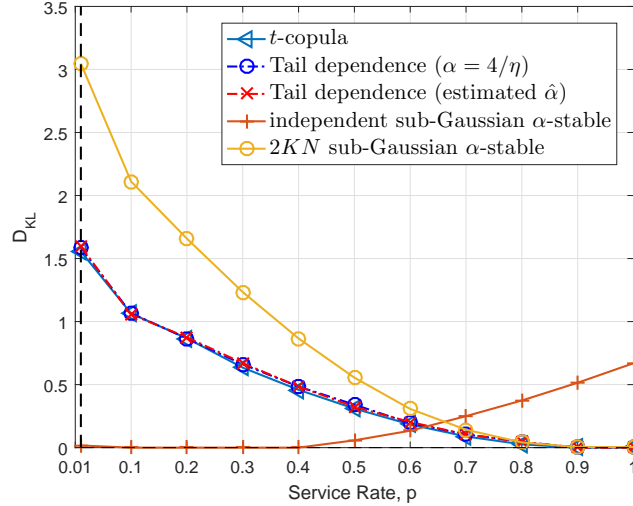
FIGURE 4.6: Plots of the KL divergence between the data generated from the models and interference samples simulated from a Matérn hard-core process of type II: we use the five different models and estimation methods: t-copula model (ML estimation, $\alpha = 4/\eta$ and $\hat{\alpha}$); independent sub-Gaussian α-stable model; and $4K$ sub-Gaussian α-stable model. We have $K = 4$ msBs and $N = 2$ eRBs in each msB.

a slightly reduced performance. This is due to the implicit assumption in the estimation procedure that the void probability is that of a HPPP. That is, the tail dependence in (4.30) is derived from (4.34), the PDF of the closest point which does not apply to the doubly Poisson point process.

Note that under the doubly Poisson cluster process, though the α-stable distribution is still a good approximation for the interference marginals, the stable parameter $\hat{\alpha}$ is not equal to $\frac{4}{\eta}$, even in the case when $r_{\min} = 0$. As a consequence, a slight improvement can be observed with an estimated α (Algorithm 1) rather than with $\alpha = \frac{4}{\eta}$ (algorithm 2).

Matérn hard-core process of type II

Fig. 4.6 plots the KL divergence for each of the proposed models for locations governed by a Matérn hard-core process of type II with the following parameters:

- Density of parent process: $\lambda_p = 0.001$ devices/m^2;

- Hard-core distance: $r_h = 20$ m.

Observe again that all five models have a very similar behavior in terms of KL divergence as under the HPPP in Fig. 4.4. The proposed model is valid on a large range of values of p, but exhibits a degradation when p becomes small. This is consistent with Theorem 3.3.1 and previous

works establishing that the Matérn hard-core process of type II can be well-approximated by a homogeneous Poisson point process [CKJ13; Hae11]. Under the Matérn hard-core process of type II, at most one point is kept within the hard-core distance based on its underlying HPPP.

Besides, unlike the doubly Poisson cluster process, the distribution of the closest interferer can also be approximated by (4.34) as shown in [IEEK13, Lemma 1]. As such, the low-complexity estimation procedures in Algorithm 1 and Algorithm 2 yields an estimate that well approximates the ML estimate.

4.5 Conclusion

We have shown that the dependence structure in an interference vector when devices are transmitting on several eRBs grouped in several msB is non-trivial. When the set of interferers remains the same, i.e., we consider the eRBs belonging to the same msB or the case where service rate $p \approx 1$, a sub-Gaussian α-stable model is theoretically obtained for a homogeneous Poisson point process (HPPP) in an infinite plane without guard zone. And when $p \approx 0$, an independent α-stable model is obtained as well. These two models remain accurate for different point processes (Doubly Poisson Cluster Process and Matérn hard-core process of type II).

Although the independent sub-Gaussian α-stable and the $2KN$-dimensional sub-Gaussian α-stable models are good models when, respectively, p is small and p is close to one, the t-copula model is the most appropriate one for a large range of service rates p. It degrades for small values of p, which probably comes from the strong dependence in msBs and weak one between eRBs. Taking a single degree of freedom to represent these contradictory effects is no longer efficient. A hierarchical model should be proposed and further studied.

The proposed estimation algorithms for the t-copula parameters exhibit a significantly lower complexity but do not degrade the accuracy of our model. The validation was made using the KL divergence. This again justifies the proposed t-copula α-stable model.

Chapter 5

Receiver Design in IoT networks

In previous chapters, we studied and characterized the interference in IoT networks. The marginal interference is well modeled as α-stable and the joint distribution of the interference vector is fitted with different interference models which reflect the service rate p.

At the receiver side, the received signal is mixed with this additive interference, which we consider as a noise. The optimal decoding strategy in the interference-limited regime is based on ML. We recall here the problem to be solved as discussed in Section 2.7, equation (2.13).

$$\max_{\mathbf{X}} f_{\mathbf{Z}}(\mathbf{Y} - \mathbf{g}\mathbf{X}),$$

where $f_{\mathbf{Z}}(\cdot|\mathbf{X}, \mathbf{g})$ is the PDF of the interference, given that the symbol $\mathbf{X}$ is transmitted, and the channel coefficient is $\mathbf{g}$.

Calculating (2.13) requires the evaluation of the measure $f_{\mathbf{Z}}(\cdot)$, which is tricky to implement in the sense that it requires the knowledge of the joint PDF of the interference vector.

Although the marginals have been proved to be symmetric α-stable, their densities are not known in closed form except for a few values of α: $\alpha = 0.5$, 1, and 2. What is more, the joint distribution of $\mathbf{z}$ is not known in the general case, and it may even not be joint α-stable [Ega+18; Zhe+19a]. As such, getting the densities of the interference vector involves more computation for estimation and non-linear signal processing. Due to the constraints of IoT features, i.e., low power, low cost and low complexity, IoT devices cannot afford to employ too complicated receiver structure. Therefore, a viable solution is through the sub-optimal receiver based on linear combining. Compared with optimal receiver from ML, linear combining is easier and simpler to implement as it only requires the knowledge of optimal weights w_i.

In the following, we will focus on the linear receiver. It appears that the optimal combiner with sub-Gaussian α-stable interference, i.e. when p

is close or equal to 1, is Maximum Ratio Combining (MRC). Even if it remains suboptimal in a more general context, when $0 < p < 1$, its simplicity justifies a careful study of its performance in such settings. We provide an exact characterization of the interference random vector and show that it is, in fact, α-stable as a random vector. Using this exact characterization, we derive the optimal combiner.

In this chapter, we evaluate the impact of the interference on the receiver design in terms of BER. For the ease of analysis, we made some modifications on the model proposed in Chapter. 2.

5.1　Previous works

In the following, we do not try to be exhaustive about the existing receiver strategies but instead give a few details about previous works about receiver design in impulsive noise, α-stable or not. It is to be noted that most of these works rely on an *i.i.d.* assumption.

5.1.1　Noise distribution approximation

When the interference distribution is too complex to be handled, a first way to solve (2.13) is to find a distribution that would approximate well the true interference PDF $f_{\mathbf{Z}}(\cdot)$ with an analytical expression and parameters that can be simply estimated. Erseghe *et al.* used a Gaussian mixture for UWB communications [ECD08]. In [Nam+06], the ϵ-contaminated is used to study the impact of impulsive noise on Parity Check Codes. However, the importance to take the real noise model into account during the decoding is underlined. And a review on the receiver design in the UWB case can be found in [BY09]. For instance, Fiorina [Fio06] proposed a receiver based on a generalized Gaussian distribution approximation. Beaulieu and Niranjayan [BN10] considered a mixture of Laplacian and Gaussian noise. The Cauchy model is proposed in [Gha+10]. Each solution is shown to significantly improve the performance in their specific context.

5.1.2　LLR inspired solutions

When noise is impulsive, the optimal Log-Likelihood Ratio (LLR) is no longer a monotonic increasing function but tends to reduce the weight of large values in the decision, as shown in the case of α-stable distributions in [Dim+14]. It means that we should not trust large positive or negative received values, contrary to the decision weight that the linear receiver would attribute.

This idea leads to a modification of the LLR function, and classical examples are the soft limiter and the hole puncher [NS95; AIH94; TNS95; SMET12; Maa+13]. For small received samples, a linear function is used;

and for large samples, respectively, a constant value or a zero are used as output of the LLR function. Another approximation is given by [Mes+19]:

$$LLR(y) = \text{sign}(y) \min\left(a\,|y|, \frac{b}{|y|}\right), \tag{5.1}$$

where $\text{sign}(x)$ is the sign of x. It was proposed in [Dim+14] for Low-Density Parity-Check (LDPC) codes. The model fits the linear part of the LLR for small values of x, and the $1/x$ approximation is inspired from the limit of the likelihood ratio for high values of x in the α-stable case. Parameters a and b are estimated with different methods. Good results are obtained in α-stable and Middleton class A interference.

Other works for weak signal detection approximate the function $f'_{\mathbf{Z}}(.)/f_{\mathbf{Z}}(.)$ where $f'(.)$ is the derivative of $f(.)$. Zozor *et al.* [ZBA06], for instance, used a polynomial approximation of the function. Spaulding and Middleton [SM77a; SM77b] proposed optimal and suboptimal strategies for coherent and non-coherent detection in Middleton Noises. In the coherent case, the optimal detector necessitates evaluating a ratio of infinite sums, too complex to be implemented. A locally optimum detector is proposed, using a series expansion for small signals. It results in applying a logarithm to the received signal followed by the linear operation.

5.1.3 Linear approaches

The previous approaches induce approximation on the interference distribution and do not completely resolve the issue of complexity. It is then important to evaluate the linear approaches for their simple implementation structures. It is well known that MRC maximizes the Signal-to-Noise Ratio (SNR) in Gaussian noise. In [Joh96], Johnson proposes a general study of linear optimal receivers in non-Gaussian noise and takes the specific example of α-stable noise. This is further studied for a rake receiver in [NB08; NB09; NB10] and for diversity combining schemes in a multi-antenna receiver in [CE12] in presence of symmetric α-stable interference.

Previous works have assumed *i.i.d.* additive impulsive noise or interference. Recently, few works considered the receiver under dependent α-stable interference. We can find the first trials in [Yan+15; Sor+17], which introduce copula for modeling dependence. In the following, we are focusing on the linear receiver strategy. It offers a low complexity and is optimal, as we will see, in the sub-Gaussian α-stable case.

5.2 System model

As fully described in Chapter 2, we consider a Single-Input and Single-Output (SISO) system on K orthogonal msBs, each containing N eRBs. The transmitter seeks to send a binary symbol $x \in \{+1, -1\}$. We simplify (2.12)

by choosing a repetition code for the source, meaning that the transmitted word is composed of NK_0 times the same bit x. Given x, the receiver observes an output $\mathbf{y} \in \mathbb{R}^{2NK_0}$ defined by

$$\mathbf{y} = \mathbf{h}x + \mathbf{z} + \mathbf{n}, \tag{5.2}$$

where $\mathbf{h} \in \mathbb{R}^{2NK_0}$ corresponds to channel fading and $\mathbf{z} \in \mathbb{R}^{2NK_0}$ is the interference in a set of NK_0 orthogonal eRBs, real and imaginary parts. $\mathbf{n}$ is the thermal noise. The channel fading is assumed to be perfectly known to the receiver; e.g., using pilots to estimate CSI.

The statistical model for the interference $\mathbf{z}$ was introduced in Chapter 2. For the analytical derivations we will only consider a network of the interfering devices located according to the HPPP over the whole plane, denoted by Φ with intensity λ. We further assume that the thermal noise has a negligible impact on the distribution of $\mathbf{z} + \mathbf{n}$ and can be ignored.

After stacking the interference on each eRB, real and imaginary parts, the resulting interference random vector is given by $\mathbf{z} = (z_1, \ldots, z_{2NK_0})^T$. Each component can be modeled by an α-stable distributed random variable. Theorem 3.2.1 gives their (marginal) distributions:

Theorem 5.2.1. *Consider the interference on a given eRB, real or imaginary part, denoted by z_i:*

$$z_i = \sum_{j \in \Phi_i} r_j^{-\frac{\eta}{2}} x_{j,i}, \quad i \in \{1, \cdots, K\}, \tag{5.3}$$

where Φ_i is the set of interferers that transmit on the i-th eRB, r_j is the distance from device j in Φ_i to the desired receiver, η is the path-loss exponent, and $x_{j,i} \in \mathbb{R} \sim \mathcal{N}(0, \sigma_I^2)$ are i.i.d. and correspond to the combination of baseband emission and small-scale fading.

Then, z_i converges almost surely to a symmetric $4/\eta$-stable random variable with the scale parameter given by

$$\gamma_{z_i} = \left(\pi \lambda p C_{\frac{4}{\eta}}^{-1} \mathbb{E}[|x_{j,i}|^{\frac{4}{\eta}}] \right)^{\frac{\eta}{4}}, \tag{5.4}$$

where C_α is given in (3.11).

Given the observation $\mathbf{y}$ and equally likely symbols (i.e., $+1$ and -1), the BER is minimized by the LLR test

$$\Lambda(\mathbf{y}) = \frac{f(\mathbf{y}|x=1)}{f(\mathbf{y}|x=-1)} \overset{x=1}{\underset{x=-1}{\gtrless}} 1. \tag{5.5}$$

Due to the interference models studied in previous chapters, the likelihoods in (5.5) do not admit tractable closed-form solutions. Consequently,

we will base our decoding on a statistic obtained from linear combining. The resulting detection rule is then given by

$$\tilde{y} = \mathbf{w}^T \mathbf{y} \underset{x=-1}{\overset{x=1}{\gtrless}} 0, \tag{5.6}$$

where the weights $\mathbf{w} \in \mathbb{R}^{2NK_0}$ satisfy $\|\mathbf{w}\| = 1$.

5.3 Optimal linear receiver for sub-Gaussian α-stable interference

When the network is heavily loaded, i.e., p close to one, the set of interference is the same on all eRBs, which means that the set of interferers verifies $\Phi_i = \Phi$ almost surely. In that case, as shown in Section 4.2.2, the interference vector $\mathbf{z}$ is sub-Gaussian α-stable.

The optimal linear combiner is well known in the case of Gaussian noise. It has also been studied in more general non-Gaussian settings [Joh96] and the optimal weights $\mathbf{w}$ are known for the *i.i.d.* symmetric α-stable interference case [NB09; NB10].

However, when the *i.i.d.* assumption is dropped, for instance with the sub-Gaussian α-stable interference we consider, little work has been proposed.

5.3.1 Optimal linear combiner when $p = 1$

Assume $\mathbf{z}$ is sub-Gaussian α-stable. We take $x \in \{+1, -1\}$ with equal probability. Using the linear detection rule in (5.6), the BER can be expressed by

$$P_e(\mathbf{w}) = \frac{1}{2} \left[\mathbb{P}(\mathbf{w}^T \mathbf{y} > 0 | x = -1) + \mathbb{P}(\mathbf{w}^T \mathbf{y} \leq 0 | x = 1) \right]. \tag{5.7}$$

Expressing $\mathbf{y}$ with (5.2), it follows that

$$\mathbb{P}(\mathbf{w}^T \mathbf{y} > 0 | x = -1) = \mathbb{P}(-\mathbf{w}^T \mathbf{h} + \mathbf{w}^T \mathbf{z} > 0)$$
$$= \mathbb{P}(\mathbf{w}^T \mathbf{z} > \mathbf{w}^T \mathbf{h}), \tag{5.8}$$

and

$$\mathbb{P}(\mathbf{w}^T \mathbf{y} \leq 0 | x = 1) = \mathbb{P}(\mathbf{w}^T \mathbf{h} + \mathbf{w}^T \mathbf{z} \leq 0)$$
$$= \mathbb{P}(\mathbf{w}^T \mathbf{z} \geq \mathbf{w}^T \mathbf{h}). \tag{5.9}$$

Therefore, we have

$$P_e(\mathbf{w}) = \mathbb{P}(\mathbf{w}^T \mathbf{z} \geq \mathbf{w}^T \mathbf{h}). \tag{5.10}$$

Since $\mathbf{z}$ is a sub-Gaussian α-stable, a special case of a symmetric α-stable random vector, $\mathbf{w}^T\mathbf{z}$ is symmetric α-stable according to Theorem B.2.22. The optimal linear combiner is given in the following theorem.

Theorem 5.3.1. *Let $\mathbf{z}$ be a sub-Gaussian α-stable random vector with underlying Gaussian vector $\mathbf{G} \sim \mathcal{N}(0, \sigma_{\mathbf{z}}\mathbf{I})$ and parameter $\sigma_{\mathbf{z}} > 0$. Then, the optimal weight vector $\mathbf{w}$ minimizing the BER in (5.10) is given by*

$$\mathbf{w} = \frac{\mathbf{h}}{\|\mathbf{h}\|}, \tag{5.11}$$

where $\|\mathbf{h}\|$ is the Euclidean norm of $\mathbf{h}$. That is, the optimal linear combiner is maximal ratio combining.

Proof. We first establish that

$$P_e(\mathbf{w}) = \mathbb{P}\left(\tilde{z} > \frac{1}{\|\mathbf{w}\|}\mathbf{w}^T\mathbf{h} \right), \tag{5.12}$$

where

$$\tilde{z} = \frac{1}{\|\mathbf{w}\|}\mathbf{w}^{\mathbf{T}}\mathbf{z} \sim \mathcal{S}_\alpha\left(\gamma_{\mathbf{z}}, 0, 0\right), \quad \gamma_{\mathbf{z}} = \frac{\sigma_{\mathbf{z}}}{\sqrt{2}}. \tag{5.13}$$

Since $\mathbf{z}$ is sub-Gaussian α-stable with parameter $\sigma_{\mathbf{z}}$, it admits the scale-mixture representation

$$\mathbf{z} = A^{\frac{1}{2}}(G_1, G_2, \ldots, G_{2NK_0})^T, \tag{5.14}$$

where $A \sim S_{\alpha/2}\left(\left(cos\frac{\pi}{4}\alpha\right)^{2/\alpha}, 1, 0\right)$ and $G_k \sim \mathcal{N}(0, \sigma_{\mathbf{z}})$, $k = 1, \ldots, 2NK_0$, all independent. As such,

$$\mathbf{w}^T\mathbf{z} = A^{\frac{1}{2}}\sum_{k=1}^{2NK_0} w_k G_k \overset{d}{=} A^{\frac{1}{2}}\tilde{G}, \tag{5.15}$$

where $\tilde{G} \sim \mathcal{N}\left(0, \sigma_{\mathbf{z}}^2 \sum_{k=1}^{2NK_0} w_k^2\right)$, which after dividing by $\|\mathbf{w}\|$ yields (5.13).

By the fact that $\tilde{z} \sim \mathcal{S}_\alpha\left(\gamma_{\mathbf{z}}, 0, 0\right)$—i.e., the parameters are independent of $\mathbf{w}$—in (5.12) and the cumulative distribution of $\tilde{z}$ is non-decreasing, it follows that minimizing $P_e(\mathbf{w})$ is equivalent to maximizing $\frac{1}{\|\mathbf{w}\|}\mathbf{w}^T\mathbf{h}$.

Applying the Cauchy-Schwarz inequality then yields

$$|\mathbf{w}^T\mathbf{h}|^2 \leq \|\mathbf{w}\|^2\|\mathbf{h}\|^2. \tag{5.16}$$

In (5.16), equality holds if and only if $\mathbf{w}$ and $\mathbf{h}$ are linearly dependent; i.e., $\mathbf{w} = c\mathbf{h}$, for some $c > 0$. Setting $c = \frac{1}{\|\mathbf{h}\|}$ to satisfy the constraint $\|\mathbf{w}\| = 1$, the equality (5.11) is obtained. $\square$

5.3.2   Bit error rate

We now want to characterize the BER when the interference random vector is sub-Gaussian α-stable. The basis of the analysis is the following lemma of symmetric α-stable random variables, which is derived from Property B.2.12 in Appendix B.

Lemma 5.3.2. *Let $X \sim S_\alpha(\gamma, 0, 0)$. Then as $b \to \infty$,*

$$\mathbb{P}(X > b) = \frac{1}{2}C_\alpha \gamma^\alpha b^{-\alpha} + o(b^{-\alpha}), \tag{5.17}$$

where C_α is given in (3.11).

   With Lemma 5.3.2, it is straightforward to characterize the BER. We note $n = 2NK_0$, and we have the following theorem:

Theorem 5.3.3. *Let $\mathbf{z}$ be an n-dimensional sub-Gaussian α-stable random vector with underlying Gaussian vector $\mathbf{G} \sim \mathcal{N}(0, \sigma_\mathbf{z}^2 \mathbf{I})$ and the linear combining weights be $\mathbf{w} \in \mathbb{R}^n$. Then, as $\|\mathbf{h}\| \to \infty$,*

$$P_e(\mathbf{w}) = \frac{1}{2}C_\alpha \gamma_\mathbf{z}^\alpha \left(\frac{1}{\|\mathbf{w}\|}\mathbf{w}^T\mathbf{h} \right)^{-\alpha} + o\left(\left(\frac{1}{\|\mathbf{w}\|}\mathbf{w}^T\mathbf{h} \right)^{-\alpha} \right), \tag{5.18}$$

where $\gamma_\mathbf{z} = \sigma_\mathbf{z}/\sqrt{2}$.

   When the optimal linear weights are used, the BER is given by

$$P_e(\mathbf{h}) = \frac{1}{2}C_\alpha \gamma_\mathbf{z}^\alpha \|\mathbf{h}\|^{-\alpha} + o(\|\mathbf{h}\|^{-\alpha}). \tag{5.19}$$

Proof. We apply Lemma 5.3.2 to calculate (5.12). To do so we replace X and b with $\tilde{z}$ and $\frac{1}{\|\mathbf{w}\|}\mathbf{w}^T\mathbf{h}$ and apply (5.17). This directly gives us (5.18). $\qquad\square$

   One observation is that the form of BER in (5.18) bears striking similarities with the BER of linear combining in Rayleigh fading with Gaussian noise. In particular, the exponent α plays a role similar to a fractional diversity gain with the key difference from the Rayleigh fading scenario that it lies in $0 < \alpha < 2$. Similarly, the factor $\frac{1}{2}C_\alpha \gamma_\mathbf{z}^\alpha$ plays the role of an array gain.

5.4   Optimal linear receiver for general α-stable interference

We now turn to the general interference model detailed in Section 4.1. We study the case in two dimensions. It means we consider two msBs containing a single eRB, and the transmission is made with real signal (no complex digital modulation schemes), which is different with the model in Section 4.1. This real-valued model arises in the case where signaling is only

performed on either the in-phase or quadrature components. This choice offers us a clear way to explicitly write analytical analysis. The framework can, however, be extended to higher dimensions.

We first establish that the interference random vector remains symmetric α-stable. This is non-trivial as, unlike the Gaussian noise case, a random vector with symmetric α-stable marginals is not necessarily symmetric α-stable as a random vector, which is formally defined in Appendix B. We then develop new bounds on the error probability.

5.4.1   Interference statistics

Let Φ be a HPPP with intensity λ. We consider two msBs containing a single eRB. The transmission is made with one-dimensional digital modulation schemes (e.g. BPSK). Under the model in Section 5.2, the interference on each eRB is given by

$$z_1 = \sum_{j \in \Phi_1} r_j^{-\frac{\eta}{2}} x_{j,1}, \tag{5.20}$$

$$z_2 = \sum_{j \in \Phi_2} r_j^{-\frac{\eta}{2}} x_{j,2}, \tag{5.21}$$

where $x_{j,i}$, $i = 1, 2$ is defined in (5.3).

A general exact characterization of the interference random vector $\mathbf{z} = [z_1, z_2]^T$ is given in the following theorem.

Theorem 5.4.1. *The interference random vector $\mathbf{z} = (z_1, z_2) \in \mathbb{R}^2$ given by (5.20) and (5.21) has the CF*

$$\begin{aligned}
\Phi_{\mathbf{z}}(\boldsymbol{\theta}) &= \mathbb{E}\left[\exp\{i(\theta_1 z_1 + \theta_2 z_2)\}\right] \\
&= \exp\left(i\gamma_1^\alpha |\theta_1^2 + \theta_2^2|^{\frac{\alpha}{2}} + i\gamma_2^\alpha |\theta_1|^\alpha + i\gamma_2^\alpha |\theta_2|^\alpha\right),
\end{aligned} \tag{5.22}$$

where

$$\gamma_1 = \sigma_I \left(\pi\lambda p^2 C_{\frac{4}{\eta}}^{-1} \mathbb{E}[|Z_0|^{\frac{4}{\eta}}]\right)^{\frac{\eta}{4}},$$

$$\gamma_2 = \sigma_I \left(\pi\lambda p(1-p) C_{\frac{4}{\eta}}^{-1} \mathbb{E}[|Z_0|^{\frac{4}{\eta}}]\right)^{\frac{\eta}{4}} \tag{5.23}$$

with $Z_0 \sim \mathcal{N}(0,1)$. That is, $\mathbf{z}$ is a symmetric α-stable random vector with spectral measure on the unit sphere $\mathbb{S}^1$ of $\mathbb{R}^2$ given by $\Gamma = \Gamma_1 + \Gamma_2$, with Γ_1 uniform on $\mathbb{S}^1$ and Γ_2 concentrated on $(\pm 1, 0), (0, \pm 1)$.

Proof. Since each device independently chooses to access each eRB B_i, $i = 1, 2$ with probability p, it follows that the processes $\Phi_1 \cup \Phi_2$, $\Phi_1 \setminus \Phi_2$ and

$\Phi_2 \setminus \Phi_1$ are independent HPPPs with intensities, respectively.

$$\lambda_1 = p^2\lambda,$$
$$\lambda_2 = \lambda_3 = p(1-p)\lambda. \qquad (5.24)$$

The CF $\Phi_{\mathbf{z}}(\boldsymbol{\theta})$ is then given by

$$\Phi_{\mathbf{z}}(\boldsymbol{\theta}) = \mathbb{E}[\exp\{i(\theta_1 z_1 + \theta_2 z_2)\}]$$
$$= \exp\left\{i\left[\sum_{k_1 \in \Phi_1 \cup \Phi_2} r_{k_1}^{-\frac{\eta}{2}}(\theta_1 x_{k_1,1} + \theta_2 x_{k_1,2})\right.\right.$$
$$\left.\left. + \sum_{k_2 \in \Phi_1 \setminus \Phi_2} r_{k_2}^{-\frac{\eta}{2}}\theta_1 x_{k_2,1} + \sum_{k_3 \in \Phi_2 \setminus \Phi_1} r_{k_3}^{-\frac{\eta}{2}}\theta_2 x_{k_3,2}\right]\right\}. \qquad (5.25)$$

Noting that $\{r_{k_j}^2\}$ are one-dimensional Poisson point process with parameters $\pi\lambda_j$ [IH98] and using the LePage series representation of symmetric α-stable random variables [ST94, Corollary 1.4.3], it follows that

$$V_1 = \sum_{k_1 \in \Phi_1 \cup \Phi_2} r_{k_1}^{-\frac{\eta}{2}}(\theta_1 x_{k_1,1} + \theta_2 x_{k_1,2}),$$
$$V_2 = \sum_{k_2 \in \Phi_1 \setminus \Phi_2} r_{k_2}^{-\frac{\eta}{2}}\theta_1 x_{k_2,1},$$
$$V_3 = \sum_{k_3 \in \Phi_2 \setminus \Phi_1} r_{k_3}^{-\frac{\eta}{2}}\theta_2 x_{k_3,2} \qquad (5.26)$$

are each independent symmetric α-stable random variables. In particular, let $Z_0 \sim \mathcal{N}(0, 1)$, then

$$V_1 \sim \mathcal{S}_\alpha\left(\sigma_I\sqrt{\theta_1^2 + \theta_2^2}\left(\pi\lambda p^2 C_\alpha^{-1}\mathbb{E}[|Z_0|^\alpha]\right)^{\frac{1}{\alpha}}, 0, 0\right),$$
$$V_2 \sim \mathcal{S}_\alpha\left(\sigma_I|\theta_1|\left(\pi\lambda p(1-p)C_\alpha^{-1}\mathbb{E}[|Z_0|^\alpha]\right)^{\frac{1}{\alpha}}, 0, 0\right),$$
$$V_3 \sim \mathcal{S}_\alpha\left(\sigma_I|\theta_2|\left(\pi\lambda p(1-p)C_\alpha^{-1}\mathbb{E}[|Z_0|^\alpha]\right)^{\frac{1}{\alpha}}, 0, 0\right), \qquad (5.27)$$

where $\alpha = \frac{4}{\eta}$.

As such,

$$V = V_1 + V_2 + V_3 = \theta_1 z_1 + \theta_2 z_2 \qquad (5.28)$$

is also a symmetric α-stable random variable, irrespective of the choice $\boldsymbol{\theta} \in \mathbb{R}^2$. Specifically, we have

$$V \sim \mathcal{S}_\alpha\left(\sigma_I\left[p^2(\theta_1^2 + \theta_2^2)^{\frac{\alpha}{2}} + p(1-p)(|\theta_1|^\alpha + |\theta_2|^\alpha)\right]^{\frac{1}{\alpha}}\left(\pi\lambda C_\alpha^{-1}\mathbb{E}[|Z_0|^\alpha]\right)^{\frac{1}{\alpha}}, 0, 0\right),$$
$$(5.29)$$

where $\alpha = \frac{4}{\eta}$.

By Theorem 2.1.5 in [ST94], it then follows that $\mathbf{z}$ is a symmetric α-stable random vector with its CF given by

$$\begin{aligned}
\Phi_{\mathbf{z}}(\boldsymbol{\theta}) &= \mathbb{E}[\exp\{i(\theta_1 z_1 + \theta_2 z_2)\}] \\
&= \mathbb{E}[\exp\{ibV\}]|_{b=1} \\
&= \exp\left(i\gamma_1^\alpha|\theta_1^2 + \theta_2^2|^{\frac{\alpha}{2}} + i\gamma_2^\alpha|\theta_1|^\alpha + i\gamma_2^\alpha|\theta_2|^\alpha\right),
\end{aligned} \tag{5.30}$$

where γ_1 and γ_2 are given in (5.23). $\qquad\qquad\square$

As expected, when $p \to 1$, we recover the sub-Gaussian α-stable CF studied in Section 5.3.

5.4.2   Optimal linear combining

We now study the BER for the general interference statistics in Theorem 5.4.1.

Theorem 5.4.2. *Let $\mathbf{z}$ have the CF given in Theorem 5.4.1, corresponding to the general interference model in Section 5.4.1. Then, the optimal combining weights are the solution of*

$$\max_{\mathbf{w}\in\mathbb{R}^2:\|\mathbf{w}\|=1} \frac{\mathbf{w}^T\mathbf{h}}{\left[\gamma_1^\alpha(w_1^2 + w_2^2)^{\frac{\alpha}{2}} + \gamma_2^\alpha|w_1|^\alpha + \gamma_2^\alpha|w_2|^\alpha\right]^{\frac{1}{\alpha}}}. \tag{5.31}$$

Proof. According to (5.10), the BER is given by

$$P_e = \mathbb{P}\left(w_1 z_1 + w_2 z_2 > w_1 h_1 + w_2 h_2\right). \tag{5.32}$$

Now,

$$\begin{aligned}
&w_1 z_1 + w_2 z_2 \\
&= \sum_{k\in\Phi_1\cap\Phi_2} r_k^{-\frac{\eta}{2}}(w_1 x_{k,1} + w_2 x_{k,2}) + \sum_{k\in\Phi_1\setminus\Phi_2} w_1 r_k^{-\frac{\eta}{2}} x_{k,1} + \sum_{k\in\Phi_2\setminus\Phi_1} w_2 r_k^{-\frac{\eta}{2}} x_{k,1}.
\end{aligned} \tag{5.33}$$

Suppose that $x_{k,j} \sim \mathcal{N}(0, \sigma_I^2)$ and call the three terms above V_1, V_2, V_3, respectively. Then

$$V_1 \sim S_\alpha\left(\gamma_1\sqrt{w_1^2 + w_2^2}, 0, 0\right),$$

$$V_2 \sim S_\alpha(\gamma_2|w_1|, 0, 0),$$

$$V_3 \sim S_\alpha(\gamma_2|w_2|, 0, 0). \tag{5.34}$$

As such,

$$w_1 z_1 + w_2 z_2 \sim S_\alpha \left(\left(\gamma_1^\alpha (w_1^2 + w_2^2)^{\frac{\alpha}{2}} + \gamma_2^\alpha |w_1|^\alpha + \gamma_2^\alpha |w_2|^\alpha \right)^{\frac{1}{\alpha}}, 0, 0 \right). \quad (5.35)$$

Hence,

$$P_e = \mathbb{P} \left(N > \frac{\mathbf{w}^T \mathbf{h}}{\left(\gamma_1^\alpha (w_1^2 + w_2^2)^{\frac{\alpha}{2}} + \gamma_2^\alpha |w_1|^\alpha + \gamma_2^\alpha |w_2|^\alpha \right)^{\frac{1}{\alpha}}} \right), \quad (5.36)$$

where $N \sim S_\alpha(1, 0, 0)$.

An examination of (5.36), reveals that scaling $\mathbf{w}$ does not affect the BER. Without loss of generality, we therefore set $\|\mathbf{w}\| = 1$. Under this condition $w_1^2 + w_2^2 = 1$, the optimal weights are given by the solution of (5.31). $\qquad \square$

5.5 Numerical results

5.5.1 Sub-Gaussian α-stable interference

In this section, we validate our analysis by evaluating the BER through Monte Carlo simulations. To study the BER in the presence of sub-Gaussian α-stable interference as described in Section 5.3, we set $\gamma_\mathbf{z} = 1$, $\alpha = 0.8$ and $x = \pm 1$. For the clarity of illustration, we select a single channel vector

$$\begin{aligned} \mathbf{h} = \sqrt{\rho} \times [&0.0949, 0.3237, 0.3988, 0.1522, 0.0563, 0.2308 \\ &0.0765, 0.0605, 0.6317, 0.4889], \end{aligned} \quad (5.37)$$

where $\|\mathbf{h}\|^2 = \rho$.

The system behavior under this choice of channel vector is representative. Indeed, it was validated through an extensive simulation study for other choices of $\mathbf{h}$. While it is also possible to study the average behavior under, for example, Rayleigh fading, the choice of a fixed $\mathbf{h}$ enables an easier interpretation of the resulting curves.

Fig. 5.1 plots BER for varying $\|\mathbf{h}\|^2 = \rho$ and both the optimal combiner, i.e., MRC (by Theorem 5.3.1) and Equal Gain Combining (EGC) as a comparison. As expected from Theorem 5.3.1, the MRC combiner performs better than EGC, even if the gap is limited. In fact in such impulsive interference ($\alpha = 0.8$), the RB with a set including one or several strong interferers is difficult to recover, whatever the combining solution used. For small values of $\|\mathbf{h}\|$—that is, the received signal is very week compared to the interference— the gap disappears between MRC and EGC, but this is not relevant because interference is strong and the situation is bad on every channel. However, as $\|\mathbf{h}\|$ increases, the gap becomes obvious. Moreover, the asymptotic approximation of the BER of sub-Gaussian α-stable in (5.19) of Theorem 5.3.3, is plotted as well. It is in very good agreement with the
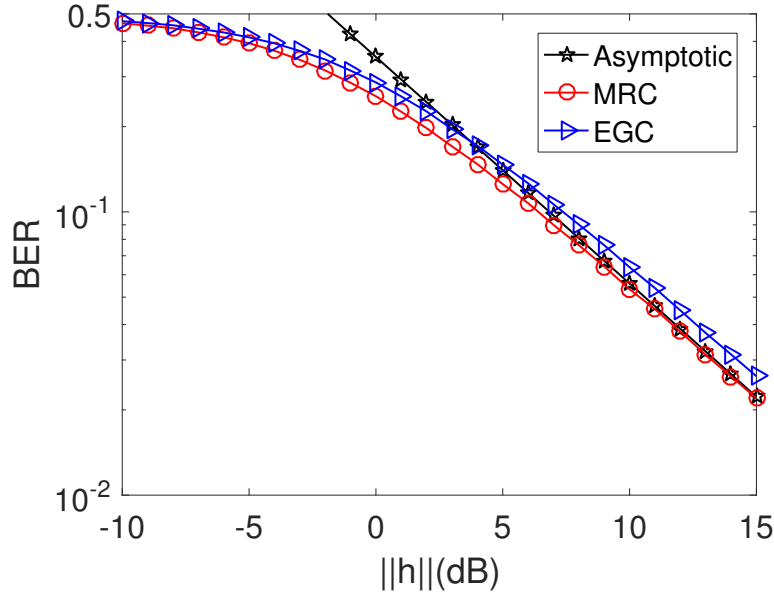
FIGURE 5.1: Bit error rates comparison of MRC and EGC
for sub-Gaussian α-stable interference under different $\|h\|$
with $K = 10$ channels, $\gamma_{\mathbf{z}} = 1$, $\alpha = 0.8$ and $x = \pm 1$.

Monte Carlo simulation for sufficiently large $\|\mathbf{h}\|$. For large values of $\|\mathbf{h}\|$, the curves for MRC and EGC become straight lines, which can be deduced from (5.18).

5.5.2 Symmetric α-stable random vector

We now turn to the model in Section 5.4.1 in 2 dimensions. To validate the model is consistent with Theorem 5.4.1, we first make a visual inspection of the samples simulated from the system model and the samples generated from (5.22). They are plotted in Fig. 5.2 and the corresponding joint PDFs in Fig. 5.3.

We can observe that the samples and the joint PDF from the model in Theorem 5.4.1 are consistent with the samples and the joint PDF from the simulated set detailed in Section 4.1.

Fig. 5.4 plots the BER for varying p with parameters: $\lambda = 0.001$ m^{-2}, $\|\mathbf{h}\| = 10^{-3}$, $\eta = 5$, and $\sigma_I = 1$. Optimal linear combining (OLC) based on Theorem 5.4.2, MRC and EGC are considered.

The BER for $p \approx 1$ under OLC and MRC approximately equal. This is consistent with the result of Theorem 5.3.1, stating that the optimal combiner for sub-Gaussian α-stable interference is MRC.

In Fig. 5.4, when p is low, i.e., each device transmits with a low probability, and the BER gets smaller, which is consistent with the fact that interference becomes smaller.

(A) Simulated samples.

(B) Model in (5.22).
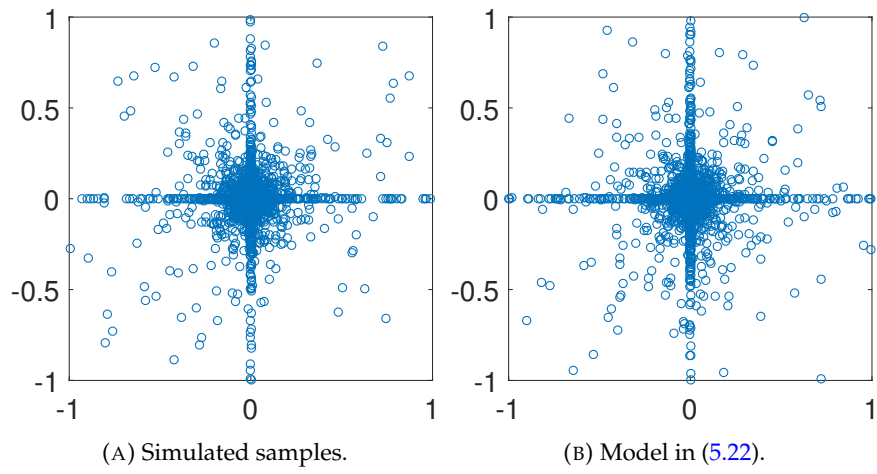
FIGURE 5.2: Scatter plots of the interference random vector with $p = 0.5$, $\lambda = 0.001 \ \mathrm{m}^{-2}$, $\eta = 5$, and $\sigma_I = 1$.

(A) Simulated samples.

(B) Model in (5.22).
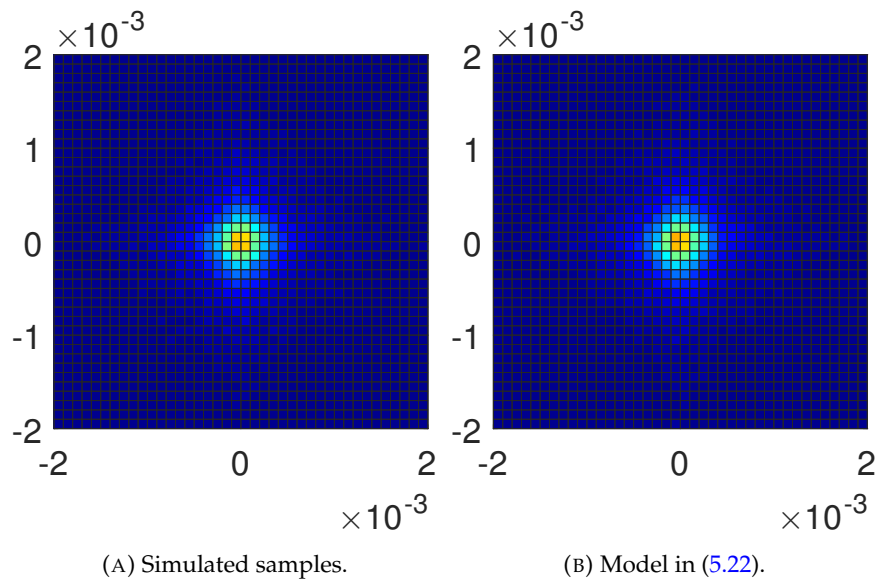
FIGURE 5.3: Probability density functions of the interference random vector with settings as in Fig. 5.2.
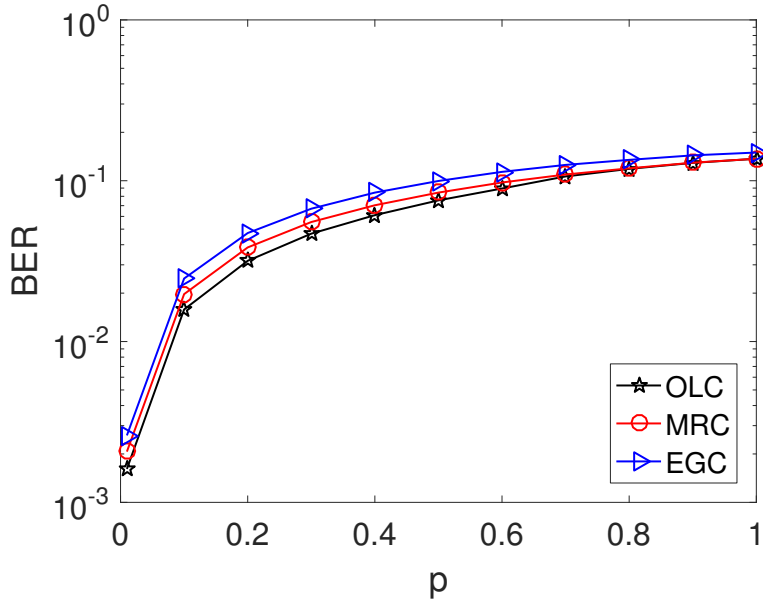
FIGURE 5.4: Bit error rates of OLC, MRC and EGC under different p with $\lambda = 0.001$ m^{-2}, $\|\mathbf{h}\| = 10^{-3}$, $\eta = 5$, and $\sigma_I = 1$.

Increasing p changes the statistics of the interference vector in two ways. First, it increases the scale parameter of each marginal—i.e., γ_{z_i} given in (5.4)– leading to a higher BER. Second, the dependence structure is modified, and the interference vector becomes approximately sub-Gaussian α-stable when $p \approx 1$, which—for equal scale parameters—reduces the BER.

In particular, for the sub-Gaussian α-stable and independent α-stable vector with the same marginal distributions, the scale parameter—$\gamma_\mathbf{w}$ of the weighted sum $z_w = w_1 z_1 + w_2 z_2$—is different. Observe that $\gamma_\mathbf{w}$ for sub-Gaussian α-stable is less than $\gamma_\mathbf{w}$ for independent case. For instance, when $z_w = w_1 z_1 + w_2 z_2$, $w_1 = w_2 = 1$ and $z_i \sim S_\alpha(1, 0, 0)$, we have $\gamma_\mathbf{w} = \sqrt{2}$ for (z_1, z_2) following sub-Gaussian α-stable and $\gamma_\mathbf{w} = 2^{1/\alpha}$ for independent α-stable.

We conclude from Fig. 5.4 that increasing p will increase the scale parameter of the marginal interference and therefore increase the scale parameter, γ_w of their weighted sum. On the other hand, the increase of p also changes the dependence structure of the interference vector, which makes it more "sub-Gaussian", which decrease the scale parameter γ_w. But the former takes dominance.

5.5.3 General case and non-linear receiver.

We now turn to the general scenario from Chapter 4. In this section, we study the impact of the dependence structure, parametrized by the service rate p, on the receiver performance. To do so, we use our tractable interference models detailed in Section 4.2.

The simulation is as follows. We assume that a transmitter seeks to send a binary symbol $x \in \{+1, -1\}$ in the presence of interference. We choose $K_0 = 4$ msBs with $N = 2$ eRBs per msB, i.e., an interference vector of dimension $2NK_0 = 16$.

Given the transmitted symbol x, the receiver observes an output $\mathbf{y} \in \mathbb{R}^{2NK_0}$ defined by

$$\mathbf{y} = \mathbf{g}Ax + \mathbf{z}, \tag{5.38}$$

where $A = \sqrt{P}r^{-\eta/2}$ is the combination of path loss and transmitted signal power P, $\mathbf{g} \in \mathbb{R}^{2NK_0}$ corresponds to channel fading stacking the real and imaginary components in NK_0 eRBs, and $\mathbf{z} \in \mathbb{R}^{2NK_0}$ is interference stacking the real and imaginary components in NK_0 eRBs, detailed in Section 4.1.

Each eRB experiences *i.i.d.* Rayleigh fading, i.e., $\mathbf{g} = [g_1, \cdots, g_{2NK_0}]$, where $g_i \sim \mathcal{N}(0, 1)$ is *i.i.d.*. We also assume that $\mathbf{g}$ for the desired link is known to the receiver, which comes to assuming that the channel estimation is perfect.

Given the observation $\mathbf{y}$ and equally likely symbols x, the probability of error is minimized by the likelihood ratio test

$$\Lambda(\mathbf{y}) = \frac{f(\mathbf{y}|x=1, \mathbf{g})}{f(\mathbf{y}|x=-1, \mathbf{g})} \underset{x=-1}{\overset{x=1}{\gtrless}} 1, \tag{5.39}$$

where $f(\cdot|x, \mathbf{g})$ is the PDF of the received signal given that the symbol x is transmitted and the fading is $\mathbf{g}$.

Applying the copula function, (5.39) is expressed as

$$\Lambda(\mathbf{y}) = \frac{f(\mathbf{y}|x=1, \mathbf{g})}{f(\mathbf{y}|x=-1, \mathbf{g})} \tag{5.40}$$
$$= \frac{c_{\mathbf{z}}(F(y_1 - g_1 A), \cdots, F(y_{2NK} - g_{2NK}A))}{c_{\mathbf{z}}(F(y_1 + g_1 A), \cdots, F(y_{2NK} + g_{2NK}A))} \prod_{i=1}^{2NK} \frac{f_{z_i}(y_i - g_i A)}{f_{z_i}(y_i + g_i A)},$$

where $f(z_i)$ are the densities of the marginals, and $c_{\mathbf{z}}(\cdot)$ is the density of copula.

To evaluate the impact of the receiver design, we consider the following solutions:

1. the *t-copula α-stable* receiver: it assumes that interference follows the *t*-copula α-stable model detailed in Section 4.2.3;

2. the MRC receiver: a linear combiner optimal for Gaussian and sub-Gaussian α-stable interference;
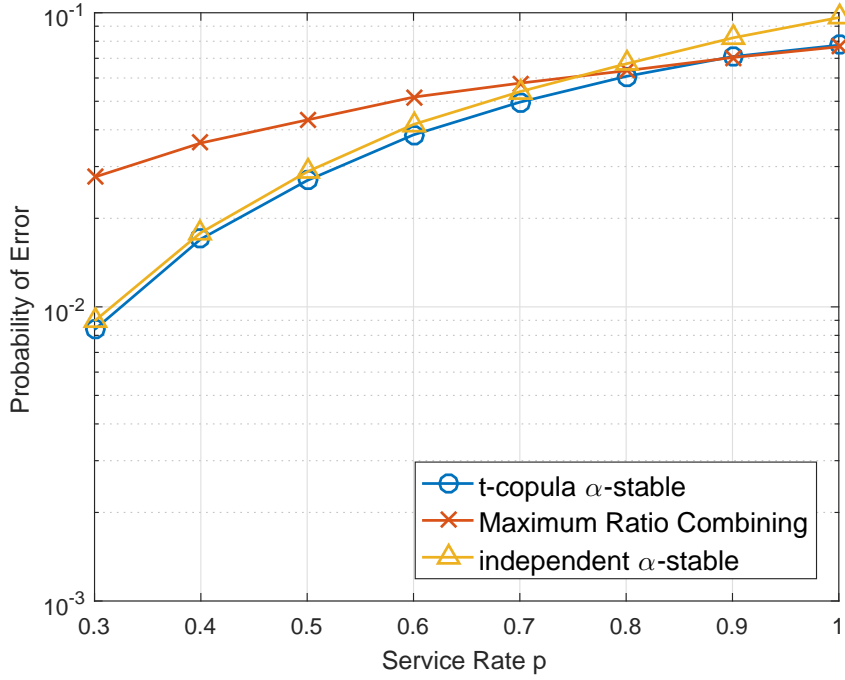
FIGURE 5.5: Probability of error under different service
rates, $\eta = 3$, $A = 0.01$ and $\lambda = 0.001$ devices/m^2.

3. the independent α-stable receiver: it assumes independent α-stable
components in the interference vector.

The α-stable densities can be computed using the method in [Nol97] via
the stblpdf MATLAB package [Sta]. The density of sub-Gaussian α-stable
distribution is given in [Nol13, eq.13]. The density of the t-copula α-stable
model is given in (4.15) and (C.24).

To evaluate the different models in terms of the probability of error, we
study the impact of the service rate, p. Recall that the service rate is the key
parameter which controls the dependence between interference on different
eRBs. In our study, we consider the following parameters:

- $h_{j,i} \sim \mathcal{CN}(0, 1)$;

- $\lambda = 0.001$ devices/m^2;

- $x_{j,i}$ is uniformly drawn from $\{+1, -1\}$, $\forall i, j$;

- $K_0 = 4$; and $N = 2$.

Fig. 5.5 gives the probability of error under each of the different re-
ceivers. The transmitted signal amplitude is $A = 0.01$. Results are based
on $200,000$ Monte Carlo iterations.

We observe that when $p \to 1$, the MRC receiver gives a lower BER than the other receivers. It is indeed optimal [Zhe+20] in sub-Gaussian α-stable interference. However, there is a negligible performance improvement over the t-copula α-stable receiver. As $p < 0.8$, the MRC receiver has significantly degraded performance.

On the other hand, the t-copula α-stable receiver exhibits better performance than the receiver tailored to independent α-stable noise [NB09; NB10], when $p \in [0.3, 1]$. This suggests that the t-copula α-stable receiver is a tractable means of obtaining improved performance for a wide range of network parameters.

5.6 Conclusion

The optimal linear receiver under the independent α-stable noise has been proved by Niranjayan[NB08; NB09; NB10] to be either MRC for $1 < \alpha < 2$ or Selection Combining (SC) for $0 < \alpha < 1$. However, the effect of dependent α-stable interference on receiver design was neglected and lacks study.

In this chapter, we prove that the optimal linear receiver is MRC in sub-Gaussian α-stable interference. This shows that the dependence structure, along with the marginal distributions, has a non-trivial impact. What is more, we also give an asymptotic approximation of the BER. Under 2 dimensions, we derive the exact CF of the interference. With the exact characterization of interference, we are able to study the impact of the service rate p, on the performance of linear receiver. For high dimensions, we study the impact of dependence structure on the performance with different receiver under different values of p. The p impacts the receiver in two different ways: First, it increases or reduces the scale parameter of marginal interference; Second, it changes the dependence structure of the interference. Results show that the t-copula has a better performance for a wide range of p. This allows us to account for this dependence structure and obtain a tractable receiver.

These preliminary results pave the way towards further studies. Knowing the dependence structure in the interference vector allows us to significantly improve the receiver design. As long as this dependence is controlled by a system parameter (p in our case), the receiver can be *a priori* optimized.

Chapter 6

Conclusion

This thesis focus on characterizing interference and designing receivers in the IoT networks. The performance of the receiver is mainly degraded by the interference which is accumulative undesired signals from other devices. However, the interference arising in IoT networks is not *i.i.d.* Gaussian. Hence, an exact characterization of the interference statistics becomes a prerequisite for improving the receiver designs.

Motivated by NB-IoT and SCMA, we first develop a mathematical formulation for the physical layer and access scheme. The point process is applied for modeling the interferers' location. In addition to the assumption of the HPPP over the whole plane, two general point processes are introduced as well: doubly Poisson cluster process and Matérn hard-core process of type II, which can account for either the clustering due to human activity or the repulsion caused by CSMA. Besides, a guard zone is introduced and a finite network radius is considered. A simple access scheme model based on a probability p is proposed. This probability p can be interpreted as the service rate which is the amount of data to be transmitted and thus the average frequency resources occupied. Although it is built on NB-IoT, our framework is kept as generic as possible so that it is also suitable for other IoT networks.

We then verify the validity of the α-stable model on a single subcarrier. We first consider a HPPP with guard-zone radius $r_{\min}$. The impact of $r_{\min}$ on the α-stable model is well studied in terms of estimated $\hat{\alpha}$, Quantile-Quantile plot (Q-Q plot), Probability-Probability plot (P-P plot) and copula space. It is verified that the fitted stable model (with estimated $\hat{\alpha}$) is a good approximation under different $r_{\min}$. The interference induced by the doubly Poisson cluster point process and Matérn hard-core process of type II is then studied. In theory, it is proved to converge in distribution to the interference induced by HPPP. The approximation of α-stable under these two point processes is also proved through simulation with practical parameters in terms of KL divergence.

The interference on multiple subcarriers is studied in the next. Based on the simple access scheme we developed, we first derive the joint distribution of the interference vector under HPPP for two limiting cases: *1)* heavily

loaded network ($p \approx 1$) where interferers transmit on all msBs, the interference follows the sub-Gaussian α-stable distribution; *2)* lightly loaded network ($p \approx 0$) where interferers transmit on one msB at most, the interference follows the independent sub-Gaussian α-stable distribution. For the general case ($0 < p < 1$), we propose a t-copula α-stable model. Tailored to this model, a low complexity estimation algorithm is proposed and its accuracy is further proved. Considering the aforementioned three point processes, we study and compare the accuracy of the five models in terms of KL divergence: the fully sub-Gaussian α-stable model, independent sub-Gaussian α-stable model and the t-copula α-stable model (which are three models based on three estimation algorithms).

In the last, we study the impact of the interference on the receiver performance. We prove that the optimal linear receiver under the sub-Gaussian α-stable distribution ($p \approx 1$) is the MRC. And an accurate approximation of the BER is derived. Furthermore, the exact characterization of the interference with 2 dimensions is derived for $p < 1$, and the optimal linear receiver for such case is studied. To obtain further insight, we study the three receivers under different service rates p: the t-copula α-stable receiver, the MRC receiver and the independent α-stable receiver.

The work in this thesis can be further improved and extended in many aspects. One is to fit α-stable distribution with practical data. Although α-stable distribution has been studied and proves to be a good approximation in theory, its validity in practice has not been proved. To the best of our knowledge, only the work in [Cla+20] studied the accuracy of α-stable model for practical measurement data. The t-copula model proposed in this work is a good approximation for a wide range of p, but a more accurate model may exist by exploiting a hierarchical copula which incorporates t-copula to model the dependence structure interference on eRBs associated with different msBs. Time dependence should also be considered as devices usually stay active and transmit on several consecutive slots. A Markov chain may be an approach to introduce such dependence, or the life session introduced in [YP03]. Analogous to the dependence in frequency, the impact of time dependent interference on receiver design can be explored. A more wide range of dependence structure may exist in IoT networks, for instance, the channel fading may be correlated and the interference on msB is not isotropic sub-Gaussian. What is more, trade-offs between the performance and complexity in the receiver also need to be accounted for.

Appendices

Appendix A

Preliminaries on Point Processes

In this section, definitions and properties on point processes are given as complementary to the three general point processes introduced in Section 2.5

A.1   Point process

Loosely speaking, a point process is a random collection of points within some spatial region. Its formal definition is given as [Hae13]

Definition A.1.1. *A point process is a countable random collection of points that reside in some measure space, usually the Euclidean space $\mathbb{R}^d$.*

A common representation of the point process is through counting measure. That is to count the number of points falling into the set $B \subset \mathbb{R}^d$:

$$N(B) = \sum_{i=1}^{\infty} \mathbb{1}(x_i \in B), \tag{A.1}$$

where $N(B)$ denotes the number of points in B and $\mathbb{1}$ is the indicator function. N is called the (random) counting measure.

The expectation of the counting measure is the intensity measure:

Definition A.1.2. *The intensity measure is defined as*

$$\Lambda(B) = \mathbb{E}[N(B)], \tag{A.2}$$

where $B \subset \mathbb{R}^d$.

A.2   Binomial point process

Definition A.2.1. *A point process $\Phi = \{x_1, \cdots, x_n\}$ consisting of n i.i.d. points with intensity λ on the set B is called a Binomial Point Process (BPP).*

And for independent subsets $A_i \subset B$, we have

$$P(x_1 \in A_1, \cdots, x_n \in A_n) = \frac{|A_1| \cdots |A_n|}{|B|^n}, \qquad (A.3)$$

where $|\cdot|$ is the Lebesgue measure.

The Poisson point process can be treated as a conditional BPP:

Theorem A.2.2 (**Conditional property for HPPP**). *Consider a HPPP in $\mathcal{R}^2$ with density λ. Let $A \subset \mathcal{R}^2$ be any subset with $0 < |A| < \infty$. Given that $N(A) = n$, the distribution of $N(B)$ for $B \subset A$ is binomial:*

$$P(N(B) = k | N(A) = n) = \binom{n}{k} p^k (1-p)^{(n-k)}, \qquad (A.4)$$

where $p = |B|/|A|$.

In addition, this theorem also provides an approach to simulate the homogeneous Poisson point process over the region A:

1. Draw a random number from the Poisson distribution with mean $\lambda|A|$, say n;

2. Distributed n points uniformly over the area of A.

A.3   Transformation of Poisson point process

A.3.1   Mapping

For a point process, each point may be mapped to another point in the same space or the space of other dimensions. In most cases, the resulting process keeps as Poisson point process when it applies to the Poisson point process.

Theorem A.3.1. *Let Φ be a Poisson point process (PPP) with intensity measure Λ and intensity function λ. And let $f : \mathbb{R}^d \to \mathbb{R}^s$ and $\Lambda(f^{-1}(y)) = 0, \forall y \in \mathbb{R}^s$. Then*

$$\Phi' = f(\Phi) = \cup_{x \in \Phi} \{f(x)\} \qquad (A.5)$$

is also a Poisson point process with intensity measure

$$\Lambda'(B') = \Lambda(f^{-1}(B')) = \int_{f^{-1}(B')} \lambda(x) \mathrm{d}x. \qquad (A.6)$$

Therefore, the relationship between HPPP over the plane ($\mathbb{R}^2$) and Poisson distribution ($\mathbb{R}^1$) is given in the following proposition:

Proposition A.3.2. *For a HPPP in the plane with the rate λ, assuming that points are at distances $r_i(r_1 < r_2 < \cdots)$ from the origin, $\Gamma_i = r_i^2$ represents Poisson arrival times on the line with the constant arrival rate $\lambda\pi$.*

This proposition is linked with the LePage series representation in Appendix B and serves as the part of the proof that the interference under the Poisson network is α-stable.

A.3.2 Thinning

Generally, thinning is the removal of certain points from the point process. According to [Hae13], the thinning is called **independent** if the removal is independent for each point. And in particular, we have

Theorem A.3.3. *For a HPPP with intensity λ, each point is retained with probability p and deleted with probability $1 - p$ independent of all other points. The resulting process is still a HPPP with $p\lambda$.*

Appendix B

Preliminaries on α-stable Distribution

In this section, preliminaries of α-stable distribution are given which are used throughout this thesis. Definitions and properties on α-stable distribution are introduced. LePage series representation based on the Poisson process is elaborated. Sub-Gaussian α-stable, isotropic α-stable and their relationships are given in detail.

B.1 Gaussian distribution

The most common approach to modeling interference is the Gaussian model. Such a model is widely used due to its analytical expression and tractability. The probability density function (PDF) of $X \sim N(\mu, \sigma^2)$ is given as:

$$f(x) = \frac{1}{\sigma\sqrt{2\pi}} e^{-\frac{(x-\mu)^2}{2\sigma^2}}, \tag{B.1}$$

where μ is the mean and σ^2 is the variance.

The validity of the Gaussian model is also proved by the classical Central Limit Theorem (CLT):

Theorem B.1.1 (Classical CLT). *Let $\{X_1, \cdots, X_n\}$ be an* i.i.d *sequence with $E[X_i] = \mu$ and $\mathrm{Var}[X_i] = \sigma^2 < \infty$. Then as $n \to \infty$, we have*

$$\sqrt{n}\,(S_n - \mu) \overset{d}{\to} N(0, \sigma^2), \tag{B.2}$$

where $S_n = \frac{1}{n}\sum_{i=1}^{n} X_i$.

Fig. B.1 shows the Gaussian samples, there is no "outlier" out of the frame, which indicates the Gaussian model an inappropriate method for modeling impulsiveness.

Fig. B.2 shows PDF of Gaussian distribution in which its tail probability decreases in an exponential way implying a low probability of having large values.
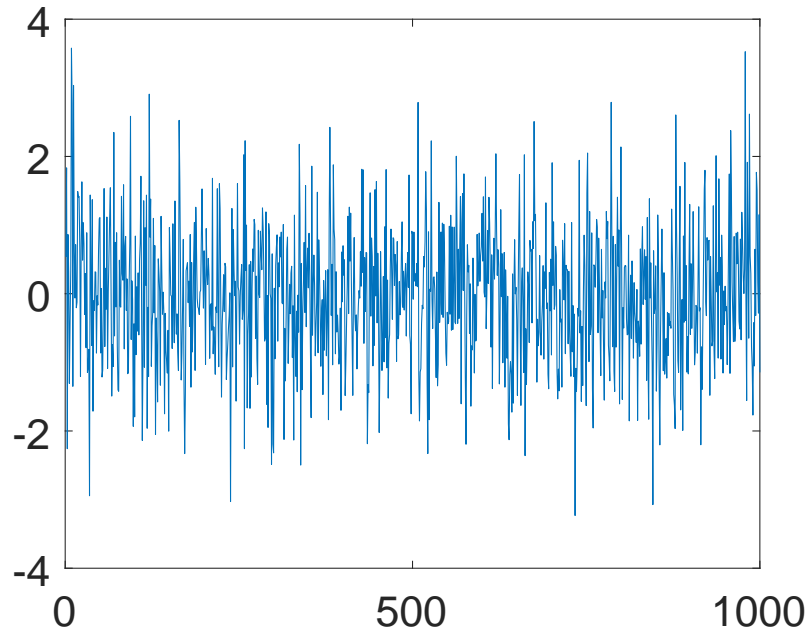
FIGURE B.1: Gaussian samples with $\mu = 0$ and $\sigma^2 = 1$.
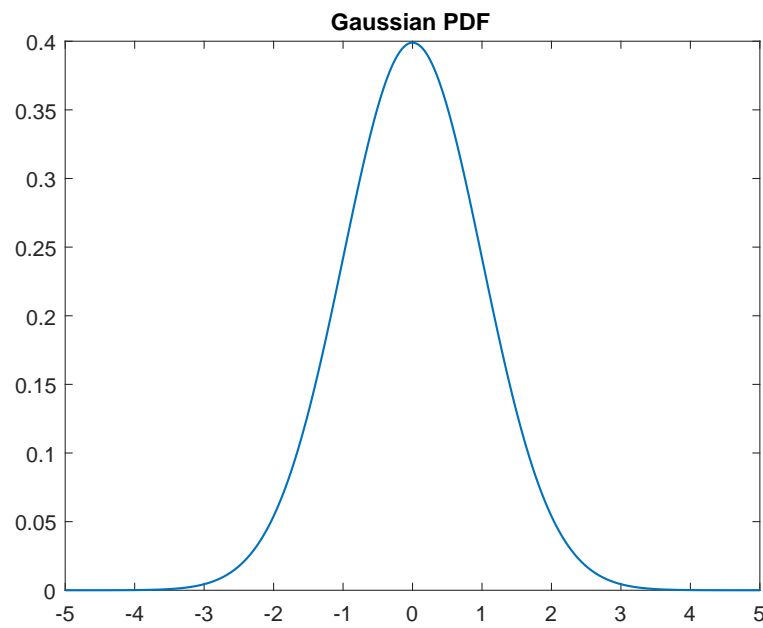
FIGURE B.2: Gaussian PDF with $\mu = 0$ and $\sigma^2 = 1$.

B.2 α-stable distribution

In many scenarios, the interference exhibits impulsiveness, i.e., there exist heavy tails in its PDF. Such an impulsive or non-Gaussian behavior can not be well captured by the Gaussian model and hence, distributions with heavy tails are introduced such as Middleton Class A and B or α-stable models. Among all the heavy-tailed models, it has been shown that α-stable distribution is a promising one.

The α-stable distribution is a generalization of Gaussian distribution and shares many properties of Gaussian distribution such as stability and isotropy. It is usually characterized by its CF due to the lack of closed-form PDF. Nevertheless, methods of parameters estimation and sample generation for α-stable have been extensively studied and already exist, which guarantees its tractability.

In this section, we give definitions of α-stable distribution. In addition, we also outline the properties and theorems related with α-stable distribution such as Lepage series representation theorem. These properties and theorems will be used in the rest of this thesis.

B.2.1 Definitions

According to [ST94], the α-stable distribution can be defined in terms of stability, GCLT and CF. We will give four equivalent definitions in this section. And each definition provides a different perspective for interpretation. The first two are defined in terms of stability:

Definition B.2.1. *A random variable X is said to have a* stable *distribution if for any positive number A and B, there is a positive number C and a real number D such that*

$$AX_1 + BX_2 \stackrel{d}{=} CX + D, \tag{B.3}$$

where X_1 and X_2 are independent copies of X.

A random variable X is called *strictly* stable if $D = 0$. And X is called *symmetric* stable if it is symmetric, i.e., $X \stackrel{d}{=} -X$.

Theorem B.2.2. *For any stable random variable X, there is a number $\alpha \in (0, 2]$ such that*

$$C^\alpha = A^\alpha + B^\alpha, \tag{B.4}$$

where A, B and C are in (B.3).

Definition B.2.3. *A random variable X is said to have a* stable *distribution if for any $n \geq 2$, there is a positive number C_n and a real number D_n such that*

$$X_1 + X_2 + \cdots + X_n \stackrel{d}{=} C_n X + D_n, \tag{B.5}$$

where $X_1, X_2, \cdots, X_n$ are independent copies of X.

It is shown that $C_n = n^{1/\alpha}$.

Although the variance of α-stable distribution is infinite, it keeps the property as GCLT, which is shown in the third definition.

Definition B.2.4 (**Generalized CLT**). *A random variable X is said to have a stable distribution if it has a domain of attraction, i.e., if there is a sequence of i.i.d. random variables $Y_1, Y_2, \cdots$ and sequences of positive numbers $\{d_n\}$ and real numbers $\{a_n\}$, such that*

$$\frac{Y_1 + Y_2 + \cdots + Y_n}{n} + a_n \xrightarrow{d} X. \tag{B.6}$$

When Y_i are *i.i.d.* with finite variance and X is Gaussian, it is classical CLT.

Generally, the α-stable distribution doesn't have a closed-form PDF. Hence, it is often characterized by its CF:

Definition B.2.5. *A random variable X is said to have a stable distribution if there are parameters: $0 < \alpha \le 2$, $\gamma > 0$, $-1 < \beta < 1$ and δ real such that its CF has the following form*

$$\mathbb{E}[e^{i\theta X}] = \begin{cases} \exp\left\{-\gamma^\alpha|\theta|^\alpha(1 - i\beta(\mathrm{sign}(\theta))\tan\frac{\pi\alpha}{2}) + i\delta\theta\right\}, & \alpha \ne 1 \\ \exp\left\{-\gamma|\theta|(1 + i\beta\frac{2}{\pi}(\mathrm{sign}(\theta))\log|\theta|) + i\delta\theta\right\}, & \alpha = 1 \end{cases}, \tag{B.7}$$

where $\mathrm{sign}(\cdot)$ is the sign function.

It is fully determined by four parameters: α, β, γ and δ, where

- α – characteristic exponent ($0 < \alpha \ne 2$): It controls the heaviness of the tail of the stable density. Small values of α imply strong impulsiveness. And large values of α exhibit more Gaussian behavior. Special cases are Gaussian ($\alpha = 2$), Cauchy ($\alpha = 1$) and Lévy ($\alpha = 0.5$);

- γ – scale parameter ($\gamma > 0$) or dispersion: It is similar to the variance of the Gaussian distribution. And in the Gaussian case, it equals to half of the variance;

- β – symmetry parameter ($-1 < \beta < 1$): It characterizes the symmetry or skewness of the density function. It is symmetric when $\beta = 0$. And when $\beta = \pm 1$, the distribution is totally skewed to the right or left;

- δ – the location parameter ($\delta \in \mathbb{R}$).

Notation. *Since* (B.7) *is fully described by the aforementioned four parameters:*

$$\alpha \in (0, 2]; \quad \gamma \in (0, \infty); \quad \beta \in [-1, 1]; \quad \delta \in \mathbb{R}. \tag{B.8}$$

we will denote the stable distribution by $S_\alpha(\gamma, \beta, \delta)$ and write

$$X \sim S_\alpha(\gamma, \beta, \delta) \tag{B.9}$$

to indicate X follows stable distribution $S_\alpha(\gamma, \beta, \delta)$.

When $\beta = \delta = 0$, X is symmetric α-stable since $X \overset{d}{=} -X$ according to (B.7). And we write

$$X \sim S\alpha S. \tag{B.10}$$

The PDFs of α-stable distribution exist and are continuous, but in general are not in closed form with only a few exceptions:

a). The Gaussian distribution $X \sim S_2(\gamma, 0, \delta) \overset{d}{=} N(\mu, \sigma^2)$, where $\delta = \mu$ and $\sigma = \sqrt{2}\gamma$. Its PDF is given as

$$f_G(x) = \frac{1}{2\sqrt{\pi}\gamma} e^{-\frac{(x-\delta)^2}{4\gamma^2}}, \quad x \in (-\infty, +\infty). \tag{B.11}$$

And its CF is given as

$$\phi_G(\theta) = \exp\left\{-\gamma^2\theta^2 + i\delta\theta\right\}. \tag{B.12}$$

b). The Cauchy distribution $X \sim S_1(\gamma, 0, \delta)$, its PDF is given as

$$f(x) = \frac{1}{\pi} \frac{\gamma}{(x-\delta)^2 + \gamma^2}, \quad x \in (-\infty, +\infty). \tag{B.13}$$

And its CF is given as

$$\phi_C(\theta) = \exp\left\{\gamma|\theta| + i\delta\theta\right\}. \tag{B.14}$$

c). The Lévy distribution $X \sim S_{\frac{1}{2}}(\gamma, 1, \delta)$, its PDF is given as

$$f(x) = \left(\frac{\gamma}{2\pi}\right)^{1/2} \frac{1}{(x-\delta)^{3/2}} \exp\left\{-\frac{\gamma}{2(x-\delta)}\right\}, \quad x \in (0, +\infty). \tag{B.15}$$

And it CF is given as

$$\phi_L(\theta) = \exp\left\{-|\gamma\theta|^{1/2}(1 - i\mathrm{sign}(\theta)) + i\delta\theta\right\}. \tag{B.16}$$

Fig. B.3 shows the PDFs of α-stable distribution under different α with $\delta = 0$ and $\gamma = 1$.

B.2.2 Properties

The α-stable distribution keeps the stable property of Gaussian distribution:
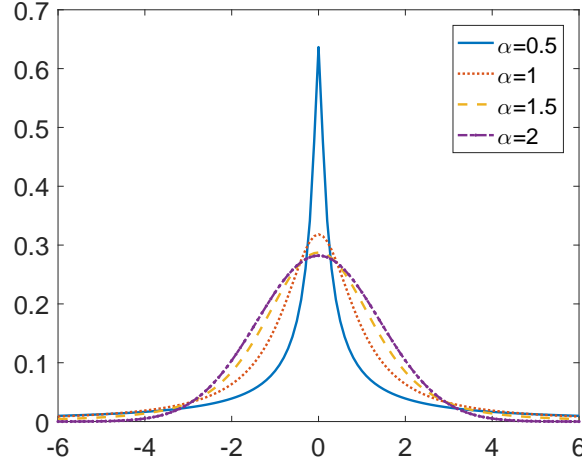
FIGURE B.3: α-stable PDFs with $\delta = \beta = 0$ and $\gamma = 1$.
$\alpha = 0.5, 1, 1.5, 2$.

Property B.2.6 (Stable Property). *Suppose that X_1 and X_2 are independent random variables with $X_1 \sim S_\alpha(\gamma_1, \beta_1, \delta_1)$ and $X_2 \sim S_\alpha(\gamma_2, \beta_2, \delta_2)$. Then $X_1 + X_2 \sim S_\alpha(\gamma, \beta, \delta)$, where*

$$\gamma = (\gamma_1^\alpha + \gamma_2^\alpha)^{\frac{1}{\alpha}} ; \quad \beta = \frac{\beta_1 \gamma_1^\alpha + \beta_2 \gamma_2^\alpha}{\gamma_1^\alpha + \gamma_2^\alpha}; \quad \delta = \delta_1 + \delta_2. \tag{B.17}$$

For the summation of several **SαS** random variables, we have the following corollary:

Corollary B.2.7. *Let $X_i \sim S_\alpha(\gamma_i, 0, 0), i = 1, 2, \cdots, K$, then $\sum_{i=1}^{K} X_i \sim S_\alpha(\gamma, 0, 0)$, where $\gamma = \left(\sum_{i=1}^{K} \gamma_i^\alpha\right)^{\frac{1}{\alpha}}$.*

Property B.2.8 (Shifting Property). *Let $X \sim S_\alpha(\gamma, \beta, \delta)$ and let a be a constant. Then $X + a \sim S_\alpha(\gamma, \beta, \delta + a)$*

For $X \sim G(\mu, \sigma^2)$, $aX \sim G(a\mu, a^2\sigma^2)$. Stable distribution has similar properties as Gaussian.

Property B.2.9 (Scaling Property). *Let $X \sim S_\alpha(\gamma, \beta, \delta + a)$ and a as a non-zero real constant. Then*

$$aX \sim S_\alpha(|a|\gamma\text{sign}(a)\beta, a\delta) \qquad\qquad if \ a \neq 1; \tag{B.18}$$

$$aX \sim S_\alpha(|a|\gamma\text{sign}(a)\beta, a\delta - \frac{2}{\pi}a(\ln(|a|))\gamma\beta) \qquad if \ a = 1. \tag{B.19}$$

Property B.2.10. *For any $0 < \alpha < 2$,*

$$X \sim S_\alpha(\gamma, \beta, 0) \Leftrightarrow -X \sim S_\alpha(\gamma, -\beta, 0). \tag{B.20}$$

Property B.2.11 (Symmetric Property). *$X \sim S_\alpha(\gamma, \beta, \delta)$ is symmetric if and only if $\beta = 0$ and $\delta = 0$. It is symmetric about δ if and only if $\beta = 0$.*

Unlike Gaussian, α-stable has heavy tails

Property B.2.12 (Tail Probability). *Let $X \sim S_\alpha(\gamma, \beta, \delta)$ with $0 < \alpha < 2$. Then*

$$\begin{cases} \lim_{t \to \infty} t^\alpha P\{X > t\} = C_\alpha \dfrac{1 + \beta}{2} \gamma^\alpha \\ \lim_{t \to \infty} t^\alpha P\{X < -t\} = C_\alpha \dfrac{1 - \beta}{2} \gamma^\alpha \end{cases}, \tag{B.21}$$

where

$$C_\alpha = \left(\int_0^\infty x^{-\alpha} \sin x \right)^{-1} = \begin{cases} \frac{1 - \alpha}{\Gamma(2 - \alpha) \cos \frac{\pi}{2} \alpha} & if \ \alpha \neq 1 \\ \frac{2}{\pi} & if \ \alpha = 1 \end{cases}, \tag{B.22}$$

Property B.2.13 (Order of Moments). *Let $X \sim S_\alpha(\gamma, \beta, \delta)$ with $0 < \alpha < 2$. Then*

$$E|X|^p < \infty, \quad 0 < p < \alpha; \tag{B.23}$$

$$E|X|^p = \infty, \quad p \geq \alpha. \tag{B.24}$$

The α-stable distribution ($\alpha \neq 2$) does not have finite variance. And for $0 < \alpha < 1$, $E|X| = \infty$.

B.2.3 Series representation of α-stable distribution

An α-stable random variable can also be represented as the convergent sum of infinite series involving Poisson arrival in one dimension. Such an infinite series is called LePage series. The following theorem in this section shows the relationship between the α-stable random variable and the LePage series.

Let $\{\epsilon_1, \epsilon_2, \dots\}$, $\{W_1, W_2, \dots\}$, $\{\Gamma_1, \Gamma_2, \dots\}$ be three independent sequences of random variables such that

- $\epsilon_1, \epsilon_2, \dots$ is an *i.i.d.* sequence of Rademacher variables, i.e., $P[\epsilon_i = 1] = P[\epsilon_i = -1] = \frac{1}{2}$;

- $W_1, W_2, \dots$ is an *i.i.d.* sequence of random variables;

- $\Gamma_1, \Gamma_2, \dots$ is a sequence of arrival times of Poisson process with unit arrival rate, i.e., $\Gamma_i = \sum_{j=1}^i e_j$, where e_j are *i.i.d.* exponential random variables with $E[e_j] = 1$.

Theorem B.2.14 (LePage Series). *Suppose $0 < \alpha < 2$. then $\sum_{i=1}^\infty \epsilon_i \Gamma_i^{-\frac{1}{\alpha}} W_i \xrightarrow{a.s.} X \sim S_\alpha(\gamma, 0, 0)$, where C_α is the constant defined in (B.22), and*

$$\gamma = (C_\alpha^{-1} E[|W_i|^\alpha])^{\frac{1}{\alpha}}. \tag{B.25}$$

The notation $X_n \xrightarrow{a.s.} X$ denotes that the sequence X_n converges almost surely to X or $P\left[\lim_{n\to\infty} X_n = X\right] = 1$.

According to [ST94], we have the following remark:

Remark B.2.15. *The first summand $\epsilon_1\Gamma_1^{-\frac{1}{\alpha}}W_1$ is stochastically the greatest in absolute value. Its probability tail has the same asymptotic rate of growth as the α-stable random variable:*

$$\lim_{t\to\infty} t^\alpha P\left[\left|\epsilon_1\Gamma_1^{-\frac{1}{\alpha}}W_1\right| > t\right] = E\left[|W_1|^\alpha\right]. \tag{B.26}$$

Proof. Let $F_{|W_1|}$ be the distribution of $|W_1|$. Since $\Gamma_1^{-\frac{1}{\alpha}}W_1$ is symmetric, it follows that

$$
\begin{aligned}
&\Pr\left(\Gamma_1^{-\frac{1}{\alpha}}W_1 > t\right) \\
&= \frac{1}{2}\Pr\left(\left|\Gamma_1^{-\frac{1}{\alpha}}W_1\right| > t\right) \\
&= \frac{1}{2}\int_0^\infty \Pr(\Gamma_1 < w^\alpha t^{-\alpha})F_{|W_1|}(dw) \\
&= \frac{1}{2}\int_0^\infty \left(1 - e^{-w^\alpha t^{-\alpha}}\right) F_{|W_1|}(dw) \\
&= \frac{1}{2}\int_0^\infty \left[w^\alpha t^{-\alpha} - \sum_{n=2}^\infty \frac{(-1)^n w^{n\alpha}t^{-n\alpha}}{n!}\right] F_{|W_1|}(dw) \\
&= \frac{1}{2}\mathbb{E}[|W_1|^\alpha]t^{-\alpha} - \sum_{n=2}^\infty \frac{(-1)^n\mathbb{E}[|W_1|^{n\alpha}]t^{-n\alpha}}{n!} \\
&= \frac{1}{2}\mathbb{E}[|W_1|^\alpha]t^{-\alpha} + o(t^{-\alpha}). \tag{B.27}
\end{aligned}
$$

Using (B.25), it then follows that

$$E[|W_1|^\alpha] = \gamma^\alpha C_\alpha, \tag{B.28}$$

and hence,

$$\Pr\left(\Gamma_1^{-\frac{1}{\alpha}}W_1 > t\right) = \frac{C_\alpha}{2}\gamma^\alpha t^{-\alpha} + o(t^{-\alpha}) \tag{B.29}$$

as required.

Let $X = \sum_{i=1}^\infty \epsilon_i\Gamma_i^{-\frac{1}{\alpha}}W_i \sim S_\alpha(\gamma, 0, 0)$, according to Property B.2.12, we have

$$\frac{1}{2}\lim_{t\to\infty} P\{X > t\} = C_\alpha\gamma^\alpha t^{-\alpha}. \tag{B.30}$$

$\square$

B.2.4 Symmetric α-stable distribution

When $X \sim S\alpha S$, its CF becomes

$$\mathbb{E}[e^{i\theta X}] = \exp\left\{-\gamma^\alpha |\theta|^\alpha\right\}. \tag{B.31}$$

The $S\alpha S$ random variable is only characterized by its characteristic exponent α and its scale parameter γ. A random variable X is called *standard* $S\alpha S$ if $\gamma = 1$. For $S\alpha S$ with $\alpha = 2$, it follows Gaussian distribution with zero mean and variance as $2\gamma^2$.

The following proposition shows that any $S\alpha' S$ random variable can be transformed into another $S\alpha S$ random variable as long as $0 < \alpha < \alpha'$.

Proposition B.2.16. *Let $X \sim S_{\alpha'}(\gamma, 0, 0)$ with $0 < \alpha' \leq 2$ and let $0 < \alpha < \alpha'$. Let A be a skewed α/α-stable variable where $A \sim S_{\alpha/\alpha'}\left(\left(\cos\frac{\pi\alpha}{2\alpha'}\right)^{\alpha'/\alpha}, 1, 0\right)$. If X and A are independent, then*

$$Z = A^{\frac{1}{\alpha'}} X \sim S_\alpha(\gamma, 0, 0). \tag{B.32}$$

In particular, this leads to the following remark which shows the link between α-stable distribution and Gaussian distribution.

Remark B.2.17. *If $X \sim \mathcal{N}(0, \sigma^2)$ where $\sigma^2 = 2\gamma^2$, $A \sim S_{\alpha/2}\left(\left(\cos\frac{\pi\alpha}{4}\right)^{2/\alpha}, 1, 0\right)$ and X and A are independent, then*

$$Z = \sqrt{A}X \sim S\alpha S. \tag{B.33}$$

Hence, every $S\alpha S$ random variable is conditional Gaussian. And Z can be treated as $\mathcal{N}(0, \sigma^2 A)$, i.e., the Gaussian distribution with variance $\sigma^2 A$.

B.2.5 Multivariate α-stable distribution

It is possible to extend the notion of an α-stable random variable to the multivariate setting, i.e., the α-stable vector.

Definition B.2.18. *A random vector $\mathbf{X} = [X_1, \cdots, X_d]$ is said to be a stable random vector in $\mathbb{R}^d$ if for any positive numbers A and B there is a positive number C and a vector $\mathbf{D} \in \mathbb{R}^d$ such that*

$$A\mathbf{X}^{(1)} + B\mathbf{X}^{(2)} \stackrel{d}{=} C\mathbf{X}^{(3)}, \tag{B.34}$$

where $\mathbf{X}^{(1)}$ and $\mathbf{X}^{(2)}$ are independent copies of $\mathbf{X}$.

We note that each element in $\mathbf{X}$ is an α-stable random variable if $\mathbf{X}$ is an α-stable vector, but not all random vectors with symmetric α-stable marginals form symmetric α-stable random vectors.

The vector "**X**" is called *strictly stable* if (B.34) holds for with **D** $= $ **0**, $\forall A, B$. The vector is called *symmetric stable* if it is stable and satisfies

$$P(\mathbf{X} \in A) = P(-\mathbf{X} \in A) \tag{B.35}$$

for any Borel set A of $\mathbb{R}^d$.

Theorem B.2.19. *Let* $\mathbf{X} = [X_1, \cdots, X_d]$ *be a stable (respectively strictly stable, symmetric stable) vector in* $\mathbb{R}^d$. *Then there is a constant* $\alpha \in (0, 2]$, *such that in* (B.34), $C^\alpha = A^\alpha + B^\alpha$. *Moreover, any linear combination of the components in* $\mathbf{X}$ *of the type* $Y = \sum_{i=1}^d b_i X_i = \mathbf{b} \cdot \mathbf{X}$ *is also* α-*stable (respectively strictly stable, symmetric stable).*

Corollary B.2.20. *A random vector in* $\mathbf{X}$ *is stable if and only if for any* $n \leq 2$, *there is an* $\alpha \in (0, 2]$ *and a vector* $\mathbf{D}_n$ *such that*

$$\mathbf{X}^{(1)} + \mathbf{X}^{(2)} + \cdots + \mathbf{X}^{(n)} \stackrel{d}{=} n^{\frac{1}{\alpha}} \mathbf{X} + \mathbf{D}_n, \tag{B.36}$$

where $\mathbf{X}^{(1)}, \mathbf{X}^{(2)}, \cdots, \mathbf{X}^{(n)}$ *are independent copies of* $\mathbf{X}$.

Definition B.2.21. *A random vector in* $\mathbf{X}$ *in* $\mathbb{R}^d$ *is called* α-*stable if* (B.34) *holds with* $C = (A^\alpha + B^\alpha)^{\frac{1}{\alpha}}$ *or equivalently, if* (B.36) *holds.*

Theorem B.2.22. *Let* $\mathbf{X}$ *be a random vector in* $\mathbb{R}^d$.

(a) *If all linear combinations* $Y = \sum_{k=1}^d b_k X_k$ *have strictly stable distribution, then* $\mathbf{X}$ *is a strictly stable random vector in* $\mathbb{R}^d$;

(b) *If all linear combinations are symmetric stable, then* $\mathbf{X}$ *is a symmetric stable random vector;*

(c) *If all linear combinations are stable with the index of stability greater or equal to* 1, *then* $\mathbf{X}$ *is a stable vector.*

Theorem B.2.23. *Let* $0 < \alpha < 2$. $\mathbf{X} = [X_1, \cdots, X_d]$ *is an* α-*stable vector in* $\mathbb{R}^d$ *if and only if there exists a finite measure* Γ *on the unit sphere* S^{d-1} *of* $\mathbb{R}^d$ *and a vector* $\boldsymbol{\mu}$ *in* $\mathbb{R}^d$ *such that:*

(a) *If* $\alpha \neq 1$

$$E\left[\exp\{i\boldsymbol{\theta} \cdot \mathbf{X}\}\right]$$
$$= \exp\left\{-\int_{S_d} |\boldsymbol{\theta} \cdot \mathbf{s}|^\alpha \left(1 - i\, \text{sign}(\boldsymbol{\theta} \cdot \mathbf{s}) \tan \frac{\pi \alpha}{2}\right) \Gamma(d\mathbf{s}) + i(\boldsymbol{\theta} \cdot \boldsymbol{\mu})\right\}; \tag{B.37}$$

(b) *If* $\alpha = 1$

$$E\left[\exp\{i\boldsymbol{\theta} \cdot \mathbf{X}\}\right]$$
$$= \exp\left\{-\int_{S_d} |\boldsymbol{\theta} \cdot \mathbf{s}| \left(1 + i\, \frac{2}{\pi} \text{sign}(\boldsymbol{\theta} \cdot \mathbf{s}) \ln |\boldsymbol{\theta} \cdot \mathbf{s}|\right) \Gamma(d\mathbf{s}) + i(\boldsymbol{\theta} \cdot \boldsymbol{\mu})\right\}. \tag{B.38}$$

Definition B.2.24. *The vector* $\mathbf{X} = [X_1, \cdots, X_d]$ *is said to have* spectrum representation $(\Gamma, \boldsymbol{\mu})$. *The measure* Γ *is called the* spectrum measure *of the α-stable random vector* $\mathbf{X}$.

B.2.6 Multivariate sub-Gaussian α-stable distribution

A particular class of α-stable random vectors is sub-Gaussian α-stable vector, which is defined based on Remark B.2.17.

Definition B.2.25. *Any vector* $\mathbf{X}$ *distributed as* $\mathbf{X} = A^{1/2}[G_1, \cdots, G_d]^T$ *is called a sub-Gaussian α-stable random vector in $\mathbb{R}^d$ with underlying Gaussian vector* $\mathbf{G} = [G_1, \ldots, G_d]^T$ *if it satisfies*

$$A \sim S_{\alpha/2}\left(\left(cos\frac{\pi}{4}\alpha\right)^{2/\alpha}, 1, 0\right), \tag{B.39}$$

where A and $\mathbf{G}$ are independent. If $\mathbf{G} \sim \mathcal{N}(0, \sigma^2\mathbf{I})$, *then* $X_i \sim S_\alpha(\gamma, 0, 0)$ *where* $\gamma = \sigma/\sqrt{2}$ *and σ is called the parameter of* $\mathbf{X}$.

Sub-Gaussian α-stable random vectors are typically characterized by either the scale-mixture representation in Definition B.2.25 or via their CFs in the following proposition.

Proposition B.2.26. *The CF of sub-Gaussian α-stable vector* $\mathbf{X}$ *is given as*

$$\mathbb{E}[e^{i\boldsymbol{\theta}\cdot\mathbf{X}}] = \exp\left\{-\left|\frac{1}{2}\sum_{i=1}^{d}\sum_{j=1}^{d}\theta_i\theta_j R_{ij}\right|^{\alpha/2}\right\}, \tag{B.40}$$

where $R_{ij} = E[G_iG_j]$ are the covariances of the underlying Gaussian vector $\mathbf{G}$.

A special case of sub-Gaussian α-stable vectors is the one with its underlying Gaussian vector $\mathbf{G} \sim \mathcal{N}(0, \sigma^2\mathbf{I})$ and has the following proposition according to [ST94].

Proposition B.2.27. *Let* $\mathbf{X}$ *be a $S\alpha S$ random vector in $\mathbb{R}^d$ where $\alpha < 2$. Then the following three statements are equivalent:*

1). $\mathbf{X}$ *is sub-Gaussian α-stable with an underlying Gaussian vector* $\mathbf{G} \sim \mathcal{N}(0, \sigma^2\mathbf{I})$;

2). *The CF X has the form*

$$\mathbb{E}[e^{i\boldsymbol{\theta}\cdot\mathbf{X}}] = \exp\left\{\gamma^\alpha|\boldsymbol{\theta}|^\alpha\right\}, \tag{B.41}$$

   where $\gamma = \frac{\sigma}{\sqrt{2}}$. *That is, it only depends on the magnitude of* $\boldsymbol{\theta} = (\theta_1, \cdots, \theta_d)$;

3). *The spectral measure is uniform.*

Similar to Remark B.2.17, we have

Remark B.2.28. *Every sub-Gaussian α-stable random vector is conditionally Gaussian. Specifically, if $\mathbf{X} = \sqrt{A}\mathbf{G}$ is sub-Gaussian α-stable with an underlying Gaussian vector $\mathbf{G} \sim \mathcal{N}(0, \mathbf{\Sigma})$, $\mathbf{X} \sim \mathcal{N}(0, A\mathbf{\Sigma})$ and is not independent.*

B.2.7   Complex α-stable distribution and isotropy

Note that a complex random variable X can be denoted as

$$X = X_1 + iX_2. \tag{B.42}$$

Note that it is the joint distribution of X_1 and X_2 that characterizes X.

Definition B.2.29. *A complex random variable $X = X_1 + iX_2$ is called symmetric α-stable ($S\alpha S$) if (X_1, X_2) is $S\alpha S$.*

Definition B.2.30. *A complex $S\alpha S$ random variable $X = X_1 + iX_2$ is isotropic if*

$$e^{i\phi}X \stackrel{d}{=} X, \quad \forall \phi \in (0, 2\pi]. \tag{B.43}$$

The following theorem shows that isotropy implies a special spectral measure for $\mathbf{X} = (X_1, X_2)$.

Theorem B.2.31. *Let $0 < \alpha < 2$. A complex $S\alpha S$ random variable $X = X_1 + iX_2$ is isotropic if and only if (X_1, X_2) has a uniform spectral measure.*

The following proposition ([ST94], Corollary 2.6.4) highlights the link between isotropic α-stable random variables and the sub-Gaussian α-stable.

Proposition B.2.32. *Let $0 < \alpha < 2$. A complex $S\alpha S$ random variable $X = X_1 + iX_2$ is isotropic if and only if there are two i.i.d. zero mean Gaussian random variables G_1 and G_2 and a random variable $A \sim S_{\alpha/\alpha'}\left(\left(\cos\frac{\pi\alpha}{2\alpha'}\right)^{\alpha'/\alpha}, 1, 0\right)$ independent of (G_1, G_2) such that (X_1, X_2) is sub-Gaussian with the underlying Gaussian vector (G_1, G_2).*

Appendix C

Preliminaries on Copula

A popular method in statistics for tractably modeling the dependence of a random vector is based on *copulas*. The word "Copula" is a Latin word which means "a link, tie, bond". It is a multivariate distribution function whose one-dimensional margins are uniform on the interval $[0, 1]$.

Definition C.0.1. *The copula $C : [0, 1]^n \to [0, 1]$ is defined as the joint CDF of $(U_1, \cdots, U_n)$:*

$$C(u_1, \cdots, u_n) = P(U_1 \leq u_1, \cdots, U_n \leq u_n), \tag{C.1}$$

where U_i are uniformly distributed on $[0, 1]$

Consider a continuous random vector $(X_1, \cdots, X_n)$ and its marginal CDFs are $F_i(x_i) = P[X_i \leq x_i]$, the vector

$$(U_1, \cdots, U_n) = (F_1(x_1), \cdots, F_d(x_n)) \tag{C.2}$$

has marginals that are uniformly distributed on the interval $[0, 1]$. Therefore, from another point of view, copula is treated as a function that joins or couples multivariate distribution functions to their one-dimensional marginal distribution functions. Such a role that copula plays between joint distribution and marginals is elucidated in Sklar's theorem.

C.1 Sklar's theorem

Sklar's theorem, named after Abe Sklar, provides the theoretical foundation for the application of copulas.

Theorem C.1.1 (Sklar's Theorem). *Let H be a d-dimensional multivariate joint distribution function of $(X_1, \cdots, X_n)$ with marginal CDFs $F_1, \cdots, F_n$. There exists a copula function C, such that*

$$H(x_1, \cdots, x_n) = C(F_1(x_1), \cdots, F_n(x_n)) \tag{C.3}$$

for all $x_i \in (-\infty, \infty), i = 1, \cdots, n$. Furthermore, if F_i is continuous for all $i = 1, \cdots, n$, then C is unique; otherwise, C is uniquely determined only on $\mathrm{Ran}\, F_1 \times \mathrm{Ran}\, F_n$, where $\mathrm{Ran}\, F_i$ denotes the range of F_i.

Conversely, with H and its margins $F_1, \ldots, F_n$ known, we can derive its copula function:

Corollary C.1.2 (Inversion Method). *Let C, H, $F_1, \ldots, F_n$ be as in Theorem C.1.1, and let $F_1^{(-1)}, \ldots, F_n^{(-1)}$ be quasi-inverse of $F_1, \ldots, F_n$, respectively. Then for $(u_1, \cdots, u_n) \in [0, 1]^n$,*

$$C(u_1, \ldots, u_n) = H\left(F_1^{(-1)}(u_1), \ldots, F_n^{(-1)}(u_n)\right). \tag{C.4}$$

This provides a method of constructing copulas, i.e., using the inversion method with joint distribution and its marginals which are already known. One of the major families of copulas–elliptical copula–is constructed in this way. Taking the derivatives of (C.3) on both sides, we have the following proposition:

Proposition C.1.3.

$$h(x_1, \ldots, x_n) = c(F_1(x_1), \ldots, F_n(x_n)) \prod_{k=1}^{n} f_k(x_k), \tag{C.5}$$

where $h(\cdot)$ is the joint density of $\mathbf{x}$, $f_k(x_k)$ is the univariate density of x_k, and $c(\cdot)$ is the density of copula function:

$$c(u_1, \ldots, u_n) = \frac{\mathrm{d}^n C(u_1, \ldots, u_n)}{\mathrm{d}u_1 \ldots \mathrm{d}u_n}. \tag{C.6}$$

The proposition above shows that the copula density $c(\cdot)$ contains all information on the dependence structure, whereas the margins $F_1, \ldots, F_n$ contain all information on the marginal distributions. This enables us to model the dependence separately from modeling the marginals.

Theorem C.1.4. *Random variable X_i, $i = 1, \cdots, d$ are independent if and only if $C(u_1, \cdots, u_n) = \Pi(u_1, \cdots, u_n)$, where $\Pi = \Pi_{i=1}^n u_i$ is called **indepndent copula**.*

Property C.1.5 (Invariance under Monotonic Transformation). *Suppose that $X_1, \cdots, X_n$ have continuous marginals and copula $C_{\mathbf{X}}$. Let $T_i : \mathcal{R} \to \mathcal{R}$ for $i = 1, \cdots, n$ be strictly increasing functions. Then the dependence structure of random variables:*

$$Y_i = T_i(X_i), \ i = 1, \cdots, n \tag{C.7}$$

is also given by the Copula $C_{\mathbf{X}}$.

C.2 Measure of dependence

The most common measure of dependence is the Pearson correlation coefficient. Though it is a perfect measure for the linear dependence, it fails

to measure the dependence when it is nonlinear. Here we introduce other measures of dependence such as Kendall's τ and tail dependence.

Definition C.2.1 (Pearson correlation coefficient). *Given a pair of random variables (X, Y), the Pearson correlation coefficient is defined as*

$$\rho_{X,Y} = \frac{Cov(X,Y)}{\sigma_X \sigma_Y}. \tag{C.8}$$

However, the correlation coefficient can only measure the linear dependence and has the constraint of finite second order of moments. For instance, we take a symmetric random variable X and let $Y = X^2$, then $\rho_{X,Y} = 0$.

A more popular measure of dependence is rank correlation, such as Kendall's τ. Before embarking on the definition of Kendall's τ, we first give the definition of concordance.

Definition C.2.2 (Concordance). *Let (x_i, y_i) and (x_j, y_j) denote two observations from a vector (X, Y) of continuous random variables. We say that (x_i, y_i) and (x_j, y_j) are*

- **Concordant** *if $(x_i - x_j)(y_i - y_j) > 0$;*

- **Discordant** *if $(x_i - x_j)(y_i - y_j) < 0$*

C.2.1 Kendall's τ

Kendall's tau, also referred to as Kendall rank correlation coefficient is the rank correlation between two random variables. It is defined in terms of concordance as follows:

Definition C.2.3. *Let $\{(x_1, y_1), \cdots, (x_n, y_n)\}$ be a set of observations from a random vector of continuous random variables. Then Kendall's τ is defined as:*

$$\rho_\tau = \frac{N_{concordant} - N_{discordant}}{n(n-1)/2}, \tag{C.9}$$

where $N_{concordant}$ and $N_{discordant}$ are the numbers of concordant pairs and discordant pairs, respectively.

An alternative definition is based on probability.

Definition C.2.4. *For two i.i.d pairs of random variables (X_1, Y_1) and (X_2, Y_2), Kendall's τ is defined as the probability of concordance minus the probability of discordance:*

$$\rho_\tau = P[(X_1 - X_2)(Y_1 - Y_2) > 0] - P[(X_1 - X_2)(Y_1 - Y_2) < 0]. \tag{C.10}$$

The following theorem describes the relationship between Kendall's τ and copula [Nel99]:

Theorem C.2.5. *Let X and Y be continuous random variables whose copula is C. Then the population version of Kendall's τ for X and Y is given by*

$$\rho_{\tau_{X,Y}} = 4E(C(U,V)) - 1$$
$$= 4 \iint_{\mathbf{I}^2} C(u,v)dC(u,c) - 1, \qquad \text{(C.11)}$$

where $\mathbf{I}^2 = [0,1] \times [0,1]$.

Property C.2.6. *The Kendall's τ is a measure of concordance, rank correlation more precisely with*

- *$-1 \leq \rho_\tau \leq 1$;*

- *If the agreement between the two rankings is perfect (i.e., the two rankings are the same) the coefficient has value 1;*

- *If the disagreement between the two rankings is perfect (i.e., one ranking is the reverse of the other) the coefficient has value -1;*

- *If X and Y are independent, then we would expect the coefficient to be approximately zero.*

C.3   Tail dependence

Tail dependence is a concept that is relevant for the study of dependence between extreme values. It turns out that tail dependence between two continuous random variables X and Y is a copula property, and hence the amount of tail dependence is invariant under strictly increasing transformations of X and Y.

Definition C.3.1. *The lower tail dependence is defined as:*

$$\lambda_l = \lim_{u \downarrow 0} P\left(X_2 < F_2^{-1}(u) | X_1 < F_1^{-1}(u)\right). \qquad \text{(C.12)}$$

The upper tail dependence is defined as:

$$\lambda_u = \lim_{u \uparrow 1} P\left(X_2 > F_2^{-1}(u) | X_1 > F_1^{-1}(u)\right). \qquad \text{(C.13)}$$

Property C.3.2.

$$\lambda_l = \lim_{u \downarrow 0} \frac{1 - 2u + C(u,u)}{1 - u}, \qquad \text{(C.14)}$$

$$\lambda_u = \lim_{u \uparrow 1} \frac{C(u,u)}{u}. \qquad \text{(C.15)}$$

Remark C.3.3. *Tail dependence provides an approach to quantification of the dependence in extremes of a multivariate distribution and can be related directly to the parameters of the copula statistical model.*

C.4 Elliptical distribution and t-copula

C.4.1 Elliptical distribution

Definition C.4.1. *A d-dimensional random vector $\mathbf{X}$ is said to have an elliptical distribution (denoted as $\mathbf{X} \sim E_d(\boldsymbol{\mu}, \boldsymbol{\Sigma})$) with parameters $\boldsymbol{\mu}$ ($d \times 1$) and $\boldsymbol{\Sigma}$ ($d \times d$) if it has stochastic representation*

$$\mathbf{X} \overset{d}{=} \boldsymbol{\mu} + r\boldsymbol{\Lambda}\mathbf{U}, \tag{C.16}$$

where $\mathbf{U}$ is uniformly distributed on a unit sphere $\mathcal{S}^{d-1}$ in $\mathbb{R}^d$ and is independent of r, $\boldsymbol{\Lambda}$ is a $d \times d$ matrix such that $\boldsymbol{\Lambda}\boldsymbol{\Lambda}^\top = \boldsymbol{\Sigma}$, called dispersion matrix.

Remark C.4.2. *Gaussian distribution, t-distribution and sub-Gaussian α-stable distribution all belong to the family of elliptical distribution.*

For multivariate Gaussian distribution, we have the following proposition:

Proposition C.4.3. *For a multivariate Gaussian vector $\mathbf{X} = (X_1, \cdots, X_d)^T \sim \mathcal{N}(\mu, \boldsymbol{\Sigma})$, it can be represented as*

$$\mathbf{X} = \boldsymbol{\mu} + \sqrt{\chi_d^2}\boldsymbol{\Lambda}\mathbf{U}, \tag{C.17}$$

where χ_d^2 is a chi-square distributed random variable, $\mathbf{U}$ is uniformly distributed on a unit sphere $\mathcal{S}^{d-1}$ and $\boldsymbol{\Lambda}\boldsymbol{\Lambda}^\top = \boldsymbol{\Sigma}$.

Definition C.4.4 (**Multivariate t-distribution**)**.** *The d-dimensional random vector $\mathbf{X} = (X_1, \cdots, X_d)$ is said to have a multivariate t-distribution with the degree of freedom ν, mean vector $\boldsymbol{\mu}$ and positive scale matrix $\boldsymbol{\Sigma}$, denoted as $\mathbf{X} \sim t_d(\nu, \boldsymbol{\mu}, \boldsymbol{\Sigma})$, if its PDF is given by*

$$f(\mathbf{X}) = \frac{\Gamma(\frac{\nu+d}{2})}{\Gamma(\frac{\nu}{2})\sqrt{(\pi\nu)^d|\boldsymbol{\Sigma}|}} \left(1 + \frac{(\mathbf{X} - \boldsymbol{\mu})^T\boldsymbol{\Sigma}^{-1}(\mathbf{X} - \boldsymbol{\mu})}{\nu}\right)^{\frac{\nu+d}{2}}. \tag{C.18}$$

Multivariate t-distribution belongs to the class of elliptical distributions and has the following representation:

Proposition C.4.5. *For a multivariate vector $\mathbf{Y} = (Y_1, \cdots, Y_d)^T \sim t_d(\nu, \boldsymbol{\mu}, \boldsymbol{\Sigma})$, it can be represented as*

$$\mathbf{X} = \boldsymbol{\mu} + \frac{\sqrt{\chi_d^2}}{\sqrt{\chi_\nu^2/\nu}}\mathbf{U}, \tag{C.19}$$

where χ^2 is a Chi-square distributed random variable, $\mathbf{U}$ is uniformly distributed on a unit sphere $\mathcal{S}^{d-1}$, and $\boldsymbol{\Lambda}\boldsymbol{\Lambda}^\top = \boldsymbol{\Sigma}$.

Since $\lim\limits_{\nu \to \infty} \frac{\chi_\nu^2}{\nu} = 1$, we have the following remark

Remark C.4.6. *Multivariate Gaussian distribution is a special case of multivariate t-distribution when $\nu \to \infty$.*

Proposition C.4.7 (Tail Dependence). *Let $\mathbf{X} \sim E_d(\mathbf{0}, \nu, \mathbf{\Sigma})$ be regular varying with tail index α. The tail dependence for the pair (X_i, X_j) where X_i, X_j are the elements of $\mathbf{X}$, is given as [Kri+09]*

$$\lambda_{i,j} = \frac{\int_0^{\sqrt{\frac{1+\rho}{2}}} \frac{u^\alpha}{\sqrt{1-u^2}} du}{\int_0^1 \frac{u^\alpha}{\sqrt{1-u^2}} du}, \tag{C.20}$$

where ρ is the off-diagonal element of the correlation matrix $\mathbf{\Sigma}$. And α is the stable exponent for sub-Gaussian α-stable distribution or the degree of freedom for t-distribution.

Proposition C.4.8. *The Kendall's τ, ρ_τ, for elliptical distribution is given as [LMS03]*

$$\rho_\tau = \frac{2}{\pi} \arcsin \rho, \tag{C.21}$$

where ρ is the correlation coefficient from $\mathbf{\Sigma}$.

C.4.2   Student t-copula

According to the Corollary C.1.2, we can derive the copula of multivariate t-distribution, i.e., t-copula. Due to the Property C.1.5, the copula of $t_d(\nu, \boldsymbol{\mu}, \mathbf{P})$ is identical to that of $t_d(\nu, \mathbf{0}, \mathbf{\Sigma})$ where $\mathbf{\Sigma}$ is the correlation matrix implied by the dispersion matrix $\mathbf{P}$. And t-copula is given by

Definition C.4.9 (T-copula). *The t-copula has the form*

$$C^t_{\nu,\mathbf{\Sigma}}(\mathbf{u}) = \int_{-\infty}^{t_\nu^{-1}(u_1)} \cdots \int_{-\infty}^{t_\nu^{-1}(u_d)} \frac{\Gamma(\frac{\nu+d}{2})}{\Gamma(\frac{\nu}{2})\sqrt{(\pi\nu)^d|\mathbf{\Sigma}|}} \left(1 + \frac{\mathbf{x}^T \mathbf{\Sigma}^{-1} \mathbf{x}}{\nu}\right)^{\frac{\nu+d}{2}} d\mathbf{x}, \tag{C.22}$$

and t_ν^{-1} is the inverse distribution function of a standard univariate t-distribution. That is,

$$t_\nu(x) = \int_{-\infty}^x \frac{\Gamma(\frac{\nu+1}{2})}{\sqrt{\nu\pi}\Gamma(\frac{\nu}{2})} \left(1 + \frac{t^2}{\nu}\right)^{-\frac{\nu+1}{2}} dt. \tag{C.23}$$

The density of t-copula is given as

$$c^t_{\nu,\mathbf{\Sigma}}(\mathbf{u}) = \frac{f_{\nu,\mathbf{\Sigma}}\left(t_\nu^{-1}(u_1), \cdots, t_\nu^{-1}(u_d)\right)}{\prod_{i=1}^d f_\nu(t_\nu^{-1}(u_i))}, \quad \mathbf{u} \in (0,1)^d, \tag{C.24}$$

where $f_{\nu,\mathbf{\Sigma}}$ is the joint density of $t_d(\nu, \mathbf{0}, \mathbf{\Sigma})$ distributed random vector and f_ν is the density of univariate standard t-distribution with the degree of freedom, ν .

The tail dependence of t-copula is given by [DM05]

Proposition C.4.10. *For continuously distributed random variables of the t-copula with ν and $\boldsymbol{\Sigma}$, the tail dependence is also given by*

$$\lambda_{\mathbf{X}} = 2t_{\nu+1}\left(\frac{-\sqrt{\nu+1}\sqrt{\rho-1}}{\sqrt{\rho+1}}\right), \tag{C.25}$$

where ρ is the correlation coefficient from $\boldsymbol{\Sigma}$, and $t_{\nu+1}(\cdot)$ is the distribution function of a standard univariate t-distribution with the degree of freedom, $\nu + 1$.

Bibliography

[AB07]   T. C. Aysal and K. E. Barner. "Generalized mean-median filtering for robust frequency-selective applications". In: *IEEE transactions on signal processing* 55.3 (2007), pp. 937–948.

[ABG11]   J. G. Andrews, F. Baccelli, and R. K. Ganti. "A tractable approach to coverage and rate in cellular networks". In: *IEEE Transactions on communications* 59.11 (2011), pp. 3122–3134.

[AC18]   A. Azari and C. Cavdar. "Performance evaluation and optimization of LPWA IoT networks: A stochastic geometry approach". In: *2018 IEEE Global Communications Conference (GLOBECOM)*. IEEE. 2018, pp. 206–212.

[AIH94]   S. Ambike, J. Ilow, and D. Hatzinakos. "Detection for binary transmission in a mixture of Gaussian noise and impulsive noise modeled as an alpha-stable process". In: *IEEE Signal Processing Letters* 1.3 (Mar. 1994), pp. 55 –57.

[Ala18]   T. Alam. "A reliable communication framework and its use in internet of things (IoT)". In: *International Journal of Scientific Research in Computer Science, Engineering and Information Technology (IJSRCSEIT)* 3.5 (2018), pp. 450–456.

[Alh+17]   O. Alhussein, I. Ahmed, J. Liang, and S. Muhaidat. "Unified Analysis of Diversity Reception in the Presence of Impulsive Noise". In: *IEEE Transactions on Vehicular Technology* 66.2 (Feb. 2017), pp. 1408–1417.

[All17]   L. Alliance. "LoRaWAN 1.1 regional parameters". In: *technical specification* (2017).

[AP10]   N. Andreadou and F.-N. Pavlidou. "Modeling the Noise on the OFDM Power-Line Communications System". In: *IEEE Transactions on Power Delivery* 25.1 (Jan. 2010), pp. 150–157.

[Axe+17]   E. Axell, P. Eliardsson, S. Tengstrand, and K. Wiklundh. "Power Control in Interference Channels With Class A Impulse Noise". In: *IEEE Wireless Communications Letters* 6.1 (Feb. 2017), pp. 102–105.

[BB10a]   F. Baccelli and B. Blaszczyszyn. "Stochastic Geometry and Wireless Networks: Volume II Applications". In: *Foundations and Trends in Networking* 4.1-2 (2010), pp. 1–312. DOI: 10.1561/1300000026.

[BB10b]   F. Baccelli and B. Błaszczyszyn. *Stochastic geometry and wireless networks*. Vol. 1. Now Publishers Inc, 2010.

[BBM06]   F. Baccelli, B. Blaszczyszyn, and P. Muhlethaler. "An Aloha protocol for multihop mobile wireless networks". In: *IEEE Transactions on Information Theory* 52.2 (2006), pp. 421–436.

[Bey+17]   Y. D. Beyene, R. Jantti, O. Tirkkonen, K. Ruttik, S. Iraji, A. Larmo, T. Tirronen, and J. Torsner. "NB-IoT technology overview and experience from cloud-RAN implementation". In: *IEEE Wireless Communications* 24.3 (2017), pp. 26–32.

[Bła+18]   B. Błaszczyszyn, M. Haenggi, P. Keeler, and S. Mukherjee. *Stochastic geometry analysis of cellular networks*. Cambridge University Press, 2018.

[BN10]   N. Beaulieu and S. Niranjayan. "UWB receiver designs based on a gaussian-laplacian noise-plus-MAI model". In: *IEEE Trans. Wireless Commun.* 58.3 (Mar. 2010), pp. 997–1006.

[BSF08]   N. C. Beaulieu, H. Shao, and J. Fiorina. "P-order metric UWB receiver structures with superior performance". In: *IEEE Trans. Commun.* 56 (Oct. 2008), pp. 1666–1676.

[BY09]   N. C. Beaulieu and D. J. Young. "Designing time-hopping ultrawide bandwidth receivers for multiuser interference environments". In: *Proceedings of the IEEE* 97.2 (2009), pp. 255–284.

[Car10]   P. Cardieri. "Modeling interference in wireless ad hoc networks". In: *IEEE Communications Surveys & Tutorials* 12.4 (2010), pp. 551–572.

[CE12]   A. Chopra and B. Evans. "Outage Probability for Diversity Combining in Interference-Limited Channels". In: *IEEE Transactions on Wireless Communications* 12.2 (2012), pp. 550–560.

[Cho+09]   A. Chopra, K. Gulati, B. Evans, K. Tinsley, and C. Sreerama. "Performance bounds of MIMO receivers in the presence of radio frequency interference". In: *IEEE International Conference on Acoustics, Speech and Signal Processing, ICASSP 2009*. Apr. 2009, pp. 2817–2820.

[CKJ13]   B. Cho, K. Koufos, and R. Jantti. "Bounding the Mean Interference in Matérn Type II Hard-Core Wireless Networks". In: *IEEE wireless communications letters* 2.5 (2013), pp. 563–566.

[Cla+20]   L. Clavier, T. Pedersen, I. Rodriguez, M. Lauridsen, and M. Egan. "Experimental evidence for heavy tailed interference in the IoT". In: (2020).

[dc12]   O. optimal input distribution and capacity limit of Bernoulli-Gaussian impulsive noise channels. "Herath, S.P. and Tran, N.H. and Le-Ngoc, T." In: *IEEE International Conference on Communications (ICC)*. 2012.

[DF+17]   M. L. De Freitas, M. Egan, L. Clavier, A. Goupil, G. W. Peters, and N. Azzaoui. "Capacity Bounds for Additive Symmetric α-Stable Noise Channels". In: *IEEE Transactions on Information Theory* 63.8 (2017), pp. 5115–5123.

[Dim+14]   V. Dimanche, A. Goupil, L. Clavier, and G. Gellé. "On Detection Method for Soft Iterative Decoding in the Presence of Impulsive Interference". In: *IEEE Commun. Lett.* 18.6 (June 2014), pp. 945–948.

[DM05]   S. Demarta and A. McNeil. "The t-copula and related copulas". In: *International Statistical Review* 73.1 (2005), pp. 111–129.

[DRG14]   M. Di Renzo and P. Guan. "A mathematical framework to the computation of the error probability of downlink MIMO cellular networks by using stochastic geometry". In: *IEEE Transactions on Communications* 62.8 (2014), pp. 2860–2879.

[EA+19]   M. El-Aasser, R. Badawi, M. Ashour, and T. Elshabrawy. "Examining Carrier Sense Multiple Access to Enhance LoRa IoT Network Performance for Smart City Applications". In: *2019 IEEE 9th International Conference on Consumer Electronics (ICCE-Berlin)*. IEEE. 2019, pp. 168–173.

[ECD08]   T. Erseghe, V. Cellini, and G. Dona. "On UWB impulse radio receivers derived by modeling MAI as a Gaussian mixture process". In: *IEEE Transactions on Wireless Communications* 7.6 (2008), pp. 2388–2396.

[Ega+17]   M. Egan, L. Clavier, M. de Freitas, L. Dorville, J.-M. Gorce, and A. Savard. "Wireless communication in dynamic interference". In: *IEEE Global Communications Conference (GLOBECOM)*. 2017.

[Ega+18]   M. Egan, L. Clavier, C. Zheng, M. de Freitas, and J.-M. Gorce. "Dynamic interference for uplink SCMA in large-scale wireless networks without coordination". In: *EURASIP Journal on Wireless Communications and Networking* 2018.1 (2018), p. 213.

[EP18]   M. Egan and S. Perlaza. "Capacity Approximation of Continuous Channels by Discrete Inputs". In: *Proc. Annual Conference on Information Sciences and Systems (CISS)*. 2018.

[FC09]   D. Fertonani and G. Colavolpe. "On reliable communications over channels impaired by bursty impulse noise". In: *IEEE Transactions on Communications* 57.7 (2009), pp. 2024–2030.

[FI60]   K. Furutsu and T. Ishida. "On the theory of amplitude distribution of impulsive random noise and its application to the atmospheric noise". In: *Journal of the radio research laboratories (Japan)* 7.32 (1960).

[Fio06]   J. Fiorina. "A simple IR-UWB receiver adapted to Multi-User Interferences". In: *IEEE Global Telecommunications Conf., GLOBECOM 2006*. Nov. 2006, pp. 1–4.

[Fre02]   A. Fredman. "Mechanisms of Interference Reduction for Bluetooth". In: *Burlington, VT, USA* (2002).

[GAR13]   M. H. Gholizadeh, H. Amindavar, and J. A. Ritcey. "Analytic Nakagami fading parameter estimation in dependent noise channel using copula". In: *EURASIP Journal on Advances in Signal Processing* 2013.1 (2013), p. 129.

[GAR15]   M. H. Gholizadeh, H. Amindavar, and J. A. Ritcey. "On the capacity of MIMO correlated Nakagami-m fading channels using copula". In: *EURASIP Journal on Wireless Communications and Networking* 2015.1 (2015), pp. 1–11.

[GBA12]   R. Ganti, F. Baccelli, and J. Andrews. "Series Expansion for Interference in Wireless Networks". In: *IEEE Trans. Inform. Theory* 58.4 (Apr. 2012), pp. 2194 –2205.

[GC05]   A. Giorgetti and M. Chiani. "Influence of fading on the Gaussian approximation for BPSK and QPSK with asynchronous cochannel interference". In: *IEEE Transactions on Wireless Communications* 4.2 (2005), pp. 384–389.

[GDK06]   N. Guney, H. Deliç, and M. Koca. "Robust detection of ultra-wideband signals in non-Gaussian noise". In: *IEEE Transactions on Microwave Theory and Techniques* 54.4 (June 2006), pp. 1724–1730.

[GES12]   K. Gulati, B. L. Evans, and S. Srikanteswara. "Joint temporal statistics of interference in decentralized wireless networks". In: *IEEE transactions on signal processing* 60.12 (2012), pp. 6713–6718.

[GH72]   A. Giordano and F. Haber. "Modeling of atmospheric noise". In: *Radio Science* 7 (1972), pp. 1011–1023.

[Gha+10]   H. Ghannudi, L. Clavier, N. Azzaoui, F. Septier, and N. Rolland. "α-stable interference modeling and Cauchy receiver for an IR-UWB Ad Hoc network". In: *IEEE Transactions on Communications* 58.6 (2010), pp. 1748–1757.

[Gha+16]   M. Gharbieh, H. ElSawy, A. Bader, and M.-S. Alouini. "Tractable stochastic geometry model for IoT access in LTE networks". In: *2016 IEEE Global Communications Conference (GLOBECOM)*. IEEE. 2016, pp. 1–7.

[Gil+91]   K. S. Gilhousen, I. M. Jacobs, R. Padovani, A. J. Viterbi, L. A. Weaver, and C. E. Wheatley. "On the capacity of a cellular CDMA system". In: *IEEE transactions on vehicular technology* 40.2 (1991), pp. 303–312.

[GK09]   B. Garel and B. Kodia. "Signed symmetric covariation coefficient for alpha-stable dependence modeling". In: *Comptes Rendus Mathematique* 347.5 (2009), pp. 315 –320.

[GK90]   F. Gan and K. Koehler. "Goodness-of-Fit Tests Based on P-P Probability Plots". In: *Technometrics* 32.3 (1990), pp. 289–303.

[Gol05]   A. Goldsmith. *Wireless communications*. Cambridge university press, 2005.

[Gul+09]   K. Gulati, A. Chopra, B. L. Evans, and K. R. Tinsley. "Statistical modeling of co-channel interference". In: *GLOBECOM 2009-2009 IEEE Global Telecommunications Conference*. IEEE. 2009, pp. 1–6.

[Gul+10]   K. Gulati, B. Evans, J. Andrews, and K. Tinsley. "Statistics of co-channel interference in a field of Poisson-Poisson clustered interferers". In: *IEEE Transactions on Signal Processing* 58.12 (2010), pp. 6207–6222.

[HA07]   A. Hasan and J. G. Andrews. "The guard zone in wireless ad hoc networks". In: *IEEE Transactions on Wireless Communications* 6.3 (2007), pp. 897–906.

[Haa98]   J. Haartsen. "Bluetooth-The universal radio interface for ad hoc, wireless connectivity". In: *Ericsson review* 3.1 (1998), pp. 110–117.

[Hae+09]   M. Haenggi, J. G. Andrews, F. Baccelli, O. Dousse, and M. Franceschetti. "Stochastic geometry and random graphs for the analysis and design of wireless networks". In: *IEEE journal on selected areas in communications* 27.7 (2009), pp. 1029–1046.

[Hae11]   M. Haenggi. "Mean interference in hard-core wireless networks". In: *IEEE Communications Letters* 15.8 (2011), pp. 792–794.

[Hae13]   M. Haenggi. *Stochastic Geometry for Wireless Networks*. New York, NY: Cambridge University Press, 2013.

[HB08]   B. Hu and N. C. Beaulieu. "On characterizing multiple access interference in TH-UWB systems with impulsive noise models". In: *Proc. IEEE Radio Wireless Symp.* Orlando, FL, Jan. 2008, pp. 879–882.

[HG09]   M. Haenggi and R. Ganti. "Interference in Large Wireless Networks". In: *Foundations and Trends in Networking* 3.2 (2009), pp. 127–248.

[IEEK13]   A. M. Ibrahim, T. ElBatt, and A. El-Keyi. "Coverage probability analysis for wireless networks using repulsive point processes". In: *2013 IEEE 24th Annual International Symposium on Personal, Indoor, and Mobile Radio Communications (PIMRC).* IEEE. 2013, pp. 1002–1007.

[IH98]   J. Ilow and D. Hatzinakos. "Analytic alpha-stable noise modeling in a poisson field of interfers or scatterers". In: *IEEE Transactions on Signal Processing* 46.6 (1998), pp. 1601–1611.

[III07]   H. Ishikawa, M. Itami, and K. Itoh. "A Study on Adaptive Modulation of OFDM under Middleton's Class-A Impulsive Noise Model". In: *Digest of Technical Papers. International Conference on Consumer Electronics, 2007. ICCE 2007.* Jan. 2007, pp. 1–2.

[Ina+09]   H. Inaltekin, M. Chiang, H. V. Poor, and S. B. Wicker. "On unbounded path-loss models: effects of singularity on wireless network performance". In: *IEEE Journal on Selected Areas in Communications* 27.7 (2009), pp. 1078–1092.

[Joh96]   D. Johnson. "Optimal Linear Detectors for Additive Noise Channels". In: *IEEE Trans. Signal Processing* 44.12 (Dec. 1996), pp. 3079–3084.

[KKLMC09]   F. Kharrat-Kammoun, C. J. Le Martret, and P. Ciblat. "Performance analysis of IR-UWB in a multi-user environment". In: *IEEE Transactions on Wireless Communications* 8.11 (2009), pp. 5552–5563.

[KM09]   J. Kitchen and W. Moran. "Copula techniques in wireless communications". In: *ANZIAM Journal* 51 (2009), pp. 526–540.

[Kou80]   I. Koutrouvelis. "Regression-Type Estimation of the Paramters of Stable Laws". In: *JASA* 75.372 (1980).

[Kou81]   I. Koutrouvelis. "An Iterative Procedure for the estimation of the Parameters of Stable Laws". In: *Commun. Stat. - Simul. Comput.* 10.1 (1981), pp. 17 –28.

[Kri+09]   S. Kring, S. T. Rachev, M. Höchstötter, and F. J. Fabozzi. "Estimation of α-stable sub-Gaussian distributions for asset returns". In: *Risk Assessment*. Springer, 2009, pp. 111–152.

[Lau+17a]   M. Lauridsen, B. Vejlgaard, I. Kovács, H. Nguyen, and P. Mogensen. "Interference measurements in the European 868 MHz ISM band with focus on LoRa and SigFox". In: *IEEE Wireless Communications and Networking Conference (WCNC)*. 2017.

[Lau+17b]   M. Lauridsen, B. Vejlgaard, I. Z. Kovács, H. Nguyen, and P. Mogensen. "Interference measurements in the European 868 MHz ISM band with focus on LoRa and SigFox". In: *2017 IEEE Wireless Communications and Networking Conference (WCNC)*. IEEE. 2017, pp. 1–6.

[LH12]   C.-h. Lee and M. Haenggi. "Interference and outage in Poisson cognitive networks". In: *IEEE Transactions on Wireless Communications* 11.4 (2012), pp. 1392–1401.

[Lin+17]   P.-H. Lin, E. A. Jorswieck, R. F. Schaefer, M. Mittelbach, and C. R. Janda. "On Stochastic Orders and Fast Fading Multiuser Channels with Statistical CSIT". In: *arXiv preprint arXiv:1712.03692* (2017).

[Lin+19]   P.-H. Lin, E. A. Jorswieck, R. F. Schaefer, C. R. Janda, and M. Mittelbach. "Copulas and Multi-User Channel Orders". In: *ICC 2019-2019 IEEE International Conference on Communications (ICC)*. IEEE. 2019, pp. 1–6.

[LMS03]   F. Lindskog, A. McNeil, and U. Schmock. "Kendall's tau for elliptical distributions". In: *Credit Risk*. Springer, 2003, pp. 149–156.

[LPP19]   A. Lavric, A. I. Petrariu, and V. Popa. "Long range sigfox communication protocol scalability analysis under large-scale, high-density conditions". In: *IEEE Access* 7 (2019), pp. 35816–35825.

[LVK10]   H. S. Lichte, S. Valentin, and H. Karl. "Expected interference in wireless networks with geometric path loss: a closed-form approximation". In: *IEEE communications letters* 14.2 (2010), pp. 130–132.

[LWK19]   T. Lindner, D. Wyrwał, and A. Kubacki. "Low Power Wireless Protocol for IoT Appliances Using CSMA/CA Mechanism". In: *Conference on Automation*. Springer. 2019, pp. 199–207.

[Maa+13]   H. Maad, A. Goupil, L. Clavier, and G. Gelle. "Clipping Demapper for LDPC Decoding in Impulsive Channel". In: *IEEE Commun. Lett.* 17.5 (May 2013), pp. 968–971.

[Mar+15]   G. Margelis, R. Piechocki, D. Kaleshi, and P. Thomas. "Low throughput networks for the IoT: Lessons learned from industrial implementations". In: *2015 IEEE 2nd world forum on internet of things (WF-IoT)*. IEEE. 2015, pp. 181–186.

[MC17]   A. Mahmood and M. Chitre. "Optimal and Near-Optimal Detection in Bursty Impulsive Noise". In: *IEEE Journal of Oceanic Engineering* 42.3 (July 2017), pp. 639–653.

[MC20]   N. Mehrnia and S. Coleri. "Wireless Channel Modeling based on Extreme Value Theory for Ultra-Reliable Communications". In: *arXiv preprint arXiv:2002.00565* (2020).

[MCA12a]   A. Mahmood, M. Chitre, and M. Armand. "Baseband characterization of additive white symmetric α-stable noise". In: *Global Communications Conference (GLOBECOM)*. Dec. 2012, pp. 3696–3701.

[MCA12b]   A. Mahmood, M. Chitre, and M. A. Armand. "PSK communication with passband additive symmetric α-stable noise". In: *IEEE Transactions on Communications* 60.10 (2012), pp. 2990–3000.

[Mei+17]   Z. Mei, M. Johnston, S. L. Goff, and L. Chen. "Performance Analysis of LDPC-Coded Diversity Combining on Rayleigh Fading Channels With Impulsive Noise". In: *IEEE Transactions on Communications* 65.6 (2017), pp. 2345–2356.

[Mek+17]   P.-V. Mekikis, A. Antonopoulos, E. Kartsakli, N. Passas, L. Alonso, and C. Verikoukis. "Stochastic modeling of wireless charged wearables for reliable health monitoring in hospital environments". In: *2017 IEEE International Conference on Communications (ICC)*. IEEE. 2017, pp. 1–6.

[Mek+19]   K. Mekki, E. Bajic, F. Chaxel, and F. Meyer. "A comparative study of LPWAN technologies for large-scale IoT deployment". In: *ICT express* 5.1 (2019), pp. 1–7.

[Mes+19]   Y. Mestrah, A. Savard, A. Goupil, G. Gelle, and L. Clavier. "Robust and Simple Log-Likelihood Approximation for Receiver Design". In: *2019 IEEE Wireless Communications and Networking Conference (WCNC)*. IEEE. 2019, pp. 1–6.

[Mid77]   D. Middleton. "Statistical-physical models of electromagnetic interference". In: *IEEE Transactions on Electromagnetic Compatibility* 19.3 (1977), pp. 106–127.

[Mid99]   D. Middleton. "Non-gaussian noise models in signal processing for telecommunications: new methods and results for class A and class B noise models". In: *IEEE Transactions on Information Theory* 45.4 (1999), pp. 1129–1149.

[Mor02]   R. Morrow. *Bluetooth: Operation and Use*. McGraw-Hill, Inc., 2002.

[MS07]   J. Ma and Z. Sun. "Copula component analysis". In: *International Conference on Independent Component Analysis and Signal Separation*. Springer. 2007, pp. 73–80.

[MS11]   J. Ma and Z. Sun. "Mutual information is copula entropy". In: *Tsinghua Science & Technology* 16.1 (2011), pp. 51–54.

[MZW17]   A. E. Mostafa, Y. Zhou, and V. W. Wong. "Connectivity maximization for narrowband IoT systems with NOMA". In: *2017 IEEE International Conference on Communications (ICC)*. IEEE. 2017, pp. 1–6.

[NAHV14]   B. Nikfar, T. Akbudak, and A. Han Vinck. "MIMO capacity of class A impulsive noise channel for different levels of information availability at transmitter". In: *IEEE International Symposium on Power Line Communications and Its Applications*. 2014.

[Nam+06]   S. Nammi, D. Borah, C. Schneider, and R. Thoma. "Effects of impulse noise on the performance of multidimensional parity check codes". In: *IEEE Wireless Communications and Networking Conference, WCNC 2006*. Vol. 4. Apr. 2006, pp. 1966–1971.

[NB08]   S. Niranjayan and N. C. Beaulieu. "The optimal BER linear rake receiver for Alpha-Stable noise". In: *2008 IEEE International Conference on Communications*. IEEE. 2008, pp. 5013–5017.

[NB09]   S. Niranjayan and N. Beaulieu. "The BER optimal linear rake receiver for signal detection in symmetric alpha-stable noise". In: *IEEE Transactions on Communications* 57.12 (2009), pp. 3585–3588.

[NB10]   S. Niranjayan and N. Beaulieu. "BER optimal linear combiner for signal detection in symmetric alpha-stable noise: small values of alpha". In: *IEEE Transactions on Wireless Communications* 9.3 (2010), pp. 886–890.

[Nel99]   R. Nelson. *An Introduction to Copulas*. New York, NY: Springer-Verlag, 1999.

[NJ15]   R. Nasri and A. Jaziri. "On the analytical tractability of hexagonal network model with random traffic distribution". In: *CoRR* (2015).

[Nol01]   J. P. Nolan. "Maximum likelihood estimation of stable parameters". In: *Levy processes: Theory and applications* (2001), pp. 379–400.

[Nol13]   J. Nolan. "Multivariate elliptically contoured stable distributions: theory and estimation". In: *Computational Statistics* 28.5 (2013), pp. 2067–2089.

[Nol97]   J. P. Nolan. "Numerical calculation of stable densities and distribution functions". In: *Communications in statistics. Stochastic models* 13.4 (1997), pp. 759–774.

[NS95]   C. Nikias and M. Shao. *Signal processing with alpha-stable distributions and applications.* New York, NY: Wiley, 1995.

[OS16]   S.-M. Oh and J. Shin. "An efficient small data transmission scheme in the 3GPP NB-IoT system". In: *IEEE Communications Letters* 21.3 (2016), pp. 660–663.

[Pet+14]   G. W. Peters, T. A. Myrvoll, T. Matsui, I. Nevat, and F. Septier. "Communications meets copula modeling: Non-standard dependence features in wireless fading channels". In: *2014 IEEE Global Conference on Signal and Information Processing (GlobalSIP).* IEEE. 2014, pp. 1224–1228.

[Pha+03]   D. S. Pham, Y. H. Leung, A. Zoubir, and R. Brcic. "On the computational aspect of robust multiuser detection". In: *Proceedings of the 3rd IEEE International Symposium on Signal Processing and Information Technology, 2003. ISSPIT 2003.* 2003, pp. 22–25.

[Pha18]   C. Pham. "Investigating and experimenting CSMA channel access mechanisms for LoRa IoT networks". In: *2018 IEEE Wireless Communications and Networking Conference (WCNC).* IEEE. 2018, pp. 1–6.

[Pin+06]   P. Pinto, C.-C. Chong, M. Chiani, and M. Win. "Narrowband communication in a poisson field of ultrawideband interfers". In: *IEEE International Conference on Ultra-Wideband.* 2006.

[PW10a]   P. Pinto and M. Win. "Communication in a Poisson field of interferers-part I: interference distribution and error probability". In: *IEEE Transactions on Wireless Communications* 9.7 (2010), pp. 2176–2186.

[PW10b]   P. Pinto and M. Win. "Communication in a Poisson field of interferers-part II: channel capacity and interference spectrum". In: *IEEE Transactions on Wireless Communications* 9.7 (2010), pp. 2187–2195.

[Rab+07]   A Rabbachin, T. Quek, P. Pinto, I Oppermann, and M. Win. "UWB Energy Detection in the Presence of Multiple Narrowband Interferers". In: *IEEE International Conference on Ultra-Wideband, 2007. ICUWB 2007.* Sept. 2007, pp. 857–862.

[Rab+11]   A. Rabbachin, T. Quek, H. Shin, and M. Win. "Cognitive Network Interference". In: *IEEE J. Select. Areas Commun.* 29.2 (Feb. 2011), pp. 480–493.

[RM93]   P. Rousseeuw and G. Molenberghs. "Transformation of non positive definite semidefinite correlation matrices". In: *Comm. Statist. Theory Methods* 22 (1993), pp. 965–984.

[SAD17]   C. Saha, M. Afshang, and H. S. Dhillon. "Poisson cluster process: Bridging the gap between PPP and 3GPP HetNet models". In: *2017 Information Theory and Applications Workshop (ITA)*. IEEE. 2017, pp. 1–9.

[Sai+13]   Y. Saito, Y. Kishiyama, A. Benjebbour, T. Nakamura, A. Li, and K. Higuchi. "Non-orthogonal multiple access (NOMA) for cellular future radio access". In: *IEEE Vehicular Technology Conference (VTC-Spring)*. 2013.

[SC09]   C. Seol and K. Cheun. "A statistical inter-cell interference model for downlink cellular OFDMA networks under log-normal shadowing and multipath Rayleigh fading". In: *IEEE transactions on communications* 57.10 (2009), pp. 3069–3077.

[Ser90]   R. Serfozo. "Point processes". In: *Handbooks in Operations Research and Management Science Volume 2*. Ed. by D. Heyman and M. Sobel. North-Holland: Elsevier Science Publishers B.V., 1990. Chap. 1, pp. 1–93.

[Sha12]   E. Shaheen. "Non-Gaussian MAI modeling to the performance of TH-BPSK/PPM UWB communication systems". In: *8th International Wireless Communications and Mobile Computing Conference (IWCMC)*. Aug. 2012, pp. 916–920.

[Sha+20]   M. B. Shahab, R. Abbas, M. Shirvanimoghaddam, and S. J. Johnson. "Grant-free non-orthogonal multiple access for IoT: A survey". In: *IEEE Communications Surveys & Tutorials* (2020).

[Sig17]   S. Sigfox. *Sigfox technical overview*. 2017.

[SJ15]   F. Sun and Y. Jiang. "On power and quality of service trade-off in device-to-device communication". In: *2015 IEEE International Conference on Communication Workshop (ICCW)*. IEEE. 2015, pp. 614–619.

[SJL16]   F. Sun, Y. Jiang, and L. Li. "A study on further properties of wireless channel capacity". In: *2016 IEEE/CIC International Conference on Communications in China (ICCC)*. IEEE. 2016, pp. 1–6.

[SM77a]   A. Spaulding and D. Middleton. "Optimum Reception in an Impulsive Interference Environment–Part I: Coherent Detection". In: *IEEE Trans. Commun.* 25.9 (Sept. 1977), pp. 910–923.

[SM77b]   A. Spaulding and D. Middleton. "Optimum Reception in an Impulsive Interference Environment–Part II: Incoherent Reception". In: *IEEE Trans. Commun.* 25.9 (Sept. 1977), pp. 924–934.

[SMET12]   T. Saleh, I. Marsland, and M. El-Tanany. "Suboptimal Detectors for Alpha-Stable Noise: Simplifying Design and Improving Performance". In: *IEEE Trans. Commun.* 60.10 (Oct. 2012), pp. 2982 –2989.

[Sor+17]   E. Soret, L. Clavier, G. Peters, and I. Nevat. "SIMO communication with impulsive and dependent interference - the Copula receiver". In: *Actes du XXVIème Colloque GRETSI.* 2017.

[Sou92]   E. Sousa. "Performance of a spread spectrum packet radio network link in a Poisson field of interferers". In: *IEEE Transactions on Information Theory* 38.6 (1992), pp. 1743–1754.

[SSH15]   Y. Song, K. W. Sung, and Y. Han. "Coexistence of Wi-Fi and cellular with listen-before-talk in unlicensed spectrum". In: *IEEE Communications Letters* 20.1 (2015), pp. 161–164.

[ST94]   G. Samorodnitsky and M. Taqqu. *Stable Non-Gaussian Random Processes.* New York, NY: CRC Press, 1994.

[Sta]   *Alpha-Stable distributions in MATLAB.* http://math.bu.edu/people/mveillet/html/alphastablepub.html.

[SZ01]   D. Stopler and R. Zamir. "Capacity and error probability in single-tone and multitone multiple access over an impulsive channel". In: *IEEE Transactions on Communications* 49.3 (2001), pp. 506–517.

[SZ08]   E. Salbaroli and A. Zanella. "Interference analysis in a Poisson field of nodes of finite area". In: *IEEE Transactions on Vehicular Technology* 58.4 (2008), pp. 1776–1783.

[Sza14]   Z. Szabó. "Information Theoretical Estimators Toolbox". In: *Journal of Machine Learning Research* 15 (2014), pp. 283–287.

[T ca]   *Copulafit.* https://www.mathworks.com/help/stats/copulafit.html.

[T cb]   *Copularnd.* https://www.mathworks.com/help/stats/copularnd.html.

[The+02]   S. R. Theodore et al. "Wireless communications: principles and practice". In: *PHI,* (2002).

[TNS95]   G. Tsihrintzis, C. Nikias, and M. Shao. "Performance of Optimum and Suboptimum Receivers in the Presence of Impulsive Noise Modeled as an Alpha-stable Process". In: *IEEE Trans. Commun.* 43.2 (Feb. 1995), pp. 904–914.

[Vas84]   K Vastola. "Threshold detection in narrow-band non-Gaussian noise". In: *IEEE Transactions on Communications* 32.2 (1984), pp. 134–139.

[Vu+14]   H. V. Vu, N. H. Tran, T. V. Nguyen, and S. Hariharan. "Estimating Shannon and constrained capacities of Bernoulli-Gaussian impulsive noise channels in Rayleigh fading". In: *IEEE transactions on communications* 62.6 (2014), pp. 1845–1856.

[WA12]   S. Weber and J. Andrews. "Transmission capacity of wireless networks". In: *Foundations and Trends in Networking* 5.2-3 (2012), pp. 109–281.

[Win+06]   M. Win, P. Pinto, A Giorgetti, M. Chiani, and L. Shepp. "Error Performance of Ultrawideband Systems in a Poisson Field of Narrowband Interferers". In: *2006 IEEE Ninth International Symposium on Spread Spectrum Techniques and Applications.* Aug. 2006, pp. 410–416.

[WKV06]   Q. Wang, S. R. Kulkarni, and S. Verdú. "A nearest-neighbor approach to estimating divergence between continuous random vectors". In: *2006 IEEE International Symposium on Information Theory.* IEEE. 2006, pp. 242–246.

[WM19]   F. Wang and G. Ma. *Massive Machine Type Communications: Multiple Access Schemes.* Springer, 2019.

[WPS09]   M. Z. Win, P. C. Pinto, and L. A. Shepp. "A mathematical theory of network interference and its applications". In: *Proceedings of the IEEE* 97.2 (2009), pp. 205–230.

[XZA11]   J. Xu, J. Zhang, and J. G. Andrews. "On the accuracy of the Wyner model in cellular networks". In: *IEEE Transactions on Wireless Communications* 10.9 (2011), pp. 3098–3109.

[Yan+15]   X. Yan, L. Clavier, G. Peters, N. Azzaoui, F. Septier, and I. Nevat. "Skew-t copula for dependence modelling of impulsive (alpha-stable) interference". In: *IEEE International Conference on Communications (ICC).* 2015.

[YP03]   X. Yang and A. Petropulu. "Co-channel interference modeling and analysis in a Poisson field of interferers in wireless communications". In: *IEEE Transactions on Signal Processing* 51.1 (2003), pp. 64–76.

[ZBA06]   S. Zozor, J. Brossier, and P. Amblard. "A Parametric Approach to Suboptimal Signal Detection in α-stable Noise". In: *IEEE Trans. Signal Processing* 54.12 (Dec. 2006), pp. 4497–4509.

[ZD11]   X Zeng and T. Durrani. "Estimation of mutual information using copula density function". In: *Electronics letters* 47.8 (2011), pp. 493–494.

[ZD97]   M. M. Zonoozi and P. Dassanayake. "User mobility modeling and characterization of mobility patterns". In: *IEEE Journal on selected areas in communications* 15.7 (1997), pp. 1239–1252.

[Zhe+19a]   C. Zheng, M. Egan, L. Clavier, G. Peters, and J.-M. Gorce. "Copula-Based Interference Models for IoT Wireless Networks". In: *ICC 2019-53rd IEEE International Conference on Communications*. 2019, pp. 1–6.

[Zhe+19b]   C. Zheng, M. Egan, L. Clavier, G. Peters, and J.-M. Gorce. "On the Validity of Isotropic Complex α-Stable Interference Models for Interference in the IoT". In: 2019.

[Zhe+20]   C. Zheng, M. Egan, T. Pedersen, and J.-M. Gorce. "Linear combining in dependent α-stable interference". In: *Proc. IEEE International Conference on Communications (ICC)*. 2020.

[ZZ17]   D. Zucchetto and A. Zanella. "Uncoordinated access schemes for the IoT: approaches, regulations, and performance". In: *IEEE Communications Magazine* 55.9 (2017), pp. 48–54.